



HAL
open science

Synaptic fluctuations in cerebellar interneurons connected by a single synaptic contact

María Camila Pulido Puentes

► **To cite this version:**

María Camila Pulido Puentes. Synaptic fluctuations in cerebellar interneurons connected by a single synaptic contact. Neuroscience. Université Sorbonne Paris Cité, 2016. English. NNT : 2016US-PCB007 . tel-01584465

HAL Id: tel-01584465

<https://theses.hal.science/tel-01584465>

Submitted on 8 Sep 2017

HAL is a multi-disciplinary open access archive for the deposit and dissemination of scientific research documents, whether they are published or not. The documents may come from teaching and research institutions in France or abroad, or from public or private research centers.

L'archive ouverte pluridisciplinaire **HAL**, est destinée au dépôt et à la diffusion de documents scientifiques de niveau recherche, publiés ou non, émanant des établissements d'enseignement et de recherche français ou étrangers, des laboratoires publics ou privés.



Université Paris Descartes

Faculté de Médecine

Ecole doctorale 474- Frontières du Vivant

Thèse de doctorat de Neurosciences

*Synaptic fluctuations
in cerebellar interneurons
connected by a single synaptic contact*

Par María Camila PULIDO PUENTES

Dirigée par Alain Marty

Présentée et soutenue publiquement le 11 Mars 2016

Devant un jury composé de :

CASADO Mariano, MC ENS, rapporteur

KAWAGUCHI Shinya, Associate Professor à Doshisha University, examinateur

LEGAY Claire, Professor à Paris Descartes, examinateur

LEGENDRE Pascal, directeur de recherche, rapporteur

MARTY Alain, DR CNRS, directeur de thèse

RYAN Timothy, directeur de recherche à Weill Cornell Medical College, examinateur

Brain Physiology Laboratory, GABAergic Synapses in the Cerebellum (UMR 8118)



Université Paris Descartes

Faculté de Médecine

Ecole doctorale 474- Frontières du Vivant

Thèse de doctorat de Neurosciences

*Synaptic fluctuations
in cerebellar interneurons
connected by a single synaptic contact*

Par María Camila PULIDO PUENTES

Dirigée par Alain Marty

Présentée et soutenue publiquement le 11 Mars 2016

Devant un jury composé de :

CASADO Mariano, MC ENS, rapporteur

KAWAGUCHI Shinya, Associate Professor à Doshisha University, examinateur

LEGAY Claire, Professor à Paris Descartes, examinateur

LEGENDRE Pascal, directeur de recherche, rapporteur

MARTY Alain, DR CNRS, directeur de thèse

RYAN Timothy, Directeur de recherche à Weill Cornell Medical College, examinateur

Brain Physiology Laboratory, GABAergic Synapses in the Cerebellum (UMR 8118)

Résumé:

L'élément constitutif des synapses centrales est le site synaptique individuel, comprenant une zone active du côté présynaptique et une densité postsynaptique associée. Du fait de limitations techniques nos connaissances sur le mode de fonctionnement d'un site synaptique restent insuffisantes. Pour faire progresser cette question nous projetons d'effectuer des enregistrements en paires entre interneurons de la couche moléculaire du cervelet. Ces neurones forment des synapses qui ont des signaux élémentaires quantiques de grande taille, et les synapses comprennent parfois un seul site synaptique, ce qui fait qu'ils offrent des avantages décisifs pour ce projet. Les réponses postsynaptiques à des trains de potentiels d'action seront étudiées dans différentes conditions expérimentales. Les résultats seront interprétés par un modèle supposant que les vésicules synaptiques doivent se lier à un petit groupe de sites d'arrimage avant l'exocytose.

Title:

Synaptic Fluctuations in Cerebellar Interneurons Connected by a single synaptic contact

Abstract:

The unitary element of central synaptic transmission is a single synaptic site, with one active zone as presynaptic component and the postsynaptic density as postsynaptic partner. Due to technical limitations there is much uncertainty on the mode of functioning of a single synaptic site. To address this issue it is planned to perform paired recordings between interneurons of the molecular layers of the cerebellum. These neurons form synapses with a large quantal size, and occasionally displaying a single release site, and are thus favorable for this study. Postsynaptic responses will be studied in response to trains of presynaptic action potentials under various conditions. The results will be compared to a model supposing the obligatory binding of vesicles to a small complement of docking sites prior to exocytosis.

Mots clés: Docking Sites, Single synaptic contacts, GABAergic interneurons.

Keywords: Docking Sites, Single synaptic contacts, GABAergic interneurons.

*To my lovely family,
they were right:
« The most important is education »*

Acknowledgment

I arrived to France directly from Colombia with the idea of starting my thesis project, already 4th years ago. However, since my arrival I have been enriched by different experiences that make even better the process of making this PhD. I had the fortune of sharing with incredible people that, even some of them already left, make part of this adventure. There are tons of people with which I am thankful and happy to meet.

First at all, I would like to thank Mariano, Shinya, Claire, Timothy and Pascal for accepting be part of my thesis jury.

I am grateful to Alain for guiding me during this process and allowing me to be part of this beautiful project. All his advices were always relevant in order to reach a happy ending. Also, I would like to thank Isabel not just for her enthusiasm helping with some experiments and for her useful comments, also for her support and concern during all these years in Paris. Without both of you this nice experience could not be the same.

As part of my formation, I will never forget to thank my mentors Enrico and Maria del Pilar. There are no words to express my gratitude and admiration for them. Those six months sharing with you here in Paris were the best!

I would like to thank all the current and previous members of 8118 which made my time here pleasant. I would like to thank Fede, Brandon, Taka, Javier, Jorge, Kris for their nice discussions during our lunch time at Crous, and during the extra-laboratory activities that were not few. Also, I would like to thank people from the laboratory 8119, which were always happy to make alternative activities together with us.

I am glad to meet Guadalupe, the best officemate and a really, really good friend. Since always, there were countless moments of joy... We never stop having fun and yet, time flew! I am grateful to her for advising and motivating me during these years of research, even from the distance.

Also, I am happy to share once again with Gerardo, who arrived with an excellent idea of making beer by ourselves, the best of all distractions!... well, there was also

the ping-pong table idea, which was better at our minds than in practice!

Likewise, I am glad to meet people that were part of this adventure. I am grateful to my friends Jimena, Eugenia, Camilo, Ana, Paula, Philippe, Jean, Joe, Johanna, Mad for their support during these years of studies. They have become a special part of my life.

I would like also to thank Paris Descartes University and the "Fondation pour la Recherche Médicale" for funding my studies.

Finally but not less important, I am grateful to my family that despite they were in Colombia, they were always thinking on me, giving me the best of their energies.

My sincere thanks to all of you for being part of this!

Table of Contents

| | |
|---|----|
| PREFACE..... | 1 |
| A historical introduction to the mechanisms of central synapses..... | 3 |
| Chapter 1: Synaptic transmission by vesicular release..... | 3 |
| 1.1 Neuromuscular Junction Model..... | 4 |
| 1.2 Miniature Spontaneous Events..... | 5 |
| 1.3 Quantal Nature of end-plate Potentials..... | 6 |
| 1.4 Vesicle hypothesis of Quantal secretion..... | 7 |
| 1.5 Chemical transmission, speed and modulation..... | 8 |
| Chapter 2: Quantal transmission at central synapses: the release sites controversy..... | 11 |
| 2.1 Are there quantum-like components in central synapses?..... | 12 |
| 2.2 Looking for release sites at the CNS..... | 15 |
| 2.2.1 One site-One vesicle hypothesis..... | 16 |
| 2.2.2 Postsynaptic receptors occupancy and Multivesicular release hypothesis... .. | 17 |
| Chapter 3: Molecular nature of the building block of the synapses..... | 23 |
| 3.1 Active zone Material and synaptic vesicle Docking..... | 23 |
| 3.2 Molecular Machinery at the Active Zone..... | 26 |
| 3.3 Distribution of calcium channels along the active zone..... | 28 |
| 3.4 Active zone proteins and their macromolecules counterparts..... | 29 |
| Chapter 4: Physiology of docking sites..... | 31 |
| 4.1 Defining the Readily releasable Pool..... | 31 |
| 4.1.1 One site-one vesicle RRP models..... | 31 |
| 4.1.2 Capacitance membrane changes in chromaffin cells..... | 32 |
| 4.1.3 RRP at the Calyx of Held..... | 32 |
| 4.1.4 Calcium uncaging at cerebellar MLIs..... | 33 |
| 4.2 Fixed number of docking sites..... | 35 |
| 4.3 Synaptic contact heterogeneity: a docking site concern..... | 37 |
| METHODS..... | 41 |
| Chapter 1: Cerebellar Slices preparation..... | 43 |
| 1.1 Slices of young rat..... | 43 |
| 1.2 Slices of adult rat..... | 43 |
| 1.3 Cutting solutions..... | 44 |
| Chapter 2: Recording Procedures..... | 45 |

| | |
|--|-----|
| 2.1 Recording set up..... | 45 |
| 2.2 Interneuron selection..... | 45 |
| 2.3 Electrophysiology..... | 46 |
| 2.4 Paired MLI recordings..... | 46 |
| Chapter 3: Spontaneous events detection..... | 47 |
| Chapter 4: Monte Carlo simulations..... | 47 |
| RESULTS..... | 49 |
| Chapter 1: Vesicular Release Statistics and Unitary Postsynaptic Current at Single GABAergic Synapses..... | 49 |
| Chapter 2: Changes in IPSC amplitude and kinetics with extracellular calcium concentration..... | 75 |
| Chapter 3: Statistics of cumulative released vesicle numbers in elementary GABAergic synapses..... | 79 |
| 3.1 Introduction..... | 79 |
| 3.2 Extension of the 2-step model to single GABAergic synapses..... | 80 |
| Chapter 4: Modeling Changes in Synaptic Properties..... | 86 |
| 4.1 Changes in success probability induced by augmentation of spontaneous synaptic activity..... | 86 |
| 4.2 Simulations of presynaptic parameters..... | 90 |
| Chapter 5: Developmental changes in the synaptic connectivity between cerebellar interneurons..... | 96 |
| 5.1 Docking site number decreases with development..... | 97 |
| DISCUSSION..... | 102 |
| 1.1 Importance of single synaptic contact recordings and docking sites calculation.. | 102 |
| 1.2 An extension of the Variance-mean fluctuation analysis method..... | 103 |
| 1.3 2-step Model and its implications in short-term synaptic depression and recovery. | 105 |
| 1.4 Spontaneous release offers a way of modulating ρ , the occupancy of the recruitment site..... | 106 |
| CONCLUDING REMARKS..... | 108 |
| PERSPECTIVES..... | 110 |
| BIBLIOGRAPHY..... | 112 |

Figure Index

| | |
|---|----|
| Figure 1. Quantal nature of the end-plate potential at the neuromuscular junction..... | 5 |
| Figure 2. Active Zone in Electron microscopy..... | 9 |
| Figure 3. Schematic diagram to explain quantal hypothesis..... | 12 |
| Figure 4. Quantal components in central synapses..... | 13 |
| Figure 5. Multivesicular release from a single synaptic contact recording..... | 20 |
| Figure 6. Docking sites are organized together with Active Zone Material at the neuromuscular junction..... | 24 |
| Figure 7. Molecular organization of the active zone..... | 27 |
| Figure 8. Vesicular readily releasable pool estimation at single synaptic contacts..... | 34 |
| Figure 9. Estimation of docking sites number and quantal parameters by a variance-mean analysis technique..... | 36 |
| Figure 10. The number of docked vesicles correlates linearly with active zone size..... | 38 |
| Figure 11. Changes in PSC peak amplitude and kinetics with Ca_o | 76 |
| Figure 12. Statistics of cumulative released vesicle numbers in elementary GABAergic synapses..... | 82 |
| Figure 13. Increase in spontaneous release due to presynaptic depolarization affects evoked release..... | 87 |
| Figure 14. Simulation of synaptic depression during repetitive stimulation in two release models..... | 90 |
| Figure 15. The replacement site may not be fully occupied in control conditions..... | 92 |
| Figure 16. Developmental changes in synaptic parameters..... | 98 |

PREFACE

Neurons are the cells of the nervous system, characterized by having functional specialized regions, that allow the faithful transmission of information through specialized inputs and outputs. Neurons propagate codified information through a thin cable (*the axon*) until a junctional region (*the synapse*), where information is passed rapidly to another cell, usually another neuron, in a process known as synaptic transmission. Essentially, the electrical information carried by the first cell (*presynaptic cell*) causes a change in the electrical activity of the second cell (*postsynaptic cell*); where the codified information is retransmitted to a following neuron or specialized cell. Since neurons were discovered, near the end of nineteenth century, the problem arose as to how excitation was transmitted across the gap between pre- and postsynaptic cells, putting neurons and synapses in the limelight of neuroscience.

There is no doubt that the twentieth century has been the century of modern neuroscience, with an extraordinary explosion of knowledge. Since the discovery of action potentials in the giant fibers in the nerve cord of the earthworm by Lucas and Andrian in the first decades of that century, followed by the characterization of its electrical nature by Hodgkin and Huxley, an extraordinary variety of new phenomena have been described, leading to an ocean of mechanisms to interpret and understand. Many discoveries relate to the mechanisms of neuronal excitability and synaptic transmission, gradually reaching to the interpretation of whole circuits and global neuronal function.

Neuronal transmission is itself a whole universe of complexities, but for my purpose, we will focus on the precise moment when the action potential reaches the axon terminal and passes the electrical information to the following cell by the secretion of a neurotransmitter. While the nature of this step is now universally accepted, it is difficult to imagine the size of the collective effort that was involved in the elucidation of this fundamental process. And, while the main focus of modern neuroscience has

PREFACE

moved on to study more integrated phenomena, it is important to point out that this work is not actually over. Yes, we do know the most basic features of synaptic transmission, but we still need to agree on several aspects of this process. In spite of the incalculable amount of knowledge that has been produced during decades of studies, there are still fundamental questions that have been raised from the beginning of the study of synaptic physiology, and which remain unanswered. Worse, while decades of studies were not sufficient to fully explain synaptic function, they were more than sufficient to create contradictory theories and scientific disagreements. As may be guessed from what I have just said, my thesis is concerned about a problem that during years has created a lot of confusion and even some personal enmities in its path; but still, it is wonderful to see how with the patient integration of all the available evidence -obtained with fantastic and ingenious methods and experiments- there is light at the end of the tunnel, there is light at the end of synaptic transmission understanding.

Along the following introduction, I am taking you through a journey in history, by relating stories and experiments, showing how from one observation made 60 years ago, a long sequence of discoveries were made, raising new questions at each step, eventually raising the hope to discern the building blocks of the synaptic processes. This description is highly simplified and does not try to be exhaustive. Rather, I have tried to focus on conceptual advances, highlighting what in retrospect appears to pave the way to subsequent progress, and trying to extract a plausible, coherent picture from occasionally discrepant views.

A HISTORICAL INTRODUCTION TO THE MECHANISMS OF CENTRAL SYNAPSES

Chapter 1: Synaptic Transmission By Vesicular Release.

During the first half of the last century, a controversy arose about how electrical information passes through that small gap that is formed between neurons, the *synaptic cleft*. At that time, Hodgkin and Huxley had yet to elucidate how information signals are generated in the neuronal axon membrane. However, it was already assumed that these signals are electrical in nature. Therefore, the most logical and natural suggestion was that an electrical process should be involved in passing that information to the next cell. Such a process was eventually demonstrated at so-called *electrical synapses*. But in parallel to electrical synapses, a totally different type of synaptic transmission was revealed at *chemical synapses*, as already anticipated by previous discoveries suggesting the involvement of chemical transmitter substances.

The efforts of Dale (1914) and Loewi (1921) contributed to demonstrate that acetylcholine, a chemical originally isolated from the ergot, causes contraction of intestinal muscle, inhibits heartbeat and lowers blood pressure. Specifically, Loewi showed that stimulating the vagus, which innervates the heart muscle, inhibits heart beating by releasing a chemical substance which was eventually identified as acetylcholine. Later, Dale demonstrated that acetylcholine is naturally produced in the body and that it is released from the motor nerve endings in skeletal muscle .

Even though these studies pointed out chemical transmission as a fundamental part of synaptic transmission, many neurophysiologists doubted whether chemical release

could be fast enough to account for the speed of the transmission of information. The assumed chemical substance must be released in the synaptic cleft, must act postsynaptically and must be removed all within a few milliseconds; in their eyes that was very difficult to accept. This difficulty was combined with the practical challenge of recording such rapid events in a living tissue. However the latter difficulty started to be lifted in the mid century, when it became possible to make electrical recordings from neurons by the insertion of a tiny intracellular electrode, allowing the recording of both sites involved in the synaptic transmission: the presynaptic and postsynaptic cells.

1.1 Neuromuscular Junction Model.

Depending on the scientific question that is raised, the model of study and the techniques have to be adapted. For instance, the first recordings of intracellular action potential obtained independently by Hodgkin & Huxley and by Cole and Curtis, took advantage of the special features of the giant axons of squids. At that time, the electrical recordings of cellular potential were made using sharp intracellular pipettes that were literally inserted inside the cells; it was fundamental to look for animal models that were adapted to those conditions. The size of squid axons, around 0.5mm, allows the insertion of recording electrodes, a process which in other cellular models would be physically impossible as it would damage all the tissue.

In the 50s, the *neuromuscular junction* emerged as a model to study synaptic transmission, because the size of the postsynaptic element, the muscle fiber, is sufficiently large to allow the stable insertion of a glass pipette. The neuromuscular junction is a synapse, but it is not a typical one, and it differs markedly from central interneuronal synapses, as I will discuss later. The goal of this synapse is to evoke contraction of the postsynaptic muscle cell. The motor axon is demyelinated near the end, where it branches and where its terminal makes synaptic contacts with the part of the muscle fiber called the *motor end-plate*. Typically when the muscle is stimulated by the arrival of an action potential at the terminal, it produces a change in its membrane potential, the *end-plate potential*, with an amplitude around 50mV, evoking its contraction (Katz, 1969). This particular synapse provides a fine introduction to the physiology of chemical synapses and it has become an excellent

model to understand how a chemical process can account for the speed of synaptic transmission, as I will be discussing in this chapter.

1.2 Miniature Spontaneous Events.

In 1952, Fatt and Katz used a high gain amplifier with a micro-electrode inserted into a frog sartorius muscle fiber at the end plate region. They examined closely recordings from the resting muscle where they observed small fluctuations in the membrane potential. These electric discharges were similar to normal *end-plate potentials* (EPPs) except for their size. They were just 0.5mV in height, and therefore received the name of *miniature end-plate potentials* (mEPPs; [Figure 1A](#); Fatt & Katz, 1952).

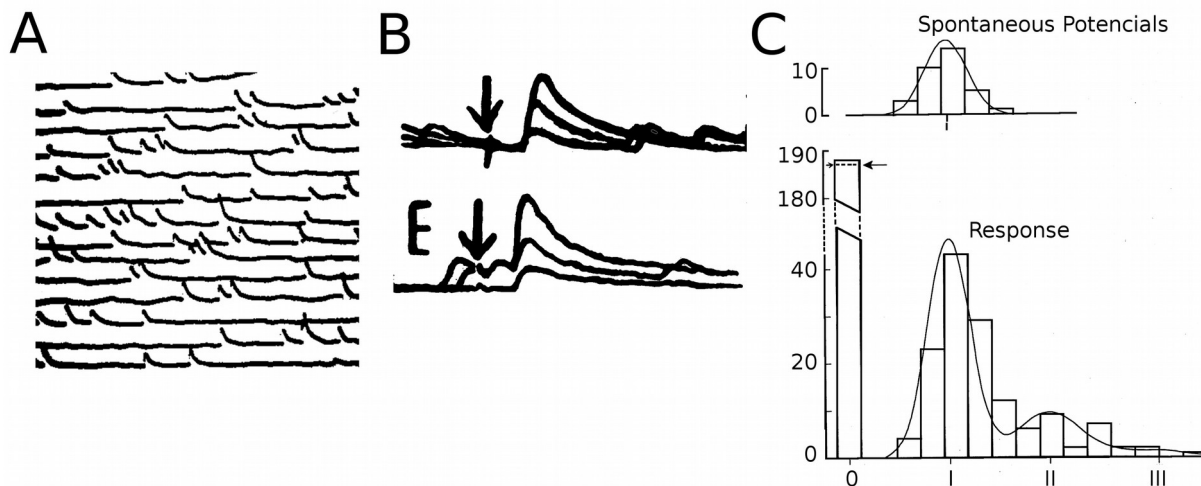


Figure 1. Quantal nature of the end-plate potential at the neuromuscular junction. (A) series of records of spontaneous changes in the membrane potential, known as miniature end-plate potentials (mEPPs, adapted from Fatt & Katz, 1952). (B) Step-wise fluctuations of EPP responses during calcium deficiency. (C) The amplitude distribution mEPPs (upper panel) and evoked EPPs responses (lower panel) after magnesium block. The expected number of failures of transmission is indicated by an arrow, and the continuous curve was calculated from a Poisson distribution, modified to take account of the variability in size of the quantal units. Peaks of the EPP amplitude histogram occur at 1, 2 and 3 times the mean amplitude of the spontaneous potentials. (B)–(C) from (del Castillo & Katz, 1954b).

Statistical analysis of the time intervals between successive mEPPs showed that their occurrence was randomly distributed in time, having a spontaneous behavior. mEPPs were just found at the end-plate region and they were not present in denervated muscle, indicating a close association with the nerve terminal. Moreover, mEPP amplitudes were reduced by curare and increased by prostigmine (an

Synaptic transmission by vesicular release.

anticholinesterase), demonstrating that mEPPS were produced by the action of acetylcholine on nicotinic receptors. These findings indicated that spontaneous activity was directly related with synaptic transmission (Fatt & Katz, 1952).

The next question was the amount of acetylcholine involved in a miniature response. An initial guess could have been to attribute a mEPP to a random collision of a single molecule. But Fatt and Katz doubted that a single molecule would be enough to cause a depolarization of 0.5mV, because that necessarily implied that just a thousand molecules are needed to produce a normal EPP of 50mV. Previously, it was estimated that the quantity of acetylcholine released by an impulse is about 10^6 molecules (Acheson, 1948), indicating that each single mEPP must be produced by several thousands of molecules. Moreover, Fatt and Katz highlighted that the response to externally applied acetylcholine is a smooth depolarization, not a series of unitary events of about 0.5mV height. Taking together these findings, it is reasonable to ask, how are those thousands of molecules released into the synaptic cleft? What is the release mechanism involved to produce the miniature discharge?

1.3 Quantal Nature of end-plate Potentials.

The neuromuscular transmission is blocked by an excess of magnesium ions. This effect is due to a reduction of the quantity of acetylcholine released per impulse (Del Castillo & Engbaek, 1954). Taking advantage of this well known effect, Fatt and Katz made remarkable findings. When the EPPs were recorded in a high Mg^{2+} and low Ca^{2+} solution its mean amplitude was smaller and surprisingly, successive EPPs responses exhibited random fluctuations in a stepwise manner. It was then found that the size of these steps approaches that of mEPPs ([Figure 1B](#); Fatt & Katz, 1952).

Integrating these results, Katz and collaborators tentatively suggested that the EPP is built by the summation of units which are identical in size with mEPPs. They further suggested that acetylcholine is released in discrete packets or *quanta* (Del Castillo & Katz, 1954). This is now known as the *quantal hypothesis*. Experimental support for this theory was initially based on impressive quantitative analysis made in collaboration with Del Castillo in 1954. This analysis was designed to estimate the mean number of quanta responding to one impulse, *m*.

Under normal conditions, the EPP is large and statistical fluctuations are small. The size of responses is maintained by a large population of packets. Each packet is assumed to be independent of the others, and to have a probability, p , to be released for each stimulus. Consequently, one might expect that quantal release would be distributed binomially under normal conditions. However, when the probability of any individual event is low (where mostly failures are observed together with occasional responses), as in quantal release recorded in high magnesium and low calcium solution, the binomial distribution degenerates and reduces to a Poisson distribution (Katz, 1969).

Using this clever idea and using the proportion of failures, Del Castillo and Katz proposed one way of calculating the quantum content (m) from Poisson's law, where m is given by the natural logarithm of the reciprocal of the proportion of failures. Alternatively, if the minis are the least unit and an EPP is made up of units of the same size, as was postulated, another way to calculate m should be the relation between the mean amplitude of the EPP responses (recorded in high magnesium) and the mean amplitude of spontaneous potentials. Furthermore, if the hypothesis is correct these two ways of calculating m should be in agreement. In fact, they showed a perfect agreement between both methods and furthermore they showed that the proportions of EPPs of different sizes are described by a Poisson distribution ([Figure 1C](#); Del Castillo & Katz, 1954).

1.4 Vesicle hypothesis of Quantal secretion.

At the same time when Katz and colleagues were making that fantastic work on quantal transmission, important observations were made by De Robertis and Bennett (1955) and Palade and Palay (1954). They showed for the first time that the nerve terminal contains large number of tiny, membrane-bound structure called *synaptic vesicles*. Taking advantage of these findings, Del Castillo and Katz (1956) suggested that vesicles represent the packets of acetylcholine that are released in response to a presynaptic action potential. They further suggested that a quantum of approximately 10,000 molecules of neurotransmitter represents the number of acetylcholine molecules contained in a single vesicle.

Synaptic transmission by vesicular release.

While the hypothesis that a quantum is represented by a single vesicle appeared very attractive, still there was not any proof in favor of that hypothesis, leaving the scene open for other suggestions about the mechanism of neurotransmitter release. Alternative options suggested that a quantum of information could be represented by the synchronized release of a group of around 7 to 10 vesicles into the synaptic cleft (Kriebel & Gross, 1974). Moreover, there was an even more drastic suggestion that the release mechanism involves the diffusion of neurotransmitter through a pore (channel) that opens during a short time interval, between the synaptic vesicle and the synaptic cleft (Falk-Vairant et al., 1996).

The controversy went on until Hurlbut and colleagues (1990) made impressive measurements on the terminal. They compared the numbers of quanta of acetylcholine released and of the synaptic vesicles lost after stimulating the nerve. Briefly, Hurlbut and colleagues measured on one side, the quantal release in low calcium/high magnesium conditions obtained with α -latrotoxin, a potent toxin extracted from the black widow spider, which causes a massive quantal release from the nerve terminals. On the other side, some muscles were fixed at various times during the secretion period and the number of synaptic vesicles remaining in the cross-sections of the terminals were counted on the electron micrographs. The relation between the quanta released and the vesicles remaining, had almost a perfect correlation, with a slope of regression line around -1.1 to -1.2 (Hurlbut et al., 1990), which means that a quantum of transmitter is derived from a single vesicle.

1.5 Chemical transmission, speed and modulation.

Now that we know that a quantum is represented by a single vesicle, it is pertinent to ask: how are these vesicles released into the extracellular medium?. Since vesicles are enclosed by a membrane, the release of neurotransmitter into the synaptic cleft requires the fusion of the vesicle membrane with the plasma membrane of the presynaptic terminal, a process called *exocytosis*.

The French neuroscientists, Couteaux and Pécot-Dechavassine (1970) first suggested that exocytotic sites are not randomly distributed, indicating that vesicles do not fuse indiscriminately with the plasma membrane. They are localized at the

active zone, (Figure 2A-B). Each active zone is represented as a dense material close to the presynaptic membrane, together with a heap of vesicles. At the end plate, active zone is localized opposite the folds of the postsynaptic membrane (Südhof, 2012). Which makes sense, since the receptors of acetylcholine are localized just in that postsynaptic membrane, making this mode of release a very efficient transmission of information.

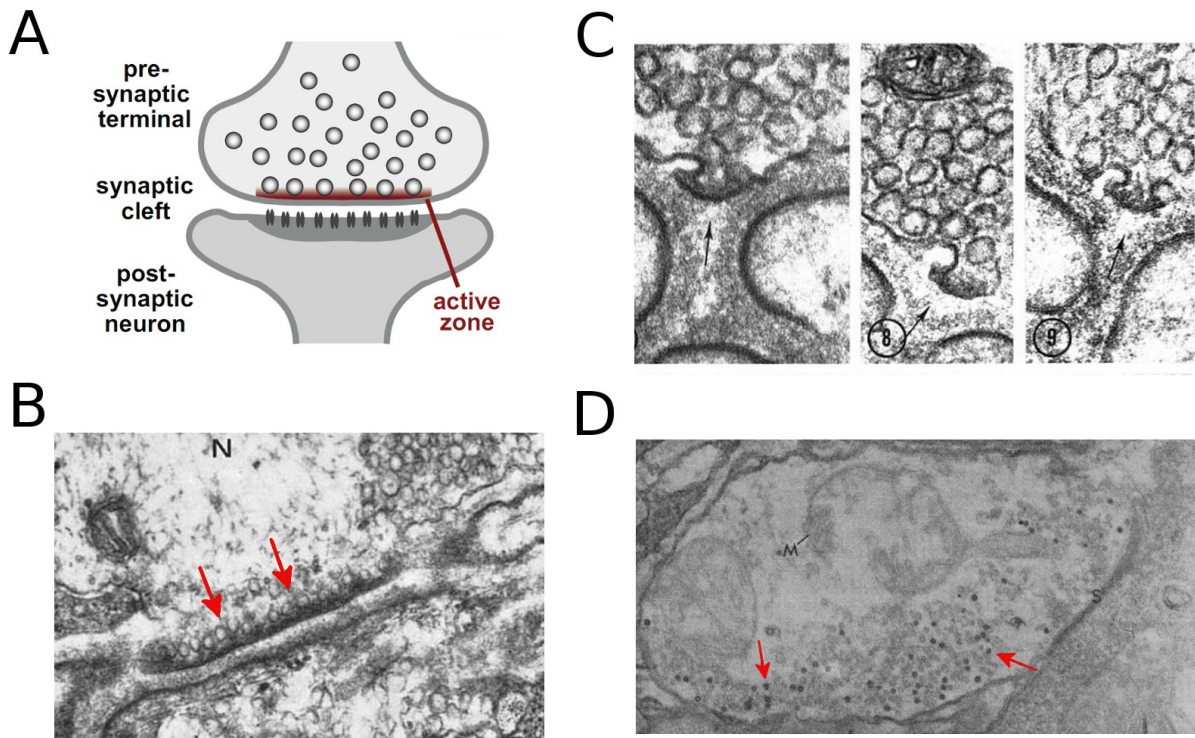


Figure 2. Active Zone in Electron microscopy. (A) Schematic drawing of a synapse (from Südhof, 2012). (B) Electron micrograph of the active zone (arrows) of the frog neuromuscular junction. Synaptic vesicles are clustered close to the active zone membrane. (C) Exocytotic opening of the synaptic vesicles into the synaptic cleft at the level of the active zone. (D) Vesicular peroxidase uptake at lobster neuromuscular junction reveals synaptic vesicle endocytosis. A few vesicles are indicated by arrows (from Holzman et al., 1971). (B) and (C) from (Couteaux & Pécot-Dechavassine, 1970).

The first direct evidence for vesicular membrane fusion was achieved by Heuser and colleagues in 1973. They produced a prolongation of action potential duration using a blocker of potassium channels, to enhance transmitter release. Then, a few milliseconds after the nerve was stimulated, the muscle was quickly cooled by slamming it onto a block of copper cooled to -269°C by liquid helium. The resulting freeze-fracture electron-micrographs showed vesicles held in the precise moment of exocytosis (Figure 2C; Heuser & Reese, 1973).

Synaptic transmission by vesicular release.

The existence of an exocytotic process, necessarily implies the existence of a counterpart, otherwise the presynaptic membrane will grow indefinitely. Evidently neurons do not behave like that. Let me describe a simple but ingenious experiment on the neuromuscular junction. Suppose that we have a certain enzyme, which oxidizes a variety of compounds and their reaction products could produce an electron-dense material. We have created a biological marker, which can be detected by electron microscopy. If we use this enzyme as a marker in the external solution in our neuromuscular junction model, and if we find that after stimulating the muscle the marker appears inside the cell, this indicates uptake of plasma membrane and some extracellular solution, proving the existence of *endocytosis* (Figure 2D; Holzmann et al., 1971). This uptake process was first established by Holzmann in the early 70s, and it occurs just after the exocytosis. Since that, it has been shown one major form of endocytosis begins with the formation of invaginations and subsequent clathrin coating, starting once again the formation of synaptic vesicles.

Chapter 2: Quantal Transmission At Central Synapses: The Release Sites Controversy.

In the previous chapter, we described synaptic transmission in the neuromuscular junction and we discussed arguments indicating that this transmission is mediated by neurotransmitter packed into vesicles. Each vesicle corresponding to a single quantum of information, fuses in the active zone at the plasma membrane and releases its content into the synaptic cleft. The transmitter reacts with the postsynaptic receptors, propagating the signal from the presynaptic neuron to the postsynaptic or cell. In this chapter, we will discuss whether the quantal statistical analysis developed by Katz and colleagues to explain the packing of information at the neuromuscular junction, also applies to synapses of the central nervous system.

According to Katz, vesicular release can occur only at specific locations, the so-called *reactive sites* or *release sites*, and he assumed a number N for these sites. As was explained before, when an impulse arrives, release of neurotransmitter occurs with a certain probability at each site, assuming that they function independently of each other. In other words, release follows binomial statistics; the average number of released quanta is the product of the total number of release sites (N) with the probability of release (p ; [Figure 3](#); Katz, 1969).

Unfortunately, attempts to adapt Del Castillo and Katz's hypothesis to the central nervous system have not been entirely successful. Trying to make sense of this literature, it is difficult for readers to disentangle the terminology created around synaptic transmission, particularly regarding release sites. Katz worked in a model where many synapses are activated by a single nerve impulse. In the context of a central synapses however, what is a release site? Is a release site a single fusion ready vesicle? A single active zone? A single synapse with perhaps, multiple active zones? There are a lot of questions and I will try to address them one by one.

Quantal transmission at central synapses: the release sites controversy.

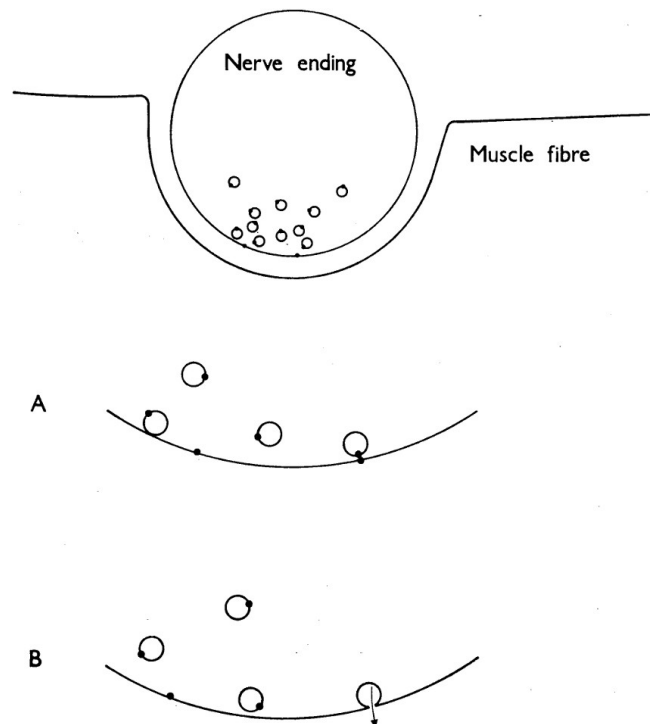


Figure 3. Schematic diagram to explain quantal hypothesis. Reactive sites on the vesicles and the active zone membrane are shown as dots. Transmitter release only occurs when two sites meet. The probability of occurrence varies directly with the number of reactive sites in the axon membrane (from Katz, 1969).

2.1 Are there quantum-like components in central synapses?

Each segment of the spinal cord includes thousands of motoneurons. The *motoneurons*, which originate from the central nervous system, are innervated by several afferent Ia neurons, the stretch-activated sensory neurons. The motoneurons are efferent nerves that propagate signals from the spinal cord to the muscle, and they emerged as a suitable model to study central synapses.

Motoneurons display *excitatory postsynaptic potentials* (EPSPs) in response to presynaptic stimuli. These EPSPs are composed of discrete units, suggesting the presence of quantal components (Kuno, 1964). However, in each motoneuron EPSPs are arising from the action of several afferent fibers; in order to distinguish responses from single terminals or see quantal release coming from a single vesicle, it is necessary to reduce the input to a single presynaptic axon, a single fiber, as was done by Redman and colleagues in the 1980ies.

In a first approach, they were able to record postsynaptic responses evoked from the stimulus of a single axon, called *unitary EPSPs* (Figure 4A). Interestingly, they showed that unitary EPSPs display amplitude variability, which cannot be explained from the background noise distribution, and they attributed this phenomenon directly to synaptic transmission (Figure 4B). Further, using a statistical computing technique known as *deconvolution*, where it is assumed that variations are discrete rather than continuous, they were able to show that EPSP amplitudes fluctuated between four discrete voltages, each with an increasing step of about $100\mu\text{V}$ (Figure 4C). They associated this step with a quantal unit in the synaptic transmission, showing for the first time quantal transmission at the CNS (Jack, Redman, & Wong, 1981).

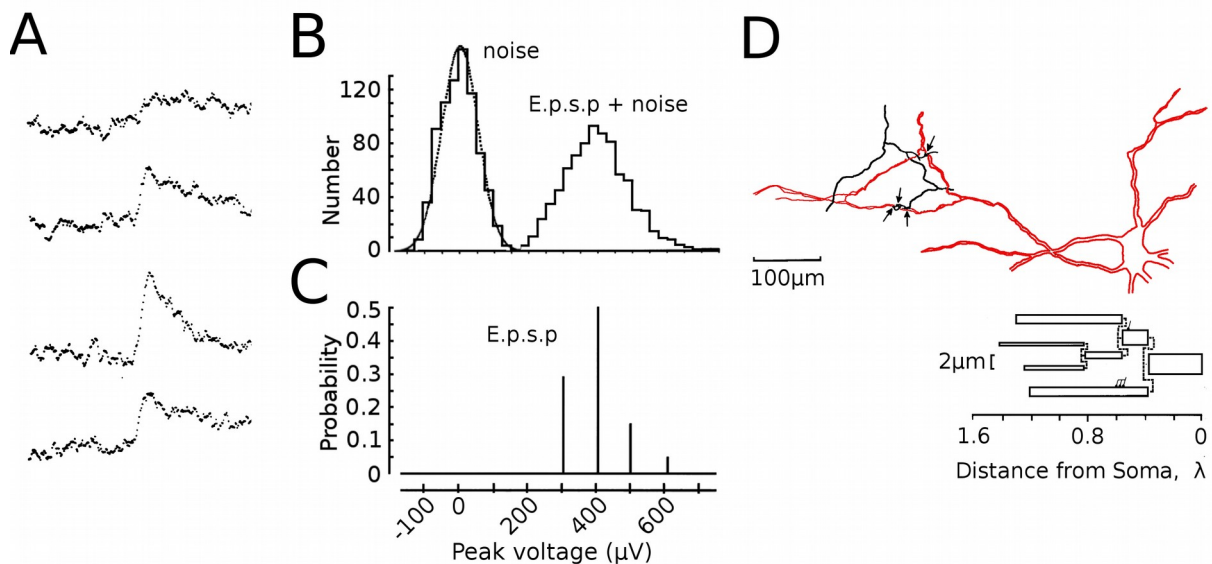


Figure 4. Quantal components in central synapses. (A) Four individual EPSPs evoked from the stimulus of a single axon. (B) The histogram of the noise, which was fitted with a Gaussian, and distribution of the peak voltage of the evoked EPSP. (C) The deconvolved release probability calculated using the Gaussian curve for the noise and the histogram in B. This result indicates that EPSP fluctuates between four discrete peak voltages, with the probabilities of each as indicated. (D) Synaptic contacts in motoneurons. Upper Panel: The dendrite of the motoneuron, together with the pre-terminal branches of the group Ia axon (black line) and synaptic contacts (arrows). Lower Panel Right: scheme representing the calculated space constant for dendritic branch. The diameter of each cylinder has been drawn to scale to represent the average diameter of the branch it represent. The $2\mu\text{m}$ bar provides the scaling for dendrite diameter. (A)-(C) adapted from (Jack et al., 1981). (D) adapted from (Redman et al., 1983).

This raises the following question: does this novel quantal unit at the CNS represent a single vesicle, as was shown in the neuromuscular junction? Unfortunately at this stage the information is not sufficient to know whether this quantum represents the release of one vesicle in a single active zone, or represents the activity of a single active zone in a multi-active zone synapse. In order to find what is the source of synaptic potential fluctuation, it becomes important to consider the morphology of the recorded neuron.

Redman and colleagues brilliantly thought that the best way to find the relation between the discrete fluctuations and their sources, was to investigate the origins of the synaptic potentials. Motoneurons and single axon fiber were filled with HRP, an enzyme that was typically used as marker for electron microscopy. Using this technique, it was possible to detect the points of contact between dendrites and axons, *the Boutons* (Figure 4D-top, Redman & Walmsley, 1983a). To corroborate that these sites were physiologically involved in the synaptic transmission, they calculated the electrical distances from the soma to each synaptic bouton, using the shape index of each recorded EPSP and the cable model (Figure 4D-bottom). Both measurements, the electrical distance and the distance obtained from the reconstruction of the synaptic contacts, were in complete agreement, concluding that fluctuations originated from different contact sources between the motoneuron and its innervating axon (Redman & Walmsley, 1983). They concluded that an evoked EPSP obtained by stimulation of a single axon, originates from a wide range of electrotonic locations on the dendritic tree, which are correlated with the location of each bouton. Redman called each location a *release site*, thinking that each contact represented the minimal unit in synaptic transmission¹. However up to here, the above findings are not enough to reach that conclusion, and it is important to clarify that a CNS release site as defined by Redman cannot be confused with the release site, with total number N, proposed by Katz; rather, it will be more associated with the active zone description.

In summary, this research showed the existence of quanta in synapses of the central nervous system. It also showed that these quanta are directly associated with the

1 This assumption is true just if there is one vesicle releasing per site, which will be discussed below.

number of synaptic boutons between axon and dendrites. Nevertheless, we still do not know whether each quantum shown by Redman represents a single vesicle or whether these discrete components are associated to the net release in each bouton. In the second alternative, this component could involve the release of multiple vesicles per active zone, which due to insufficient resolution would appear as a single component.

2.2 Looking for release sites at the CNS.

This chapter has attempted to gain insight into the mechanism by which neurotransmitters are released at the CNS. So far, it has been shown that neurons can be connected by more than one bouton. Moreover, amplitude histograms of evoked synaptic potentials can be fitted with binomial distributions, and the number of peaks are believed to correspond to the number of release sites. This correspondence requires that each synaptic contact contributes at most one quantum, either because it releases at most one vesicle (the so-called “one site-one-vesicle hypothesis”, as proposed by Triller & Korn, 1982); or because the postsynaptic receptors are close to saturation so that multivesicular release is indistinguishable from singular events (Redman, 1990).

The next logical step is to resolve the number of vesicles that are released in one active zone from the arrival of an action potential. Is there one vesicle release or multivesicular release per action potential? Reaching this apparently simple question, it will help to finally address another question raised 45 years ago: what is the “release site”, with total number N , proposed by Katz?.

In the case that the one site-one vesicle hypothesis holds true, that would imply that the release site proposed by Katz would be represented by a single active zone. Then, the probability of release p , would be the probability that one of the multiple available vesicles will be released. In the other case, if multivesicular release can be elicited by a single action potential, the release site would be each individual vesicle ready to release and p would be the fusion probability for each vesicle (Stevens, 2003). These two vesicular release hypotheses represent different interpretations of Katz's model, and distinguishing which of the two is correct becomes vital for our

comprehension of central synaptic transmission.

2.2.1 One site-One vesicle hypothesis.

Korn and Faber used the inhibitory synapses on Mauthner (M) cells as a preparation to support their one site-one vesicle hypothesis. As in motoneurons, it was found that the number of active zones established on this neuron, equals the number of binomial components obtained by statistical analysis of their *inhibitory postsynaptic potential* amplitudes (IPSPs). The estimated quantal amplitude was relatively small in size, resulting from the opening of around 1000 postsynaptic Cl⁻ channels. For them, the most parsimonious explanation of their findings was that one quantum corresponds to the amount of neurotransmitter released by one vesicle in a given active zone (Korn & Faber, 1991).

Despite the lack of direct evidence to support their interpretations, Korn and Faber proposed that the active zones were the building block of synaptic connections, or in other words that active zones and release sites were the same. They justified this assumption with the fact that in the NMJ there are 300-1000 active zones in one junction, while the mean quantal content is only about 200 (Korn & Faber, 1991). However, discerning the number of vesicles involved per active zone is difficult, particularly when a whole population of synapses are activated simultaneously. To get more accurate numbers, it is necessary to look for synaptic models where it is possible to record synaptic release from a single bouton or active zone.

As usual technical progress came to the rescue. A major improvement came with the whole-cell variant of the patch-clamp technique. This made possible an accurate control of the postsynaptic membrane voltage and a faithful recording of synaptic currents.

When a neuron is under whole-cell recording, a second micro-pipette can be approached close to the neuronal dendrites. From this second electrode, an external voltage stimulation can be applied. With some luck it is possible to excite an individual presynaptic axon and to record responses from our 'clamped' neuron. The *minimal stimulation technique* is based on these foundations. If such a connection is found, the amount of stimulation is decreased until an almost invariant amplitude

current response is obtained together with a high probability of failures (non responses). When these two conditions are met, likely the neuron is stimulated in a single bouton.

Stevens and collaborators used whole-cell recordings from CA1 hippocampal pyramidal neurons and minimal stimulation of axons to study what seems to be single synapses. However, the analysis of minimal stimulation outcome is difficult because of the uncertainty at different levels of the single synapse components: Is the number of boutons really 1? Is the number of active zones per bouton also 1? Is there multivesicular release in one active zone? Is there postsynaptic receptor saturation?. Stevens knew about these difficulties but he was forced to simplify the analysis, assuming that a single synapse had only a single active zone that can release zero or one quanta (Stevens & Wang, 1995).

In agreement with the one-site one-vesicle hypothesis, it was concluded that in one site, only one vesicle is released per action potential and then Katz's N, the number of release sites, would correspond to the number of active zones. But still, the question that remained open is whether the interpretation made by some researchers assuming inhibition of multivesicular release is correct, or whether a big fraction of postsynaptic receptors can be saturated by transmitter released by one vesicle, so that simultaneous release by several vesicles could remain undetected.

2.2.2 Postsynaptic receptors occupancy and Multivesicular release hypothesis.

How can we assay multivesicular release? What about thinking in other terms: if only one vesicle is released by a spike, the transmitter concentration in the cleft will merely depend on the amount of molecules contained in one vesicle, and it will not vary with any change in the synaptic release probability. If however, transmitter from multiple vesicles can act all at once in the same population of receptors, the peak of transmitter concentration will increase according to the number of vesicles, and thus will vary together with the release probability (Tong & Jahr, 1994).

Jahr and colleagues proposed this direct assay of multivesicular release. They estimated the concentration of free neurotransmitter (glutamate) in the synaptic cleft of hippocampal interneurons, using a rapidly competitive antagonist of the postsynaptic receptors. They measured the degree of inhibition on the excitatory postsynaptic current (EPSC), by taking into account the number of receptors free of antagonist at the instant of release and, the number of receptors that turns free of antagonism by competition at the peak of transmitter release. In theory, if there is multivesicular release and an increase in the release probability, the transmitter transient in the cleft will increase and the degree of inhibition of the EPSC will decrease. And in practice, that was exactly what they found. When they raised the probability of transmitter release by increasing calcium levels, the amount of receptor inhibition was decreased, showing for the first time that multivesicular release occurs in a single active zone (Tong & Jahr, 1994).

Although these observations are in favor of multivesicular release, some groups had still some doubt pointing out that these findings can be equally explained by *cross-talk*, where transmitter release from one synapse leads to significant activation of receptors of the neighboring synapses (Barbour & Häusser, 1997; Scanziani et al., 1997). The implications of neurotransmitter spill-over in the synaptic transmission had been estimated by the implementation of theoretical models of transmitter diffusion. These models were able to estimate, during highly synaptic activity, the levels of neurotransmitter involved in cross-talk processes, which can end activating high-affinity receptors and also desensitizing certain receptors from neighboring neurons. In that sense, two vesicles coming from independent active zones can activate the same postsynaptic receptors cluster, making difficult to distinguish between cross-talk and multivesicular release (Barbour & Häusser, 1997). Once again comes the necessity of have a single bouton, single active zone model to finally avoid any doubt.

This leads us to yet another experimental situation: Two synaptically connected inhibitory interneurons, the presynaptic cell recorded under loose cell-attach clamp and the postsynaptic cell under whole-cell clamp (Figure 5A). When the presynaptic interneuron is electrically stimulated, the postsynaptic counterpart responds with an

inhibitory postsynaptic current (IPSC, top panel in Figure 5B). Sometimes failures can occur and in most of the cases one or a few peaks can be distinguished in the amplitude histogram. These results indicated that this type of synapse includes few active zones and, several categories of connections can be distinguished by the shape of the amplitude histogram (Figure 5C). It is reasonable to propose that a connected pair of interneurons that presents low variance in amplitude and a single component in its histogram is connected by a single active zone (Figure 5B; Kondo & Marty, 1998).

Now that we have a single active zone model, let us come back to the multivesicular release issue, and try to solve another relevant problem in all this controversy: the saturation level of the postsynaptic receptors. By analogy with the neuromuscular junction, low receptor occupancy was implicitly assumed in the early formulation of the one site-one vesicle hypothesis. However, in central synapses, if one release event is sufficient to highly saturate the postsynaptic receptors, a second simultaneous vesicle signal will be reduced in amplitude or perhaps undetectable (Auger et al., 1998). Examining closely timed pairs of synaptic currents (doublets), and studying the relation between amplitude of the second event and the time interval, it was possible to conclude that the degree of receptor occupancy after release of a vesicle is high at cerebellar interneurons (Auger & Marty, 1997). In such a case, multivesicular release would be revealed in the IPSCs as closely successive events that do not sum linearly, and display small amplitude current increments as shown in the Figure 5D (red lines). In fact, the lack of linear summation of IPSCs doublets confirms that they activate the same set of receptors and come from the same active zone. Which also explains the low variance in the amplitude histogram that has just one component, interpreted as one active zone connection (Auger et al., 1998). These connections were called *simple synapses*.

Cerebellar interneuron connections have become an important model to understand synaptic transmission because they provide high resolution recordings from a single synaptic contact. Even though interneurons present high postsynaptic receptor occupancy, they were one of the first synapses showing multivesicular release, an important fact to consider along the pursuit for the building block of synapses.

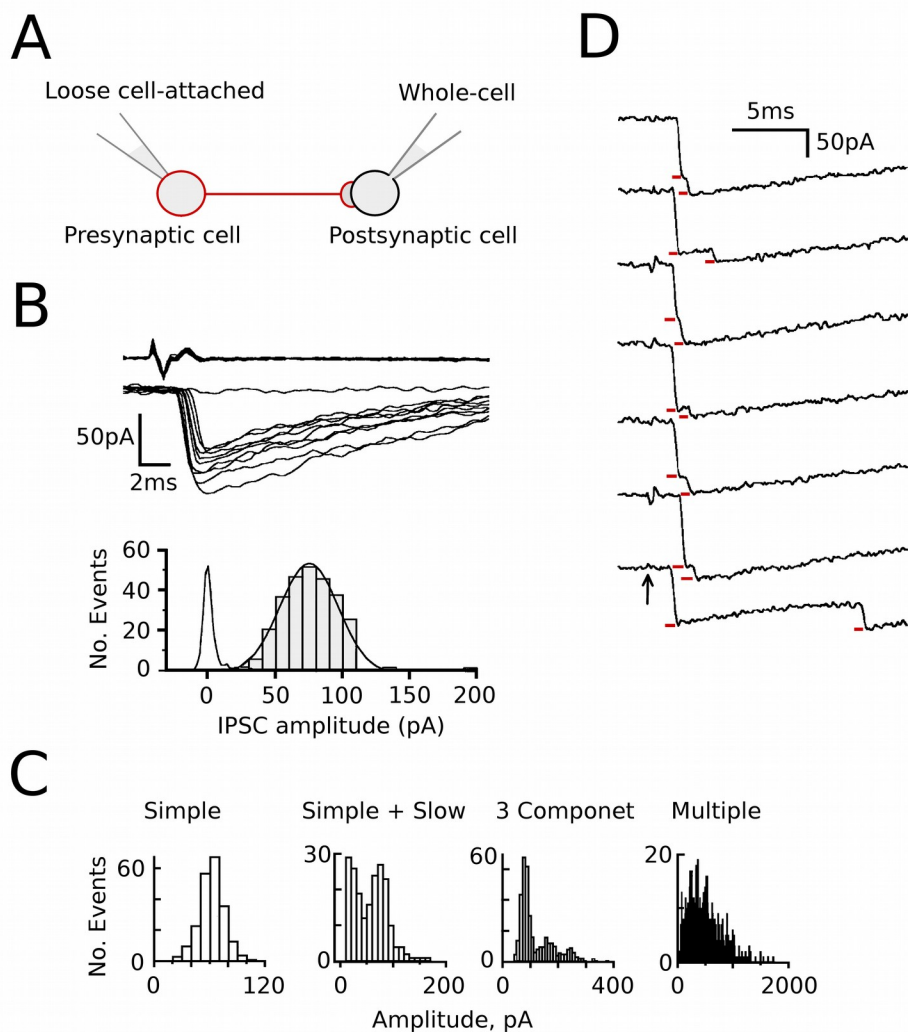


Figure 5. Multivesicular release from a single synaptic contact recording. (A) Schematic drawing of the pair-recording configuration. (B) Recording of evoked IPSCs in cerebellar interneuron. Upper Panel: pre- and postsynaptic traces at a faster time scale. Only one failure is shown, but the failure rate was 0.63. Lower Panel: amplitude distribution for successful IPSCs. The eIPSC distribution can be fitted to a single Gaussian. The histogram of the recording noise is also shown. (C) Classification of paired recording according to the shape of the amplitude histograms. The amplitude variability increases with the number of synaptic connections. The distributions fitted by one Gaussian are called Simple synapses. (D) Displaying IPSCs traces on a fast time scale, sometimes it reveals two events in close succession (red bars), showing multivesicular release at single connections. (A) - (C) adapted from (Kondo & Marty, 1998). (D) adapted from (Auger & Marty, 2000).

Considerable evidence has been obtained in recent years in favor of multivesicular release, including electro-micrographs that show the exact moment when simultaneous vesicular membrane fusion occurs (Abenavoli et al., 2002). In fact

multivesicular release occurs at many inhibitory and excitatory synapses throughout the brain, including hippocampus, cerebral cortex, cerebellum, hypothalamus and sensory synapses (Rudolph et al., 2015).

However, it appears in certain synapses that transmitter from one vesicle is far from fully occupying postsynaptic receptors and that multivesicular release can still happen (Rudolph et al., 2015). A particular case occurs at hippocampal GABAergic synapses, where due to low postsynaptic receptor occupancy, the IPSC amplitude increases by several folds in a high release probability condition. The analyses of the variance and mean of those IPSC amplitudes (method adapted by Clements and Silver in 2000 and explained in chapter 4), together with anatomical reconstructions, have shown that actually there is an increase in the signal provided by a given active zone when increasing external calcium, which indeed reflects multivesicular release (Biró et al., 2006).

Receptor occupancy is an important consideration in assessing the consequences of simultaneous release. Multivesicular release allows synapses with low receptor occupancy to enhance their dynamic range. While high occupancy synapses forfeit dynamic range due to insensitivity to changes in release probability, they operate with greater fidelity (Rudolph et al., 2015). Since multivesicular release occurs at single CNS active zones, the definition of release site should be reconsidered and may move down by one level in the synaptic hierarchy, being associated with the vesicles that are attached to the active zone, as will be discussed in the next chapter.

Chapter 3: Molecular Nature Of The Building Block Of The Synapses.

When an impulse arrives at the synaptic terminal, calcium inflow triggers vesicle fusion and neurotransmitter release. By this mechanism multiple vesicles can fuse simultaneously at the presynaptic membrane, secreting neurotransmitter into the synaptic cleft. Thus the release site contemplated by Katz, would be the physical site where each vesicle docks in close association with the active zone at the presynaptic membrane, called *docking sites* (Figure 3; Katz, 1969). Those sites where the vesicles are docked would be the building block of the synapses.

In recent years, morphological, biochemical and functional evidence has been accumulated supporting the existence of several docking sites per bouton. Docking sites are specific macromolecular structures, where vesicles must bind before undergoing exocytosis. In this chapter we will describe dense aggregates of macromolecules called *active zone material* (AZM) and discuss their role in the docking of synaptic vesicles on the presynaptic membrane. I will start describing how these macromolecules are physically distributed on the AZ and later on, I will give names to these molecules, trying to describe proteins and complexes involved in the docking sites structural formation. Finally, I will introduce some models that explain the physiology of the docking sites at the active zone.

3.1 Active zone Material and synaptic vesicle Docking.

Vesicular release is an extremely fast process triggered by the influx of calcium ions. Llinas and colleagues measured the time course of calcium ions concentration changes after an evoked presynaptic action potential. They found that the delay for triggering transmitter release by the voltage-dependent calcium influx is in the order of 200 μ s (Llinás, Steinberg, & Walton, 1981). In order to get ultrafast neurotransmitter release, it is essential that vesicles are directly located near the active zone membrane and near calcium channels. This physical conformation requires specific

Molecular nature of the building block of the synapses.

interactions between molecules located at the vesicular membrane, the active zone plasma membrane and in the cytomatrix of the active zone. Tentative candidates that could regulate these interactions are the macromolecules at the AZM, because of their prominence and of their proximity to docked vesicles and calcium channels (white arrow in [Figure 6A](#)). However, during years it has been difficult to study the AZM because of its small size, of the high density and complex arrangement of macromolecules (Szule et al., 2012).

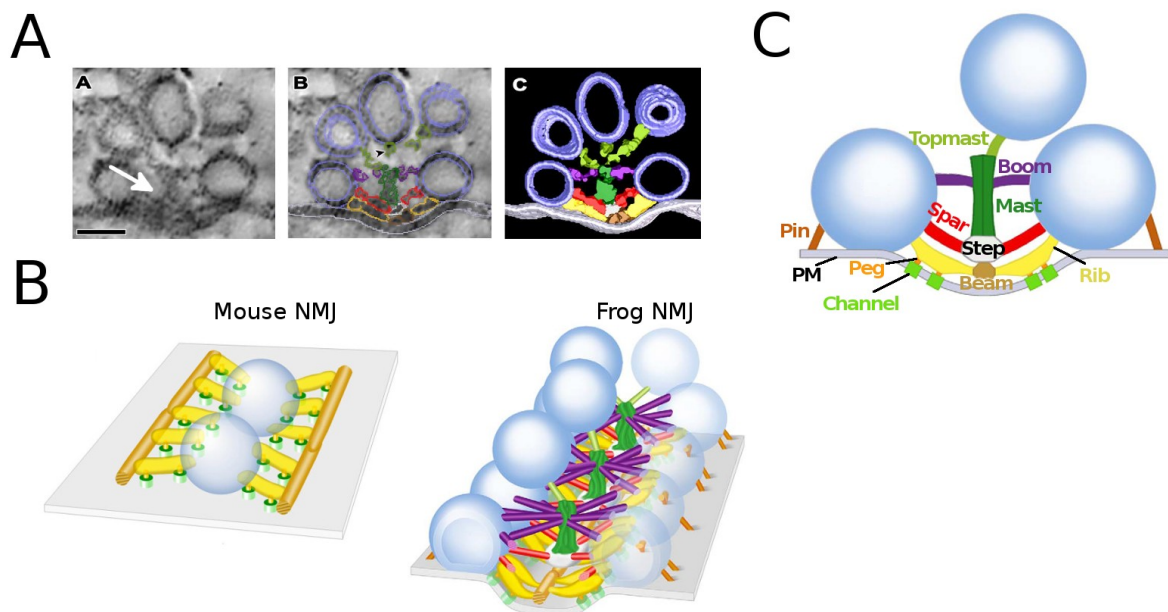


Figure 6. Docking sites are organized together with Active Zone Material at the neuromuscular junction. (A) Virtual slices showing the transverse distribution of macromolecules of the AZM (white arrow) at frog neuromuscular junction active zone. In the middle and right panel the distribution of different classes of AZM macromolecules are represented by colors. These macromolecules tether secondary vesicles, which are in line to be docked at active zone; as soon as the site turns free a series of macromolecular interactions guide the secondary vesicle to the docking site. (B) 3D schematic models of the active zone from mouse and frog neuromuscular junction, showing different distributions of AZM macromolecules: one line of vesicles in mouse (left panel; from Nagwaney et al., 2009) and two parallel lines of vesicles in frog (right panel; Szule et al., 2012). (C) Diagram of the distribution of layers of AZM macromolecules, showing in transverse plane of the active zone: the superficial layer including the macromolecules: beams, ribs and pegs; the intermediate layer: steps and spars; and the deep layer: mast, booms and topmast. (A) and (C) from (Szule et al., 2012).

In recent years, McMahan and colleagues proposed a convincing model of the architecture of the AZM molecules. They implemented the last advances in electro-tomography and virtual slices processing in tissue sections from NMJ synapses of

frog and mouse. Surprisingly, they showed that even though the same macromolecules are present in both models, their organization is different: single band in the mouse and a paired double rows of AZM in the frog ([Figure 6B](#)). This immediately indicates that AZM varies even within the same synaptic type.

More in detail, the 2D electro-microscopy micrographs and the 3D reconstructions models have shown the presence of two groups of vesicles: primary vesicles that are directly interacting with the AZM bands and are selectively docked on presynaptic membrane; and secondary vesicles, that are located at the ends of the AZM bands. These secondary vesicles are particularly relevant to the present work. They are not docked vesicles, but they are in-line to be the following vesicles positioned in release sites ([Figure 6A](#); Nagwaney et al., 2009). In order to guide vesicle docking, this model proposes the interaction of three main structural layers composed by different classes of macromolecules, which interact at different domains on the vesicle surface: the superficial layer, closer to the presynaptic membrane, the intermediate layer and the deepest layer, farther from the membrane and interacting with the recycling vesicle pool.

Briefly, this vesicle docking model describes eight classes of macromolecules distributed along the three organization layers ([Figure 6C](#)). At the superficial layer are three classes of macromolecules called *beams*, *ribs* and *pegs*. Beams are connected to beams and ribs, ribs connected to docked vesicles and pegs, and pegs, presumably connected to macromolecules in the membrane such as calcium channels. At the intermediate layer we find the *steps*, which interact with the beams, and the *spars* parallel to the ribs and connected with four docked vesicles. Finally, at the deepest layer there are *mast*, *boom* and *topmast* macromolecules. Masts are connected to the steps and to the boom, boom contacts the docked vesicle and eight booms radiate from the mast to end interacting with four docked vesicles. Finally they described topmast, an elongated macromolecule, linking the end of mast to the membrane of an undocked vesicle, keeping it near docked vesicles (Szule et al., 2012).

After a docked vesicle fuses with the membrane, undocked vesicles are directed by AZM macromolecules to the docking sites by an orderly series of interactions.

Molecular nature of the building block of the synapses.

Starting from the deepest layer, a pre-docked vesicle first establishes contact with topmast. Topmast then guides the vesicle to interact with the rest of macromolecules classes at that layer, followed by the intermediate macromolecules. Finally, the vesicle is brought to the superficial layer to the docking site position. Micrographs have shown that all macromolecular classes help to maintain the new vesicle at the docking site until it fuses with the membrane during synaptic transmission.

3.2 Molecular Machinery at the Active Zone.

As I have emphasized, vesicular release is a fast process, meaning that some vesicles should be already physically in contact with the presynaptic membrane, waiting for an action potential. McMahan nicely showed a model where macromolecules are in charge of positioning vesicles in *primed* or even in *super-primed* position, just short of the last step made by calcium influx to evoke fusion and release. Now it is time to discover the molecular nature of the machinery involved in vesicular fusion.

Let us think about this situation: we have a pool of vesicles and we want some of them to be close to the active zone membrane to start membrane fusion. For simplicity let us focus on just one vesicle, but be aware that the chain of events that I explain below could occur simultaneously in several places of the same active zone, depending on the number of sites available to dock vesicles (reviewed from: Südhof, 2013).

To keep our vesicle anchored at the AZ membrane, specific interactions would be necessary between proteins located at the vesicular membrane, at the AZ membrane and in the cytomatrix of the AZ. One of the assembly complexes made by the interactions of proteins located in these three regions is the SNARE/SM complex which triggers fusion. *Synaptobrevin*, a vesicular SNARE protein, forms a complex with its counterparts at the synaptic membrane, the SNARE proteins *Syntaxin-1* and *SNAP-25*. The assembling of this complex is tightly controlled by *Munc18*, which is a cytosolic protein involved in vesicular priming ([Figure 7A](#); Südhof, 2013; Haucke, Neher, & Sigrist, 2011). This SNARE/SM complex is one example of direct protein interaction anchoring the vesicle to the AZ membrane.

At this first stage, we have held the vesicle to the membrane, however we still need to address an important question: How is it possible that, after the inflow of calcium, a vesicle can be released in less than 200 μ s? There are still two important steps missing to gain this battle in favor of speed. One is a vesicular calcium sensor protein, as Katz already predicted; and second, an anchoring of that calcium sensor to calcium channels and to the rest of protein complexes. This tight assembling ensures that each calcium ion passing through the channels is immediately captured by the sensor, triggering all the molecular machinery involved in vesicular membrane fusion.

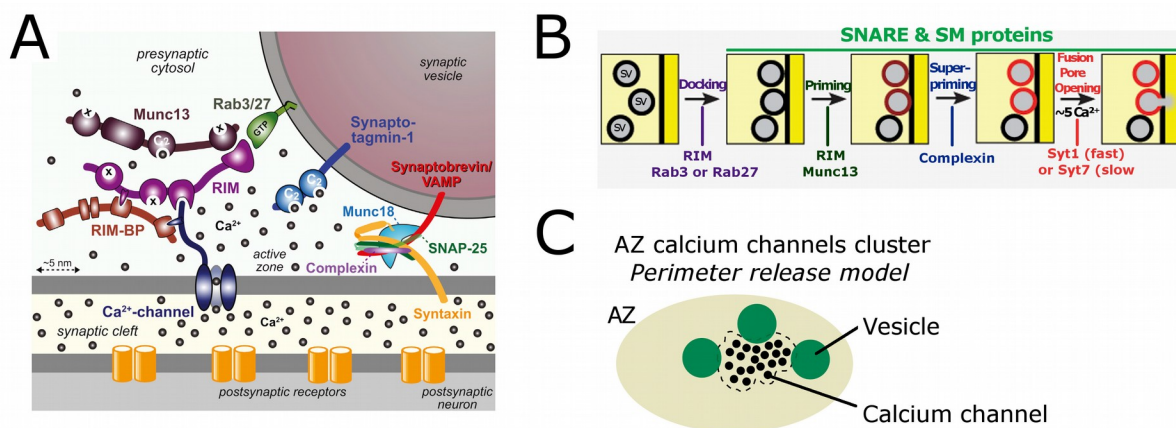


Figure 7. Molecular organization of the active zone. (A) Molecular model of the active zone protein complex coupled with calcium channels and its relation to the synaptic vesicle fusion machinery by calcium influx triggering. (B) Schematic representation of synaptic calcium-controlled neurotransmitter release. Presumably, partial SNARE complex assembly (from docking up to super-priming state) may precede calcium triggering of exocytosis. (C) Cartoon showing a possible active zone topography for calcium channels and synaptic vesicles released by a single AP in the calyx of Held. Releasable synaptic vesicles are positioned at the perimeter of calcium channel cluster. Nakamura et al. speculate that there are more than one releasable vesicle per active zone (Nakamura et al, 2015). (A) and (B) adapted from (Südhof, 2013).

Synaptotagmins are vesicular proteins with two cytoplasmic C2 domains that bind calcium. By the use of point mutations on the endogenous Synaptotagmin-1 gene, it has been shown that a decrease in their calcium binding affinity by about 2-fold, also translates into a decrease in the calcium affinity of neurotransmitter release by a factor of 2-fold, making synaptotagmins good candidates for the calcium sensors (Südhof, 2013).

Molecular nature of the building block of the synapses.

On the other hand, there is another large protein complex involving three multidomain proteins, called: *RIM*, *RIM-BP* and *Munc13*. This complex apart of mediating the docking of the vesicle at the active zone, is also important in recruiting calcium channels, placing the calcium sensor in the vicinity of the channels. RIM proteins are cytosolic proteins that bind to Munc13, calcium channels and a vesicular trans-membrane protein, *Rab3* (Südhof, 2012). RIM and RIM-BP bind to each other, and both bind to calcium channels. Electrophysiological recordings from cultured hippocampal neurons and from the calyx of Held have suggested that the deletion of RIM-BP increases the average distance between calcium channels and synaptic vesicles (Acuna et al., 2015).

Let us try to put all the process together. Our vesicle, which is coming from the reserve pool, is guided from the backfield of the synapse up to the active zone by a series of interactions mediated by *Piccolo* and *Bassoon*, proteins specific to vertebrates that have been related with vesicle clustering and tethering (Hallermann et al., 2010). The vesicular anchoring begins with the action of RIM that interacts with *Rab3*, starting the pulling of the vesicle to the proximity of calcium channels (Figure 7B). A second state is priming, which involves the binding of Munc13 to RIM, and the switching of syntaxin-1 from close to open conformation, starting the assembly of the SNARE/SM complex. Further, vesicles can reach a super-primed state by the action of *complexin*, an universal cofactor for synaptotagmin and a fundamental component in the assembling of SNARE complexes. Actually, it has been shown that loss of function of complexin could cause a decrease in calcium-triggered release, an increase of spontaneous release, and a decrease in the number of vesicles ready to be released. Finally, this super-primed vesicle is now the substrate of synaptotagmin, the synaptic calcium sensor candidate, which is positioned less than 100nm away from calcium channels. This architecture allows direct influx of calcium through channels to synaptotagmin, which triggers vesicular fusion. All these proteins form a single complex, the so-called Docking Site (Südhof, 2013).

3.3 Distribution of calcium channels along the active zone

I have been describing proteins sensitive to calcium that are close to calcium channels. The efficiency of this coupling is of special importance for securing

precision of synaptic transmission (Bucurenciu et al., 2008). It has been shown that variations in the number of calcium channels cause wide variations in release strength, and in some way this number critically influences whether release would be facilitating or depressing (Sheng et al., 2012).

A few years ago, it was shown that calcium channels form clusters at the active zone of central mammalian synapses (Holderith et al., 2012); however, their number, density and distribution were just recently described at the calyx of Held. Shigemoto and colleagues, by combining functional measurements, freeze-fracture replica, immunogold labeling of calcium channels and 3D modeling, suggested a model in which the calcium sensors are located close to the perimeter of the channel clusters ([Figure 7C](#)). More precisely, this model predicts that at the majority of docking sites multiple channels contribute to the release of each vesicle (Nakamura et al., 2015).

3.4 Active zone proteins and their macromolecules counterparts.

The composition of the active zone has been described from two different points of view: the morphology derived from electron microscopy, and the molecular identity derived from biochemistry and from knock-out studies. Is there a point where both paths merge? Due to the macromolecular distribution of synaptic proteins and of their spatial relation with the docked vesicles, it seems logical to hypothesize that many, if not all of the proteins shown by biochemistry may contribute to the composition of the AZM. McMahan and colleagues suggested a tentative correlation between morphologically derived macromolecules and specific proteins. Of course this is a speculation still lacking any direct evidence, but it is a useful working hypothesis.

The first point is to anchor a vesicle close to the active zone. The proteins that have been described to be in charge of that are mainly RIM and Rab3. Likely they could be associated with the macromolecular density formed by ribs, spars, boom and topmast, which are involved in tethering pre-docked vesicles to the site prior to docking. The following step is to bring the vesicle membrane in direct contact with the active zone membrane during docking and fusion. The cytoplasmic domains of the SNARE proteins, synaptotagmin, complexin, Munc13 and Munc18 are involved in that, corresponding to the macromolecules ribs and pins. In addition, RIM may also

Molecular nature of the building block of the synapses.

contribute to the density formation, as well as pegs, which are thought to contain the cytoplasmic portion of the calcium channel. Finally, there are several scaffolding proteins: bassoon, piccolo, RIM and spectrin, which are localized to the vicinity of the active zone. They may contribute to core AZM macromolecules described as beams, steps and masts (Szule et al., 2012).

Chapter 4: Physiology Of Docking Sites.

It was concluded on the basis of biochemistry and knock-out studies on one hand (Südhof, 2013), and of micrographs of macromolecular densities on the other hand (Szule et al., 2012), that synaptic vesicles bind to specific docking site structures. Each docking site, depending on various protein-protein interactions, holds a vesicle either in a primed or in a super-primed state. Previously, we also mentioned that in a single active zone multivesicular release is happening following one action potential (Tong & Jahr, 1994; Auger et al., 1998; Biró et al., 2006; Rudolph et al., 2015). These findings imply that in order to generate multivesicular release, each active zone should have one or several docking sites, and at least some of them should hold vesicles already docked and primed, forming the *readily releasable pool* (RRP). Next I will discuss the relation between RRP and docking sites.

4.1 Defining the Readily releasable Pool.

4.1.1 One site-one vesicle RRP models.

As we already discussed, the one site-one vesicle hypothesis considers that with the arrival of an action potential either zero or one vesicle can be released; however that does not preclude that in the active zone there may be several vesicles ready to be released. Thus, groups in favor of this hypothesis, also proposed models to calculate the RRP based on pair pulse ratio analysis (PPR), and 3D reconstruction models of the active zone. At hippocampal synapses, for instance, where the one site-one vesicle hypothesis has been advocated, it has been suggested that several vesicles are docked in one active zone, and that each of these docked vesicles has equal probability to participate to evoked release. In this situation the number of docked vesicles is proposed to represent the RRP size (Dobrunz & Stevens, 1997; Schikorski & Stevens, 1997).

Despite the observation of multiple docked vesicles, these RRP estimations have been strongly criticized, because there is not any convincing argument that explains

how vesicular release is regulated to avoid multivesicular release during one action potential. Consequently, this analysis gives an underestimated RRP value. Stevens and colleagues argue in favor of the existence of lateral inhibition, in which a negative interaction between sites prevents simultaneous release of vesicles (Triller & Korn, 1982). However, more recent experimental evidence argues against lateral inhibition at individual hippocampal synapses (Abenavoli et al., 2002).

4.1.2 Capacitance membrane changes in chromaffin cells.

How can we estimate the number of vesicles that are ready to be released during an action potential? Each time that a vesicle releases its content in the synaptic cleft, its membrane fuses with the active zone, so that for some tens of milliseconds the AZ membrane increases in size. Due to the electrical properties of neurons (or cells in general), any increase in cell surface area translates into an increase in its membrane capacitance (C_m ; Neher & Marty, 1982). Analysis of C_m changes due to vesicle fusion has provided the first and most extensive experimental basis to estimate the RRP.

Chromaffin cells, which employ the same or similar proteins used by neurons to mediate vesicular docking and fusion, were the first model used to estimate the RRP. To determine the RRP size, brief depolarizing pulses were given to restrict the measurements to vesicles that were ready to fuse and to exclude significant contributions of vesicles coming later to refill the RRP. Surprisingly, the analysis of C_m increases after depolarization, revealed a small readily releasable pool, consisting of ~ 17 vesicles per cell (Horrigan & Bookman, 1994). This was the first RRP estimated but it was far from being the last. After Bookman's estimate, numerous measurements have been produced, resulting in a broad variation in results.

4.1.3 RRP at the Calyx of Held.

This glutamatergic synapse in the auditory pathway, allows simultaneous electrical recordings from the pre- and postsynaptic compartments using patch clamp. It has become a classical model to study in detail the biophysical properties of synaptic transmission, yielding a quantitative description of the function of central synapses.

Here I focus on numbers related with RRP estimation (Neher & Sakaba, 2008 for review). It has been shown that fibers forming the calyx, fire at rates between 1 and 200Hz in complete silence and can reach up to 500Hz during tone burst. In order to follow such high frequencies the terminal has been precisely adapted. It has been calculated that the calyx holds around 500-700 active zones, and a RRP of about 1500-1800 sites at rest; moreover at high stimulation it has been shown that it can release on average 40-50 vesicles per action potential. Altogether it has been estimated that during the first second at 100Hz stimulation each release site is used three times (Neher, 2010).

Finally, it has been shown that the calyx of Held has two sets of releasable vesicles: the fast-releasing pool (FRP) and slow-releasing pool (SRP), that are distinct with respect to their release probability and speed of recruitment (Sakaba & Neher, 2001). The FRP are synchronously released at the beginning of the stimulation, while the SRP are asynchronously released late in the train (Sakaba, 2006). The relevance of these pools will be subject of discussion throughout this thesis.

4.1.4 Calcium uncaging at cerebellar MLIs.

In the last decades, advanced imaging and optical techniques have increasingly been used to study synaptic transmission. One recent study combines traditional voltage-clamp techniques together with innovative optical methods including dye-imaging and photolysis (Trigo et al., 2012). This approach is intuitively simple and robust: we have two connected cerebellar interneurons under whole-cell clamp, it does not matter whether they are connected by more than one bouton (blue traces; [Figure 8B, D](#)). Each cell is filled with a different fluorescent dye and the presynaptic cell is filled with a calcium caged compound, which is photo-releasable by a flash of UV light. Pre- and postsynaptic neurites are carefully examined until a plausible synaptic connection is identified. A laser beam (405nm) is focused on one of these potential sites, and local calcium uncaging is triggered by delivering a short flash (0.1-1ms). The uncaged calcium promotes the release of docked vesicles ([Figure 8A](#)). In parallel, the postsynaptic cell is electrically recorded ([Figure 8C](#)). A low variability in PSC amplitudes is a signature of a single synaptic contact ([Figure 8D](#)).

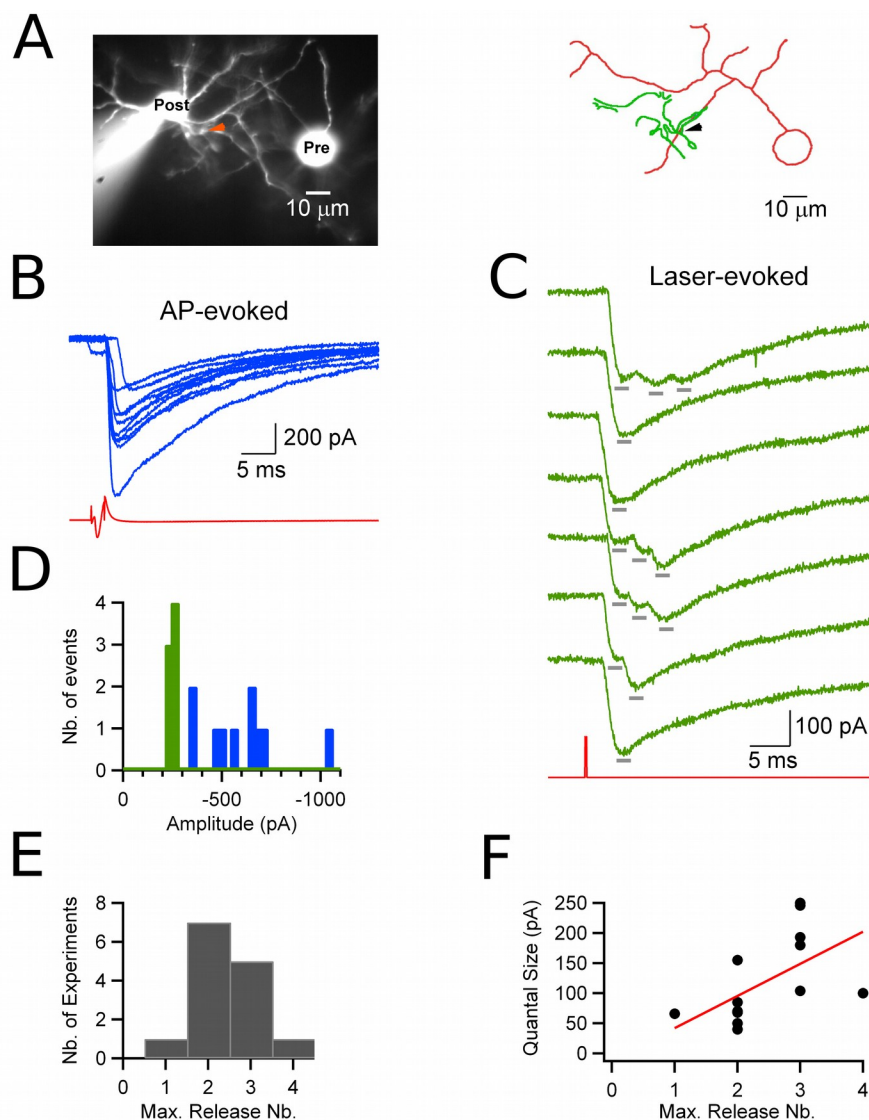


Figure 8. Vesicular readily releasable pool estimation at single synaptic contacts.

(A) In order to facilitate neurite identification, the presynaptic and postsynaptic cell are filled with red and green Alexa dyes, respectively. The presynaptic cell is filled with a calcium cage (DM-nitrophen) and a calcium fluorescent indicator (OGB-5N). Presynaptic calcium uncaging is achieved by delivering a brief laser flash confined on the synaptic contact (arrow). (B) Presynaptic APs (red trace) elicit large and variable PSCs (blue traces) which indicates a multiple site connection. (C) When calcium from the cage is released, multi-quantal release can be distinguished on the laser-evoked PSCs (green). The number of events (gray lines) can fluctuate across trials and it determines the vesicular RRP. (D) Laser stimulation can isolate records from single contacts from neurones connected by multiple synaptic sites. Peak amplitude histogram shows more variable values for AP-evoked currents (blue), than for laser-evoked currents (green). (E) The maximum number of release events observed following a single laser stimulus varies across experiments. Distribution histogram suggest variable number of docking sites ranging from 1 to 4 among simple synapses. (F) There is a linear correlation (red line) between the quantal size and the maximum number of quantal events seen at each site. From (Trigo et al., 2012).

Due to postsynaptic saturation multivesicular release appears as added steps of smaller amplitudes. Nevertheless, it is possible to count these steps to get an estimative of the number of vesicles released per photolysis flash, the RRP ([Figure 8E](#)). Following this approach the RRP at cerebellar interneurons is composed on average of about 1.9 vesicles per active zone. In a given experiment, there is a maximum value across successive trials of one to four release events per site (Trigo et al., 2012), which can be interpreted as the number of docking sites.

4.2 Fixed number of docking sites.

We are going further elaborating a vesicular release model, where prior to releasing, vesicles sit on docking sites that are physically attached to the active zone membrane. Surprisingly, this evolving CNS release model is still influenced by Katz. Namely, Katz argued that there is a limited (fixed) number of release sites, N (which we would call “Docking sites”), so that in physiological conditions release should follow a binomial distribution (Katz, 1969). Is this also the case in the CNS?

From literature just reviewed, an important fact emerged in favor of fixed number of docking sites. Trigo et al. (2012) showed that at each recorded pair of interneurons there was a maximum number of vesicles that can be released in a certain synaptic contact. That maximal number varies from one contact to another, so that some active zones can release at most 1 vesicle and others up to 4 vesicles ([Figure 8E](#), Trigo et al., 2012).

Another approach has been developed in recent years that is relevant to the study of synaptic docking sites. Clements and Silver (2000) adapted a method from sodium channels fluctuations analysis (Sigworth, 1980), which can be used to estimate quantal parameters from fits of the relationship between the variance and mean amplitude of postsynaptic responses, recorded at different release probabilities (Clements & Silver, 2000; Biró et al., 2006). Following this logic, Silver and colleagues demonstrated that the quantal amplitude fluctuation obtained under high calcium conditions (high release probability), were very small, and were in fact comparable with the variance obtained at low release probability, when mean responses were much weaker ([Figure 9A](#)). This is expected if there is a fixed number

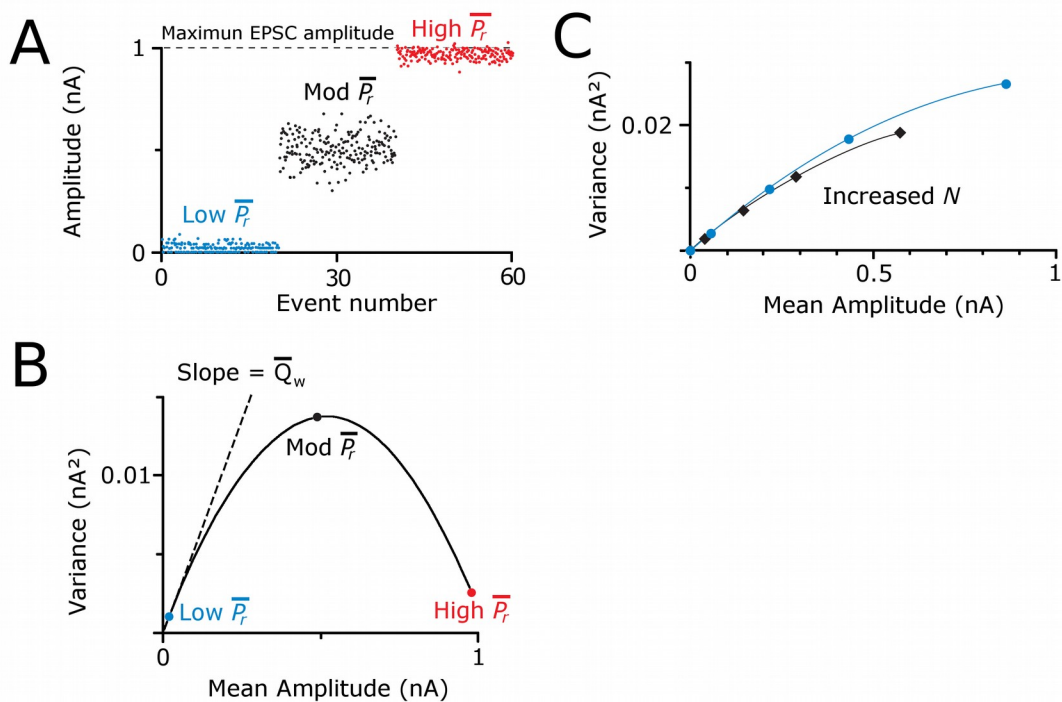


Figure 9. Estimation of docking sites number and quantal parameters by a variance-mean analysis technique. (A) Simulated EPSC data are plotted comparing peak amplitude against event number. For the simulations, Clements et al. assumed 50 independent release sites (docking sites) with uniform release probabilities. Quantal amplitude of 20pA at each site and moderate CV of 0.2. They chose three different average release probability values for separate sets of simulation, each of 190 events: low Pr at 0.02 (blue), moderate Pr at 0.5 (black) and high Pr at 1 (red). (B) The variance of the simulated EPSC amplitude against the mean amplitude for each set of events, can be fitted with a simple parabola. The number of docking sites can be estimated by the quotient between the maximum mean amplitude reached by the parabola fit (1nA) and the quantal size, which is estimated from the initial slope of the parabola (20pA), yielding 50 release sites. (C) Sets of simulation showing how the parabolic variance-mean fit changes when the number of docking sites (N) is increased from 50 docking sites (black line) to 75 docking sites (blue line). From (Clements & Silver, 2000).

N of docking sites, because in high calcium condition, the system consistently releases a number of vesicles that is close to the maximum possible number, that is N (Neher, 2010). The binomial model predicts that the variance-mean plot is parabolic, with an initial slope related with the quantal size, a maximum variance at half release probability and a maximum mean equal to the product of N with the quantal size (Figure 9B). In the case that the number of docking sites is not fixed and increases with stimulus strength, the variance-mean plot changes as shown in Figure 9C. This multiple-probability fluctuation analysis (MPFA) has been successful arguing

that at each active zone there is a fixed number of vesicles, and it has become a standard tool to estimate synaptic parameters in a given synaptic contact (Clements & Silver, 2000). However, a limitation of this model is to disregard postsynaptic receptor saturation and depends directly on the mean amplitude fluctuation, which in fact is being affected by this non-considered parameter.

Neher proposes that fixing the number of docking sites per active zone limits the rate of release during sustained synaptic activity (Neher, 2010). However, there is always the surrounding question whether all the active zones from the same family of neurons or even from the same neuron have the same strength; and whether the number of docking sites in individual active zones is fixed.

4.3 Synaptic contact heterogeneity: a docking site concern.

Connections are typically comprised of multiple synaptic contacts, but do individual synapses behave similarly? Cerebellar interneurons have become an excellent model for exploring vesicular release, and it will be again a helpful example to bring in. In these cells like in many central neurons recordings of miniature IPSCs using TTX display a large variability in amplitude. Exploring the mechanism responsible for that variability, α -latrotoxin and channel fluctuation analysis also come again to the fore (Auger & Marty, 1997).

Briefly, it has been shown that in presence of both toxins the miniature events become less variable and their amplitude distribution can be fitted by a single Gaussian, because α -latrotoxin stimulates release at just one synaptic contact at a time. Furthermore, different groups of miniature events representing independent synaptic contacts were compared by a noise analysis routine (represented by variance-mean plots), showing differences in the elementary current and the number of channels underlying the IPSCs. This analysis indicates that synaptic contacts can differ within the same type of neurons, or even within one family of synapses.

These findings beg the question of what synaptic parameters determine functional differences between synaptic contacts. In order to address this question Stevens around 1997, and more recently Nusser in 2012, have used electron-micrographs of hippocampal active zones and postsynaptic densities. They showed differences in

size and shape between active zones (Figure 10A); furthermore, by the implementation of 3D modeling algorithms both groups were able to count vesicles close to the active zone membrane that were considered primed, determining the docking sites number. This analysis led to several interesting conclusions: first, that the size and shape of the active zone, the area of the postsynaptic density, the number of docking sites per AZ, and the size of the reserve of non-docked vesicles all vary greatly from synapse to synapse; secondly and importantly, that there is a tight relationship between the active zone size and the number of docked vesicles (Figure 10B; Schikorski & Stevens, 1997; Holderith et al., 2012).

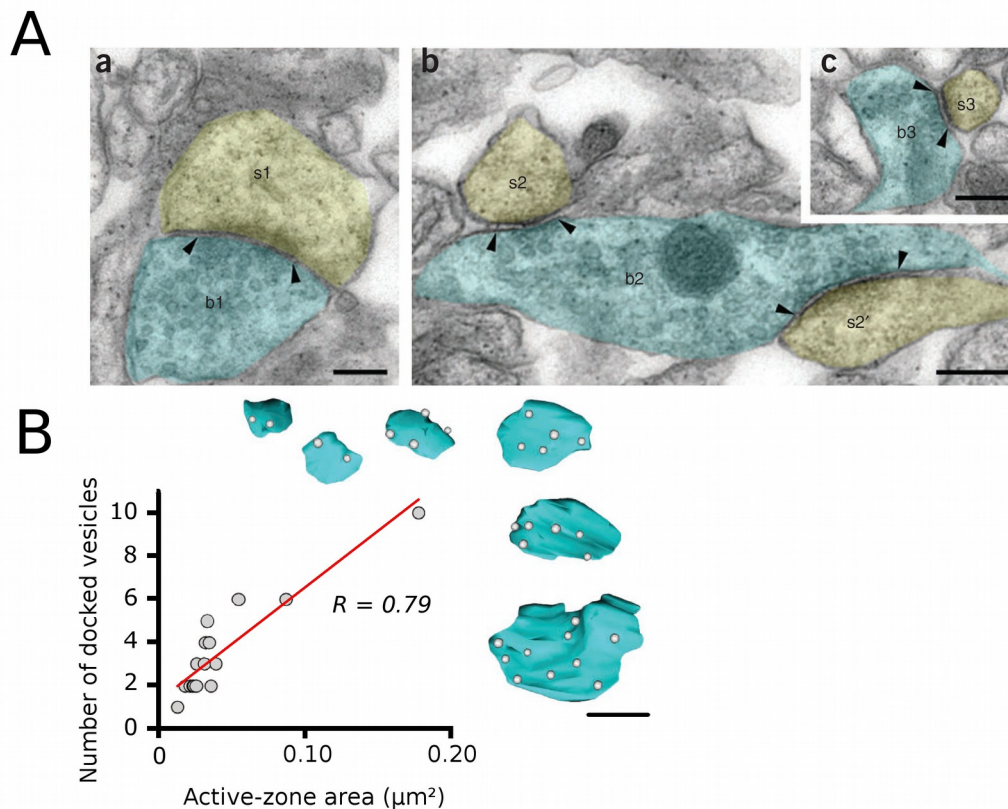


Figure 10. The number of docked vesicles correlates linearly with active zone size. (A) Electron micrographs show the morphological diversity of glutamatergic terminals (blue) and their corresponding postsynaptic spines (yellow) in the CA3 region of the hippocampus. Terminals differ in their size, active zone area (arrowheads) and the size of the postsynaptic spines. Active zone area has the same length as the corresponding PSD. (B) 3D modeling was used to reconstruct each active zone (blue), and to identify and count docked vesicles (white spheres). The number of docked vesicles was plotted against the active zone area, revealing a positive correlation. (A) and (B) Scale bar 0.2 μ m, adapted from (Holderith et al., 2012).

Trigo et al. also showed that the number of docking sites varies between synaptic contacts and is correlated with the quantal size (Figure 8F; Trigo et al., 2012), which indirectly reflects an increase in size of the active zone and the postsynaptic density, which explains the heterogeneity between synaptic contacts at interneurons.

In summary, synaptic contacts can differ between synapses or even within the same family. Differences are observed in the output of noise fluctuation analysis, and by morphological evidence, and the results suggest a correlation between the synaptic size and the different synaptic parameters (review: Branco & Staras, 2009). An interesting factor related to the synaptic contact heterogeneity is the number of vesicles that are docked in a given active zone, which are increasing in parallel with active zone size. Those vesicles are docked in specialized sites, made up from specific protein families that are constantly adjusting to allow the vesicle priming and subsequent release. The number of docking sites is tentatively considered as fixed in a given active zone, but this number can vary from one synaptic contact to another, resulting in different rates of release during sustained synaptic activity.

METHODS

Along this work I have been studying cerebellar interneurons connected by a single synaptic contact, called “simple synapse”, as previously described by Kondo & Marty (1998). Particular care was devoted to prepare cerebellar slices under the best possible conditions in order to approach physiological conditions. Pairs of healthy interneurons located in sagittal slices were recorded under whole-cell clamp, and tested for synaptic connectivity.

Posterior analysis of the synaptic responses included amplitude distribution, kinetics, charge, probabilities of responses, providing a direct description of simple synaptic connections. Based on an analysis of failure probability, the number of docking sites was finally estimated together with key synaptic parameters (docking site occupancy, release probability and recovery rate).

The following section contains a detailed description of the experimental procedures, and a brief description of the detection analysis of evoked IPSCs. The model proposed to estimate the number of docking sites in single synaptic contacts is explained in detail in the published paper shown in results section, and is not repeated here.

Chapter 1: Cerebellar Slices Preparation

1.1 Slices of young rat

Cerebellar slices were prepared following well established procedures used in the laboratory (Llano et al., 1991). Young Sprague-Dawley rats (12-16 days old) were used because neuronal connections are still developing and the probability to get pairs connected by single synaptic contact is greatly influenced by the age of the experimental animal (Kondo & Marty, 1998). Rats were killed by decapitation under anesthesia with isoflurane. The vermis was dissected by a careful section, performed parallel to the sagittal plane to avoid damaging neuronal processes. It was placed some minutes in cold bicarbonate-buffered saline (BBS; see composition below), to slow down possible metabolic degradation by deeply cooling the brain tissue. The meninges still attached to the surface, were removed under the microscope to minimize subsequent damage during slicing.

The tissue was subsequently glued to the stage of a vibroslicer and sagittally sliced with a thickness of 200 μ m. The slicer chamber solution was always kept cold ($\sim 4^{\circ}\text{C}$) and oxygenated. The slices were transferred and incubated in a vessel with BBS saline bubbled with 95% O_2 and 5% CO_2 at 34°C . This gas mixture allows first, the exchange of O_2 and CO_2 with the tissue; second CO_2 keeps the solution pH at 7.4. Slices were incubated during at least one hour to recover them from thermal shock which decreases their metabolic activity. Thereafter, slices were held at room temperature during 15min prior to the beginning of experimental recordings.

1.2 Slices of adult rat

A critical limitation in the development of the living acute brain slice preparation has been the difficulty in preparing slices from adult and aging animals. Cerebellar slices are particularly fragile and unless special measures are taken, often only Purkinje cells are more or less good enough to be patched. This unfavorable effect is well known, even though its explanation is still uncertain. In the literature many special

procedures are proposed to prepare brain slices for adult animals, varying: cutting solution, cutting temperature and mode of killing animals (Ting et al., 2014; Blot & Barbour, 2014). Each has its advantages and I have tried different combinations as explained next.

Rats between 30-35PN were considered as adult animals. The procedure was exactly the same as in young rat, except for cutting solution and cutting temperature. In some cases, the whole procedure was done at physiological temperature (~34°C): solutions and vibroslicer were kept at that temperature. In other trials temperature was kept at 4°C. At both cutting temperatures, three different solutions were interdependently tried: normal BBS, NMDG based solution (Ting et al., 2014) and potassium gluconate based solution (Blot & Barbour, 2014). In these “protective cutting solutions” sodium and calcium are replaced, with the premise that decreased sodium influx reduces the slice synaptic activity and subsequent water entry, preventing cells from swelling.

1.3 Cutting solutions.

| | <u>BBS</u> | <u>NMDG Sol.</u> | <u>K-Gluconate Sol.</u> |
|--------------------------------------|-------------------|-------------------------|--------------------------------|
| NaCl | 130 mM | – | – |
| NMDG | – | 92 mM | – |
| Na-ascorbate | – | 5 mM | – |
| Na-pyruvate | – | 3 mM | – |
| KCl | 2.5 mM | 2.5 mM | 15 mM |
| Potassium Gluconate | – | – | 130 mM |
| NaHCO₃ | 26 mM | 30 mM | – |
| NaH₂PO₄ | 1.3 mM | 1.25 mM | – |
| HEPES | – | 20 mM | 20 mM |
| CaCl₂ | 2 mM | 0.5 mM | – |
| MgCl₂ | 1 mM | 10 mM | – |
| Glucose | 10 mM | 25 mM | 25mM |
| Thiourea | – | 2 mM | – |

Chapter 2: Recording Procedures

2.1 Recording set up.

The incubated slice was placed in a perfusion chamber and held stable with a harp. The recording chamber was mounted in an Axio Examiner D1-Zeiss microscope, which was itself mounted on an independent XY movement. This chamber was continuously perfused with oxygenated BBS solution, which in most experiments was maintained at room temperature. However, a series of experiments were performed at near-physiological temperature (34-35°C) using a temperature feedback system. The preparation was observed that upright microscope equipped with a Nomarski prism and a 63x water immersion objective with a numeric aperture of 0.9, and a working distance of 1.4mm.

Micropipettes were positioned on the cell membrane by 'XYZ' motorized micro-manipulators, controlled manually by a remote interface (Luigs & Neumann, Germany). The probability to find connections with single synaptic contact is on the order of 10%. Because this probability is low I used triple recordings from MLIs using a triple EPC-10 amplifier (Heka, Lambrecht, Germany). I first established 3 cell-attached recordings from 3 neighboring MLIs, broke quickly into whole-cell recording, and tested the 6 possible connections. In this manner I got 6 possible connections with 3 recordings -a ratio of 2:1. By comparison for 2 simultaneous recordings, I could check 2 connections, a ratio 1. Thus using the triple set-up increased 2-fold my rate of success. The amplifier was controlled by Patch Master computer interface (Heka Elektronik, Germany) that allows setting all parameters for cellular recording and stimulation.

2.2 Interneuron selection

The two types of cerebellar interneurons, basket and stellate, were chosen indifferently. The cells were selected and identified according to the following criteria: (1) Morphological: including soma diameters exceeding 6µm, significantly larger than

that of migrating granule cells; avoiding superficial cells which processes likely were damaged. (2) Electrical activity: In the molecular layer, only basket and stellate cells show a significant number of spontaneous synaptic currents and large voltage-dependent inward currents.

2.3 Electrophysiology

Micropipettes were made from borosilicate tube glass, pulled twice. After filling them with a saline solution that resembles the intracellular content, the resistance was 4-5 M Ω . Membrane sealing procedure was controlled by continuous generation of a depolarizing pulse of 5ms at -10mV. The same pulse was also used to measure and compensate pipette capacitance, membrane capacitance and series resistance, along the whole experiment.

Series resistances were 50% compensated, with values generally around 15M Ω . Cells which had a series resistance larger than 30M Ω were discarded.

2.4 Paired MLI recordings

Usually three tentative interneurons were chosen and their membrane potential held under whole cell clamp configuration (Hamill et al., 1981), using a holding potential of -60mV. Cells were recorded using a high Cl⁻ internal solution to optimize the size of PSCs, GABA was included in this solution to prevent emptying of the synaptic vesicles and consequent PSC rundown (Bouhours et al., 2011). Its composition is as follows (in mM): 145 KCl, 4.6 MgCl₂, 0.1 EGTA, 10 HEPES-K, 0.4 Na-GTP, 4 Na₂ATP, 10 GABA; pH 7.4; osmolarity: 300 mosm. In some experiments the EGTA concentration was increased to 2mM in order to provide a better-defined basal calcium concentration.

Having a pair of synaptically connected MLIs, the next question was whether the connection involved a single synaptic contact. The first criterion to identify single synaptic contacts was a low variance for the peak amplitudes of postsynaptic responses. A final identification of single site connection was made after the experiment, during the analysis stage. During experiments, connected cells presenting an obvious variability in their IPSCs were discarded. A new selection of interneurons was then performed. Sometimes one of the initial cells was kept and

another neighboring interneuron was tested.

Cells that displayed low IPSCs amplitude variability were subjected to cycles of thirty sweeps of a train stimulation consisting of 5 pulses at 25Hz, with 10 seconds of recovery between sweeps. In some cases, trains of stimulation at 50Hz were also applied.

Chapter 3: Spontaneous Events Detection.

Spontaneous events from single site connected interneurons were recorded during periods of 9 seconds. Spontaneous synaptic currents originating from the postsynaptic cell were recorded, while the presynaptic cell was held at -80, -50 or -60mV. Immediately after the presynaptic prepulse, the holding potential was returned to -60mV and a train of 5 pulses at 25Hz was applied. IPSCs were recorded. Finally the presynaptic was leaved for another 9 seconds at -60mV to recover the basal conditions. 30 repetitions of this cycle were performed.

The spontaneous postsynaptic currents (sPSCs) were detected using the Igor plug-in 'TaroTools' by setting a threshold of -10pA which was at the limit of the background noise. All detected events were subjected to a kinetic analysis; those with decay kinetics faster than 20ms were discarded, as they were plausibly glutamatergic events. The remaining events were checked individually. The number of sPSCs counted per trial was normalized against the mean of sPSCs obtained at each prepulse potential.

Chapter 4: Monte Carlo Simulations

We implemented 2 stochastic synaptic release models based on Monte Carlo simulations. In each model the synapse is subjected to 30 trains of 5 spikes with inter-spike interval of 25Hz (Igor Pro, WaveMetrics, Inc., USA). In the first model, we

Monte Carlo simulations

assumed 1 docking site, which was occupied by synaptic vesicles with a probability of δ before 1st stimulating pulse. When a vesicle is present at the site, release occurs with a probability of p . After releasing, replenishment of the docking site occurs stochastically with a constant rate R .

In a second model, a replacement site is assumed to precede the docking site. Occupancy probability of the replacement site, ρ , is iterated from 0 to 1 before starting the first stimulating pulse. After consumption of the vesicle, replenishment of the replacement site occurs stochastically with a recovery probability s . The docking site is replenished only by a vesicle coming directly from the replacement site, with a net probability r that depends on ρ and a certain probability of refilling r' . Just as in the first model, when a vesicle is present at the docking site, release occurs with a probability of p . Using these binary variables we can compute the average release and we evaluate the influence of presynaptic parameters on synaptic transmission.

RESULTS

Chapter 1: Vesicular Release Statistics And Unitary Postsynaptic Current At Single GABAergic Synapses

Typical central synapses of the mammalian brain are complex structures where the building block is a single synaptic site, comprising a presynaptic active zone and its associated postsynaptic density. Much of the present knowledge on the functioning of synapses is derived from the work of Bernard Katz at the neuromuscular junction. But the neuromuscular junction is a giant synapse comprising many synaptic sites, and it remains unclear how each synaptic site releases its neurotransmitter. In particular Bernard Katz has speculated that each synaptic site may display one or several docking sites, where synaptic vesicles would have to bind prior to exocytosis. However today, much uncertainty remains concerning the nature, number, and indeed the very existence, of docking sites within one synaptic site.

The amplitude distribution of the miniature synaptic currents at the neuromuscular junction follows a single Gaussian curve, whereas in the central nervous system (CNS), neurons present a skewed amplitude distribution. In mammalian brain synapses, this amplitude variability probably originates in variations in the number of postsynaptic receptors among synaptic contacts. To address further aspects of inter-synaptic variability, it is necessary to record synaptic currents coming from a single synaptic contact.

The mammalian Molecular Layer Interneurons (MLIs) of the cerebellar cortex, generate spontaneous unitary synaptic currents (sIPSCs) with large mean amplitudes, distributed over a wide range. When comparing amplitude distributions of

sPSCs in control and in the presence of tetrodotoxin, very similar mean values are found. This implies that synapses between these interneurons involve a small number of release sites, each of them associated with a large unitary current (Llano & Gerschenfeld, 1993). It is therefore likely that at least some of these interneurons synapses involve a single synaptic contact, making them a suitable model to study synaptic fluctuations at a single synaptic contact.

When two cerebellar interneurons are connected by one synaptic site, the amplitude distribution of evoked IPSCs follows a single Gaussian curve. Additionally, as postsynaptic receptors are close to saturation, the current increments for closely succeeding events display smaller amplitudes, reflecting multivesicular release (Auger et al., 1998).

In the present thesis paired recordings involving single site MLI-MLI synapses are performed, with the purpose of examining the responses to trains of presynaptic action potentials. With this approach we assess the hypothesis that vesicular release at a single synaptic contact involves one or several docking sites. The results obtained and presented below, shed light on new aspects of synaptic transmission which have largely escaped experimental or theoretical investigation so far.

Vesicular Release Statistics and Unitary Postsynaptic Current at Single GABAergic Synapses

Camila Pulido,¹ Federico F. Trigo,¹ Isabel Llano,¹ and Alain Marty^{1,*}

¹Laboratoire de Physiologie Cérébrale, CNRS UMR 8118, Université Paris Descartes, 45 rue des Saints Pères, 75006 Paris, France

*Correspondence: alain.marty@parisdescartes.fr

<http://dx.doi.org/10.1016/j.neuron.2014.12.006>

SUMMARY

The existence of vesicular docking sites in central synapses is supported by morphological and biochemical evidence, but their functional role remains elusive. To investigate this role we have studied single depressing GABAergic synapses where multivesicular release and postsynaptic receptor saturation have been documented. We used failure/success patterns to estimate the number of vesicular docking sites, which varied from one to six among synapses. Variations of docking site numbers account for differences in release probability, as well as in the amplitude and decay kinetics of unitary postsynaptic currents. Upon repetitive stimulation, decreasing docking site occupancy likewise accounts for changes both in presynaptic and postsynaptic parameters. Finally steady-state docking site occupancy during train stimulations can be modulated by applying subthreshold presynaptic conditioning potential steps. The results suggest that differences in docking site numbers determine intersynaptic variability and that docking site occupancy is a key parameter controlling single synapse signaling.

INTRODUCTION

Central mammalian synapses differ markedly in terms of quantal size, release probability, and short-term synaptic plasticity. Even within one family of synapses, where both presynaptic and postsynaptic partners belong to single classes of neurons, very heterogeneous synaptic parameters have been reported (review: Branco and Staras, 2009).

Perhaps the most basic of these parameters is size. Individual synapses vary in size on a scale spanning one order of magnitude or more; the surface area of the presynaptic active zone, that of the postsynaptic density, the number of postsynaptic receptors, and the number of synaptic vesicles all increase in parallel with synaptic size (Harris and Stevens, 1988; Schikorski and Stevens, 1997; Nusser et al., 1997). Recently, it was shown that the number of presynaptic calcium channels at individual active

zones, as well as the corresponding release probability, increase with active zone size at the calyx of Held (where individual active zones can be investigated with local patch clamping) (Sheng et al., 2012) and at hippocampal glutamatergic synapses (where “optical quantal analysis” can be implemented) (Holderith et al., 2012). Likewise, release probability and synaptic size are correlated in cultured hippocampal neurons (Ermolyuk et al., 2012).

While these studies shed light on variations in vesicular release at single active zones, surprisingly little is known on corresponding variations at the next step of synaptic transmission: postsynaptic current (PSC). Yet the relation between transmitter release and PSCs can be complex, particularly at synapses displaying multivesicular release and/or saturation of postsynaptic receptors. A promising preparation to address these issues is offered by molecular layer interneurons (MLIs) of cerebellar slices, because a sizable fraction of MLI-MLI synapses appears to involve a single synaptic contact, with a single presynaptic active zone and a single postsynaptic density (Nusser et al., 1997; Kondo and Marty, 1998). Like other GABAergic and glycinergic synapses (Biró et al., 2006; Balakrishnan et al., 2009), MLI-MLI synapses display multiple vesicular release events in response to one action potential (AP), but because extensive postsynaptic receptor saturation occurs following vesicular release, the peak PSC amplitude histogram at individual synaptic contacts forms a single Gaussian (Kondo and Marty, 1998; Auger et al., 1998). Previous work showed that quantal size varies markedly among single synapses and that it grows with the size of the postsynaptic density and of the associated number of receptors (Nusser et al., 1997; Auger and Marty, 1997; Kondo and Marty, 1998). Whether other aspects of synaptic transmission, including release probability, the extent of multivesicular release, and short-term synaptic plasticity, also depend on synaptic size remains to be investigated.

A related question concerns possible interactions between multivesicular release and short-term synaptic plasticity in a single synapse. It is widely accepted that synaptic vesicle availability plays a key role in synaptic depression, but it is not known whether the processes of multivesicular release and synaptic depression interact with each other and, if they do, what the functional consequences of such interactions are.

Such issues touch upon elementary mechanisms of the synapse. In recent years, morphological, biochemical, and functional evidence has accumulated supporting the existence in each synaptic contact of several docking sites (sometimes called “release sites”), which are specific macromolecular structures

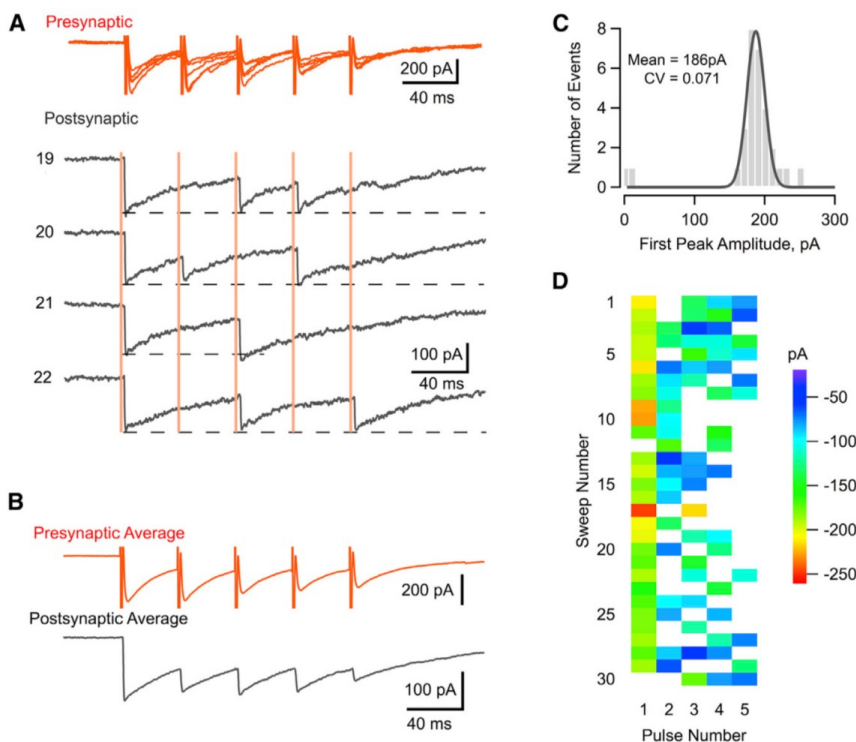


Figure 1. "Simple Synapses" Exhibit Receptor Saturation and Homogeneous PSC Amplitudes

(A) Presynaptic (red superimposed traces, showing autoreceptor currents) and postsynaptic responses (black individual traces; trace numbers correspond to sweep numbers in [D]) to trains of presynaptic APs (five pulses at 25 Hz; timing indicated by vertical pink lines) in a synaptically connected pair of MLIs. PSC peak amplitude increments (measured from the value observed just before each stimulus) are reduced within the train compared to the values for the first stimulus, but the absolute PSC peak values are almost constant within a train (dotted lines), indicating saturation of postsynaptic receptors.

(B) Average presynaptic and PSCs (30 consecutive trials), showing synaptic depression in both cases.

(C) Histogram of first peak PSC amplitudes; single Gaussian fit with low CV are diagnostic of a single synaptic site, called "simple synapse." Success rate: 93%. The position of the histogram peak gives μ , the mean amplitude of successful events ($= 186$ pA).

(D) Pattern of success/response sequences and associated peak PSC amplitudes for a series of 30 consecutive trials. Failures are depicted in white.

where vesicles must bind before undergoing exocytosis (Nagwney et al., 2009; Szule et al., 2012; reviews: Zucker et al., 2009; Neher, 2010). Variations in docking site occupancy are thought to drive short-term synaptic plasticity (Neher and Sakaba, 2008). However, inferences on the functional role of docking sites mostly originates from multisite synapses. Performing such studies at single synapses, as in the present work, has the potential to provide a more direct test of docking site function.

Recent results using local calcium uncaging indicate that in MLIs, each synaptic contact contains a fixed number of docking sites, which varies from one to four between contacts (Trigo et al., 2012). Here we investigate the influence of the number and occupancy of docking sites on synaptic signals. We first estimate the number of docking sites in individual experiments, based on failure statistics. We then show that variations of docking sites number explain signaling differences between individual synaptic contacts. These differences involve not only release probability and short-term synaptic plasticity but also PSC unitary amplitude and decay kinetics. Moreover, in individual experiments, variations in docking site occupancy during AP trains account for observed changes in failure frequency, peak amplitude, and decay kinetics of PSCs. Altogether the number and occupancy of docking sites emerge as key parameters governing unitary synaptic function.

RESULTS

Simple Synapses Display Decreasing Release Probability during Trains

In the present work, we study failure/success sequences in single synapses following trains of presynaptic APs. PSCs were

measured in functionally connected pairs of MLIs from juvenile rats. Each cell was under voltage clamp. The pipette solution contained a high concentration of Cl^- (140 mM) to maximize PSC amplitudes measured at the holding potential (-60 mV). A significant fraction of the synaptic connections between MLIs, called "simple synapses," involve single synaptic contacts (Llano and Gerschenfeld, 1993; Kondo and Marty, 1998). Our first aim was to characterize responses of simple synapses to train stimulations.

A representative recording is shown in Figure 1. Here, 30 trains of five pulses each were given at 25 Hz, with 5 s intervals between trains (ensuring a large degree of recovery between trains: Sakaba, 2008). In response to presynaptic voltage pulses, large autoreceptors/autaptic currents were recorded, reflecting the sensitivity of the presynaptic cell to the neurotransmitter that it releases (Figure 1A, red traces) (Pouzat and Marty, 1998; 1999). On the postsynaptic side, PSCs obtained in response to the first pulse displayed homogeneous amplitudes (Figure 1A, black traces), and the corresponding amplitude histogram could be fitted with a single Gaussian with a small CV (0.071; Figure 1C), indicating a simple synapse. The mean peak amplitude, called simple synapse current hereafter (symbol: i), has a value of 186 pA, in accordance with the large quantal sizes observed at MLI synapses (Llano and Gerschenfeld, 1993; Nusser et al., 1997; Auger et al., 1998). When two PSCs overlapped within a train, the second PSC had a smaller incremental amplitude than the first (Figures 1A and 1D), yet the absolute peak PSC amplitude remained approximately constant (dashed lines in Figure 1A), indicating saturation of postsynaptic receptors (Auger and Marty, 1997; Auger et al., 1998). Mean responses, both presynaptic and postsynaptic, displayed synaptic depression within

a train (Figure 1B). This reflected not only receptor saturation but also a decrease in release probability. Thus, in the example shown (Figure 1D), the probability of success was 93% for the first pulse, 63% for the second, and an average of 51% for the third to fifth pulses.

To investigate possible mechanisms underlying synaptic fluctuations, we first compared peak amplitudes of autoreceptor/autaptic currents and of PSCs across trials, finding no correlation (Figure S1 available online). Because the two sorts of signals are elicited by the same presynaptic AP, these results indicate that trial-to-trial changes in the AP waveform and associated calcium entry do not influence PSC fluctuations significantly.

At the juvenile calyx of Held, Ca^{2+} /calmodulin-dependent inactivation of presynaptic calcium channels elicits a significant decrease in release probability during repetitive stimulation (Xu and Wu, 2005). To examine whether a similar effect occurs in MLIs, we introduced the calcium-sensitive dye Oregon green 488 BAPTA-6F (100–200 μM) in the pipette solution, and we used two-photon imaging in single varicosities to analyze calcium concentration changes following one or two axonal APs (40 ms intervals, corresponding to the interspike interval used in the majority of the present experiments). The calcium responses to the first and second AP were identical (mean amplitude ratio: 0.99 ± 0.06 , $n = 6$; Figure S2). This indicates that synaptic depression occurs downstream of calcium entry.

“Temperature plots” of PSC amplitudes as a function of pulse number and sweep number (Figure 1D) give a visual characterization of functional properties of a simple synapse. As we shall now document, these properties varied markedly across experiments, and the differences followed certain patterns that give clues on the nature of underlying mechanisms.

Heterogeneity among Simple Synapses

A serial electron microscopy section study has shown that most MLI-MLI varicosities involve a single synaptic contact, that synaptic contacts vary markedly in size and in number of postsynaptic receptors, and that the number of postsynaptic receptors varies in register with synaptic size (Nusser et al., 1997). Variations between postsynaptic receptors numbers underlie the marked quantal size heterogeneity observed between simple synapses (Auger and Marty, 1997; Nusser et al., 1997). In our simple synapse recordings, i values varied across experiments from 36 to 221 pA, with a mean of 100 pA; these values are similar to those previously reported (Kondo and Marty, 1998). We next searched for correlations between i , taken as indicator of synaptic size, and other functional parameters of simple synapses.

While Figure 1 illustrates a case where a large value of i is combined with high success probability (defined as the probability to release at least one vesicle), Figure 2 exemplifies an experiment with low i ($i = 61$ pA in Figure 2C versus 186 pA in Figure 1C) and moderate success probability (54% for the first pulse responses in Figure 2D versus 93% in Figure 1). Strikingly, in spite of the relatively low success rate, the paired pulse ratio (PPR) is lower in the case of Figure 2 (with a value of 0.25; Figures 2B and 2D) compared to that of Figure 1 (with a value of 0.68; Figures 1B and 1D). Also, it may be noted that the half time of PSC decay, $t_{1/2}$, is smaller for the experiment of Figure 2 than for that of Figure 1 ($t_{1/2} = 9.9$ ms and 39.5 ms respectively).

Group results show a gradual dependence of the success probability in response to the first pulse, $P(S_1)$, as a function of i (Figure 2E; $r = 0.63$; $p < 0.0001$). The regression line indicates a change from a success rate of ~ 0.4 for the smallest synapses, with i values near 50 pA, to almost 1 for the largest ones, with i values near 200 pA. These results are in line with recent work in glutamatergic synapses suggesting a link between synaptic size and release probability (Ermolyuk et al., 2012; Holderith et al., 2012; Sheng et al., 2012).

It has been suggested that this scaling of the release probability with size results from a larger number of voltage-dependent calcium channels contributing to exocytosis in larger synapses, leading to an enhancement of spike-evoked calcium transients at the site of exocytosis (Holderith et al., 2012; Sheng et al., 2012). Here, volume-averaged peak AP-induced calcium transients did not increase with the size of presynaptic varicosities (Figure S3). In addition, the evolution of success probability during trains was not consistent with an increase of local spike-evoked calcium transients with synaptic size. If this were the case, the amount of synaptic depression would be expected to decrease with synaptic size, as found before (Sheng et al., 2012). In the present case, however, the ratio between the success rate calculated for the last three pulses, $P(S_{3-5})$, to the success rate obtained for the first pulse, $P(S_1)$, failed to decrease with i (Figure 2F). (This ratio varies in parallel to the standard PPR calculated as the ratio $P(S_2)/P(S_1)$, and it is preferred here to the PPR because it is calculated from a larger number of trials, and it is therefore statistically more robust.) These data are not consistent with the proposal that local calcium signals increase with synaptic size.

We therefore considered alternative mechanisms to explain the links between simple synapse current amplitude, release probability, synaptic depression, and PSC decay kinetics. Based on calcium photolysis experiments, it has been suggested that simple synapses contain variable numbers of docking sites and that larger synapses have a more numerous complement of docking sites than smaller ones (Trigo et al., 2012) (Figure 2G). If this is the case, release statistics of large synapses may differ from those of small synapses because they have a larger number of docking sites, rather than a larger number of calcium channels driving exocytosis. Below we explore this possibility.

Modeling Synapse Heterogeneity with Varying Numbers of Docking Sites

Release statistics for a simple synapse containing N equivalent docking sites are described in Experimental Procedures. Each docking site undergoes a cycle starting from an occupied state, followed by exocytosis and docking of a new synaptic vesicle. We call p the probability of an occupied docking site to undergo exocytosis and R the rate constant of recovery to the docked state after exocytosis. Both p and R are assumed constant within a train. Each docking site has a probability δ of being occupied by a release-ready vesicle at rest, so that the average size of the readily releasable pool (RRP) is $n = N \delta$. Making $j = 1$ in Equation 5 below gives

$$P(S_1) = 1 - (1 - \delta p)^N. \quad (1)$$

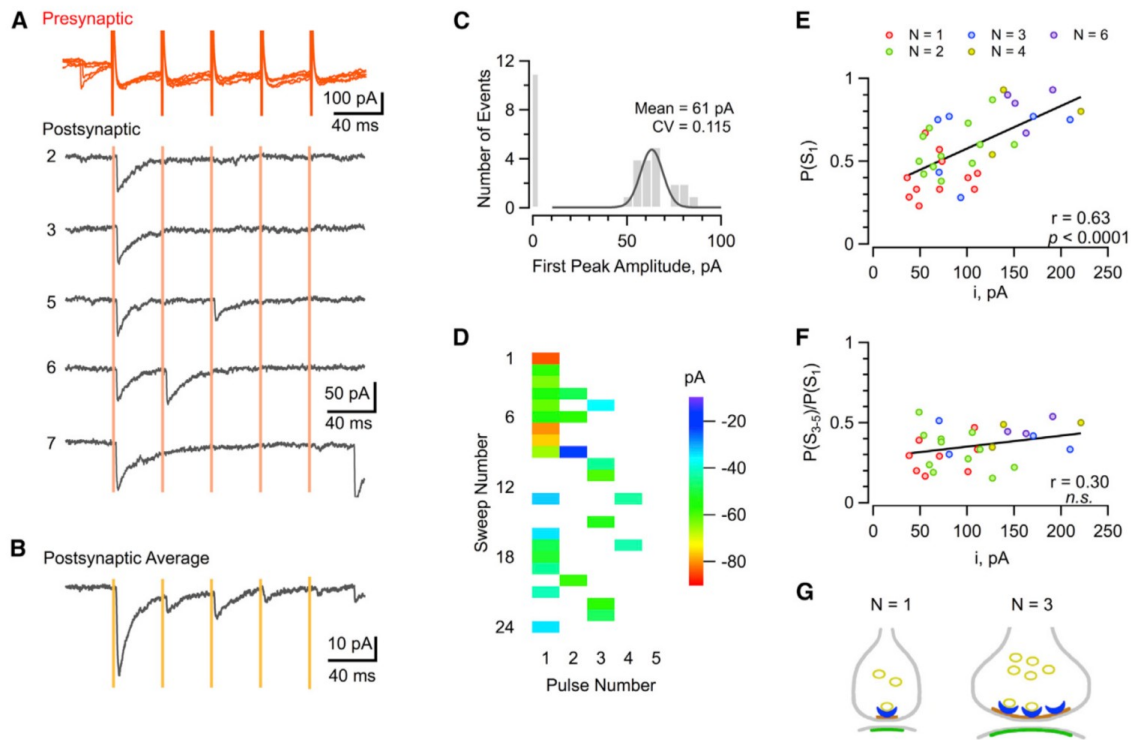


Figure 2. Functional Variability among Simple Synapses

(A) Sample responses (red: presynaptic; black: postsynaptic; trace numbers correspond to sweep numbers in [D]) to AP trains in a presumed single docking site synapse, called “elementary synapse.” Note lower PSC amplitude and lower release probability compared to the example of Figure 1, where the number of docking sites was estimated as 6.
 (B) Average PSCs from the same experiment showing very pronounced synaptic depression (PPR = 0.25) in spite of the moderate release probability ($P(S_1) = 0.67$).
 (C) Histogram of first peak PSC amplitudes ($i = 61$ pA).
 (D) Pattern of success/response sequences and associated peak PSC amplitudes for a series of 24 consecutive trials.
 (E) Summary results from 33 simple synapses showing a positive correlation between i and the corresponding probability of success, $P(S_1)$. This indicates a link between the size of simple synapses and the probability of success.
 (F) $P(S_{3-5})/P(S_1)$ as a function of i , where $P(S_{3-5})$ represents the success rate measured for stimuli 3–5, fails to show a negative correlation. This argues against release statistics being governed by a scaling of release probability with synaptic size.
 (G) Schematic model of a small and of a large simple synapse (active zone in brown and postsynaptic density in green), with respective values of 1 and 3 for N , the number of docking sites (in blue). In (E) and (F), each dot is colored according to the value of N (calculated as explained in Experimental Procedures) that is assigned to the corresponding experiment.

This is an increasing function of N , in agreement with Figure 2E, provided that δ and p are constant. This reflects the fact that $P(S_1)$ includes the contributions of each docking site, and hence increases with N .

In response to the second pulse, the probability of success is as follows:

$$P(S_2) = 1 - (1 - \delta_2 p)^N, \quad (2)$$

where δ_2 is the docking site occupancy just before the second stimulation. δ_2 is smaller than δ for a depressing synapse (Experimental Procedures), and in these conditions it may be shown that the ratio $PPR = P(S_2)/P(S_1)$ is an increasing function of N . Indeed, depression is maximally strong for $N = 1$, because once the single docking site is empty, no other site can replace it. With increasing N values, there is an increasing likelihood that other docking sites may be filled before the second pulse,

and therefore the PPR increases. Overall, the model predicts that both $P(S_1)$ and the PPR grow as a function of N .

As shown in Experimental Procedures (Equation 11), N can be calculated by using an approximate relation derived for the RRP size (n) under the assumption of no recovery ($R = 0$): $n = \log(1 - P(S_1)) / \log(\log(1 - P(S_2)) / \log(1 - P(S_1)))$.

Having calculated n from this equation, N can be obtained using the relation $N = n/\delta$. As a first approximation, we assumed that δ was 0.7, based on previous calcium photolysis data (Trigo et al., 2012), and N was taken as the integer closest to the value $n/0.7$. Values of N obtained with this method ranged from 1 to 4 (i.e., in the same range that was previously obtained with calcium photolysis experiments) (Trigo et al., 2012). These provisional N estimates were then revised as explained in Experimental Procedures. The final assignments, with a range going from 1 to 6, are illustrated by color coding in Figures 2E and 2F. Figures 1 and

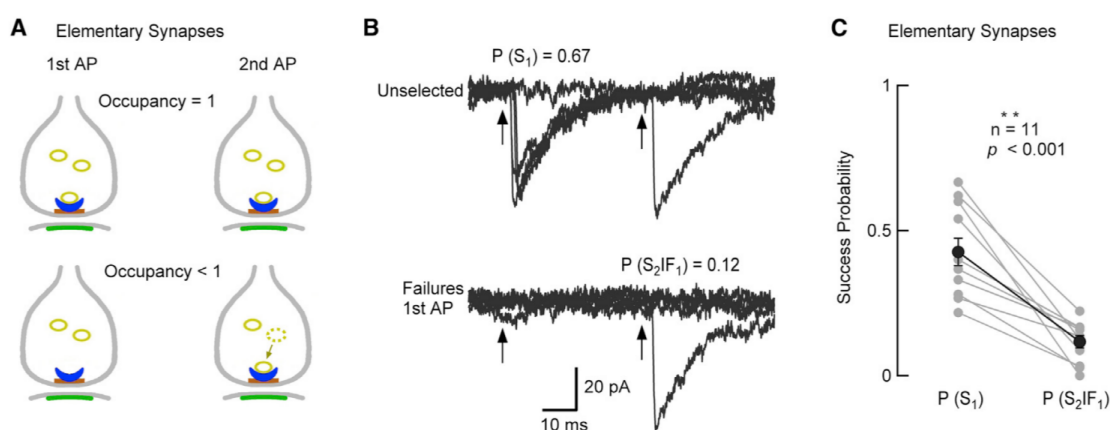


Figure 3. Release Statistics in Elementary Synapses Indicate Incomplete Docking Site Occupancy

(A) Principle of the analysis. In an elementary synapse where the docking site occupancy is 1, failure does not change the status of the synapse; hence, the probability of success for a second AP following a failure, noted $P(S_2|F_1)$, is the same as the original probability of success, noted $P(S_1)$. If on the other hand the docking site occupancy is less than 1, then some failures correspond to occupancy failure, in which case success for a second AP is unlikely because it requires previous refilling of the docking site.

(B) Representative traces from an elementary synapse. Upper panel: Unselected traces, showing a high release probability for the first AP: $P(S_1) = 0.67$. Lower panel: Selected traces showing failures for the first AP. The conditional probability of success for the second AP given that there was a failure for the first one, $P(S_2|F_1)$, is much lower than $P(S_1)$: $P(S_2|F_1) = 0.12$. Presynaptic stimulations marked with arrows.

(C) Summary results from several elementary synapses. In each experiment (gray dots) $P(S_2|F_1)$ is lower than $P(S_1)$. Average values (black dots; mean \pm SEM) are, respectively, 0.117 ± 0.021 and 0.426 ± 0.047 ($p < 0.001$; $n = 11$).

2A–2D, respectively, exemplify the cases $N = 6$ and $N = 1$. Cells with identical N values cluster together in the plots of Figures 2E and 2F. The mean value of N in these experiments was 2.5, close to the value of 2.0 previously obtained in calcium photolysis experiments (Trigo et al., 2012).

The Resting Occupancy of Docking Sites Is Less than 1

Docking site occupancy at rest is tainted with uncertainty as methods to measure this parameter have been lacking. In view of this information gap, it has often been postulated for simplicity that $\delta = 1$. At the calyx of Held δ is estimated at 0.8 or higher (Neher, 2010). This issue can be addressed by considering simple synapses with $N = 1$, which we called “elementary synapses” (Figure 2). In these synapses, we examined the conditional probability of success in response to the second pulse given that there is a failure for the first pulse, noted $P(S_2|F_1)$. The rationale to focus on this parameter is as follows. Failures represent either an occupied site that fails to release or an empty site. If $\delta = 1$, all failures belong to the first category. In this case, the site remains occupied after an initial failure, so that the second pulse has still a probability p to elicit release. This is the same probability as that applying for the first pulse (Figure 3A, upper panel). If, however, $\delta < 1$, some of the failures are due to the docking site being empty. Following this class of failure, release is less likely for a second pulse as docking site refilling is slow (Figure 3A, lower panel; see statistical analysis in Experimental Procedures). Therefore if $\delta = 1$, $P(S_1)$ and $P(S_2|F_1)$ should be identical, but if $\delta < 1$, $P(S_2|F_1)$ should be less than $P(S_1)$. Experimental results support the latter possibility. Thus, in the elementary synapse recording of Figure 3B, whereas $P(S_1)$ is 0.67, $P(S_2|F_1)$ is 0.12. In all elementary synapse recordings it was found that $P(S_2|F_1)$ was smaller than $P(S_1)$ (Figure 3C; $p < 0.001$), showing that as

a rule, docking site occupancy is less than 1 under resting conditions. (A similar discrepancy is found in experiments with $N > 1$, but the difference is less marked, and the interpretation of the effect is less direct.)

An approximate calculation of p and δ starting from $P(S_1)$ and $P(S_2|F_1)$ yields estimates of 0.84 and 0.51, respectively (Experimental Procedures). These values are very compatible with those obtained with more complete calculations as discussed next.

Simulation of Simple Synapse Release Statistics

Once N is determined (starting from $P(S_1)$ and $P(S_2)$, see above), the other model parameters (p , δ , and R) can be calculated as described in Experimental Procedures. The results fail to reveal significant differences linked to the stimulation frequency, which was varied between 25 Hz and 50 Hz (Figure S4). When group results are displayed as a function of N , no significant correlation emerges (Figure S4).

Given the homogeneity of model parameters across experiments ($n = 33$), a simulation of simple synapse release statistics was performed with a single set of parameters, close to the average values obtained from Figure S4: $p = 0.89$, $\delta = 0.45$, and $R = 3.0 \text{ s}^{-1}$. In each docking site, the mean occupancy decreases with stimulation number, from 0.45 before pulse nb. 1, to 0.164 before pulse nb. 2, 0.136 before pulse nb. 3, and 0.133 before both pulse nb. 4 and pulse nb. 5. Release/failure statistics are then obtained by combining together those of each docking site, depending on the value of N . The simulations predict larger initial success rate, and less depression, for large N values than for small N values (Figure 4A). Although $P(S)$ varies widely across experiments, results of individual experiments are close to the simulation obtained with the relevant N value (Figure 4A).

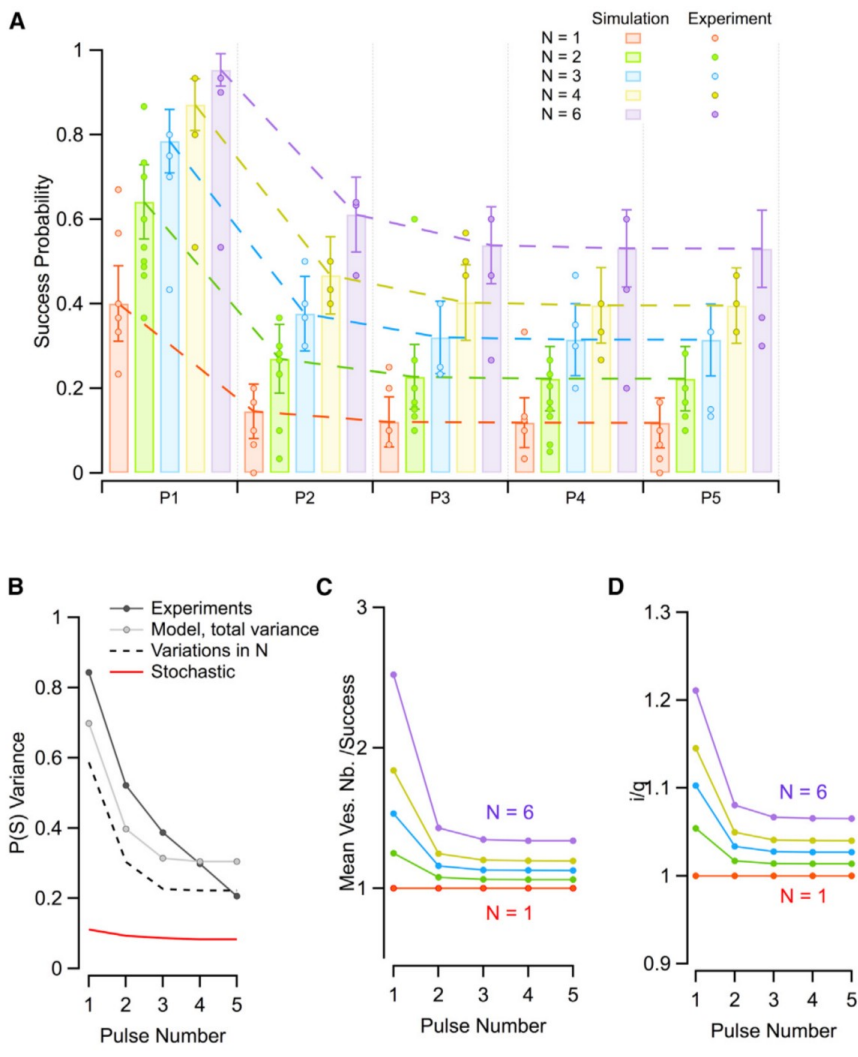


Figure 4. Simulation of Simple Synapse Statistics for Various Docking Site Numbers

(A) Experimental data (circles) and model simulations (bar histograms; error bars represent \pm the SD expected from binomial statistics given the data size), depicted P(S) as a function of stimulus number (interstimulus interval: 40 ms). Model parameters are $p = 0.89$, $\delta = 0.45$, and $R = 3 \text{ s}^{-1}$. As N increases from 1 to 6, release probability increases, and synaptic depression decreases.

(B) Comparison between estimated and observed variance of P(S) among experiments. The variance calculated from the simulations of (A) using the pattern of N values experimentally observed (dashed line) was added with the variance expected from the finite size of the data sample (red line, calculated on the basis of binomial statistics) to simulate a series of experiments with no variation in p , δ , or R (gray dots). This total variance was comparable to the observed variance (black dots), indicating little variations of p , δ , or R among synapses.

(C) Simulation of mean number of released vesicles per successful response (see [Experimental Procedures](#)). This number varies from 1 for elementary synapses to 2.5 for the first stimulus in N = 6 synapses.

(D) Normalized peak PSC amplitude as a function of pulse number and docking site number. The peak PSC estimated at a simple synapse, i , was normalized by division with the quantal amplitude (q : the peak amplitude reflecting a single vesicular release). This ratio was estimated from the results of (C) assuming a value of 0.76 for the peak receptor occupancy following one vesicular release event (see [Experimental Procedures](#)). For elementary synapses the ratio is 1; however, it is larger than 1 for $N > 1$ synapses because saturation of postsynaptic receptors is incomplete. In the simulation shown, the i/q ratio reaches a maximum of 1.21 for the first pulse response with N = 6.

Figure 4B displays the predicted interexperiment variance of the success probability calculated on the basis of differences in N (dashed black line) and the stochastic variance associated with the finite number of trials that were used in each experiment (red line). The sum of these two components (gray line and dots in Figure 4B) accounts for a large fraction (80% or more) of the observed variance (black line and dots in Figure 4B; $n = 33$). These results suggest that the primary source of heterogeneity among simple synapses lies in differences in the docking site number. The residual difference between experimental and modeled variances reflects variations in the release parameters p , δ , and R among synaptic sites. These variations appear small, in contrast with the situation found in culture (Ermolyuk et al., 2012).

Variations of PSC Peak Amplitude and Decay Kinetics with Pulse Number

So far we have treated PSCs as a binary process without attempting to disambiguate the number of vesicular release events contributing to each successful response. However, previous

work at simple synapses has revealed that responses involving larger numbers of released vesicles have larger peak amplitudes and slower decays than those with smaller vesicle numbers (Kondo and Marty, 1998). This suggests that during a train, mean values for PSC peak amplitude and decay duration should vary with pulse number. Specifically, multivesicular release is predicted to occur mostly for the first pulse, so that the peak amplitude and half time of decay should decrease as a function of pulse number. In addition, these variations should not occur if $N = 1$, because multivesicular release never happens in this case. Verifying these predictions represents a stringent test of the validity of our experimental and theoretical approaches.

We used the same model as above to describe the mean number of released vesicles per successful trial during a train (Figure 4C). This number decreases within a train following docking site occupancy. However, it also depends on N, with a maximum for the first pulse response near 2.5 in N = 6 synapses and near 1.2 in N = 2 synapses. Starting from these numbers, we simulated the modification of PSC amplitudes during trains. Due to multivesicular release and partial receptor saturation, the peak

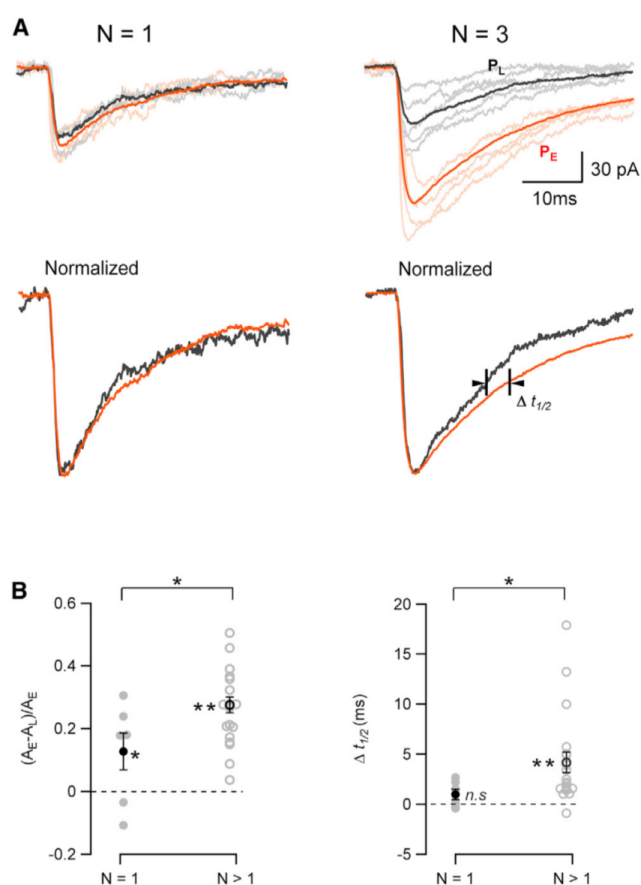


Figure 5. Variations of PSC Peak Amplitude and Decay Kinetics in Simple Synapses

(A) Data from two experiments, one with $N = 1$ (left) and the other with $N = 3$ (right). In each experiment, sweeps were selected where one early event was followed by a late event with an interval of ≥ 80 ms, and early and late events were aligned and superimposed (pink and gray traces respectively). Averages (from 30 trials) were collected for such pairs of early events (labeled P_E , in red) and late events (labeled P_L , in black). Upper panels: Peak amplitudes are larger for P_E than for P_L in the case $N = 3$ but are similar in the case $N = 1$. Lower panels: After normalization, decay kinetics appear slower for P_E than for P_L in the case $N = 3$, but kinetics are very similar in the case $N = 1$.

(B) Summary data from 11 elementary synapse experiments ($N = 1$) and 17 additional simple synapse experiments with $N > 1$. Left: Peak amplitude differences between early and late PSCs as a function of N . In each experiment the mean difference between early and late amplitudes was normalized with respect to the early event amplitude. This difference was significantly larger for $N > 1$ experiments (gray circles and associated black mean; $p < 0.05$). It is interpreted as reflecting an increased degree of receptor activation for the first stimulation following multivesicular release in the $N > 1$ experiments. Note that $N = 1$ experiments yield a significant difference in peak amplitudes between early and late PSCs ($p < 0.05$), even though this difference is markedly larger in the case $N > 1$ (where $p < 10^{-6}$). The origin of this effect is investigated in Figure S4. Right: Half decay time differences between late and early PSCs, as a function of N . Again, a significant difference between early and late events was found in $N > 1$ experiments (gray circles and black mean; $p < 0.0002$). By contrast, no difference was found in elementary synapses (gray dots and black mean; $p > 0.05$). $\Delta t_{1/2}$ values are significantly larger for $N > 1$ synapses than for $N = 1$ synapses ($p < 0.05$). The results indicate that PSC amplitude and decay duration increase with multivesicular release and, furthermore, that multivesicular release

PSC amplitude, i , is on average larger than the quantal size q . We calculated the i/q ratio by combining the results of Figure 4C with a previous estimate for the percentage of receptor occupancy at the peak of one quantal event (0.76; Auger et al., 1998). The results predict a maximum i/q ratio of 1.21 for $N = 6$ and of 1.05 for $N = 2$ (Figure 4D).

A potential difficulty of this analysis is overlap between successive responses, which could produce nonlinear PSC additivity and obscure some of the expected effects. For this reason, we only analyzed sequences obtained with low stimulation frequency (25 Hz), and we restricted the analysis to sequences that included at least one failure before a late event. In this way, we produced pairs of early and late events separated by at least 80 ms, thus minimizing overlap between paired responses. For experiments where the value of N had been estimated as 1 (elementary synapses, shown in the left column of Figure 5A), amplitude and decay time were similar for early stimulations (red traces) and for late traces (black). By contrast, in $N > 1$ experiments, early responses displayed larger amplitudes and slower decays than late responses (right column of Figure 5A).

Group results reveal that after normalization with respect to the first event amplitude, the relative difference between early and late PSC amplitudes is significantly larger for $N > 1$ experiments than for $N = 1$ experiments (respective mean values: 0.263 ± 0.026 , $n = 20$, and 0.126 ± 0.060 , $n = 6$; $p < 0.05$; Figure 5B, left). Likewise differences in $t_{1/2}$ values between early and late events are significantly larger for $N > 1$ experiments than for $N = 1$ experiments (respective mean values: 4.07 ± 1.03 ms, $n = 20$, and 0.99 ± 0.54 ms, $n = 6$; $p < 0.01$; Figure 5B, right). These results indicate that both amplitude and kinetic effects are related to a differential mean number of vesicles released per successful event.

An alternative mechanism that could lead to a lengthening of PSC decay is spillover from adjacent synapses (Balakrishnan et al., 2009). While signs of spillover were obtained in a minority of the present recordings (Figure S5), two lines of evidence argue against spillover accounting for $t_{1/2}$ changes during trains. First, spillover does not explain differences in $t_{1/2}$ results between $N > 1$ and $N = 1$ synapses, whereas multivesicular release does. Second, it is possible to correct PSC traces for spillover based on the analysis of failures (Figure S5). Results in Figure 5 were corrected in this manner, showing that spillover is insufficient to account for the observed $t_{1/2}$ changes.

Modulation of PSC Amplitude by Receptor Saturation/Desensitization during Trains

Differences between early and late $t_{1/2}$ values, as quoted above, were not significant for elementary synapses ($p > 0.05$), consistent with the notion that no multivesicular release occurs in such cases. Early PSC amplitudes were, however, significantly larger than late PSC amplitudes in elementary synapses ($p < 0.05$). To investigate the origin of this effect we performed GABA uncaging experiments using the fast caged GABA, DPNI-GABA (Trigo

decreases as a function of stimulus number for $N > 1$ experiments, but not in $N = 1$ experiments.

Error bars represent \pm SEM.

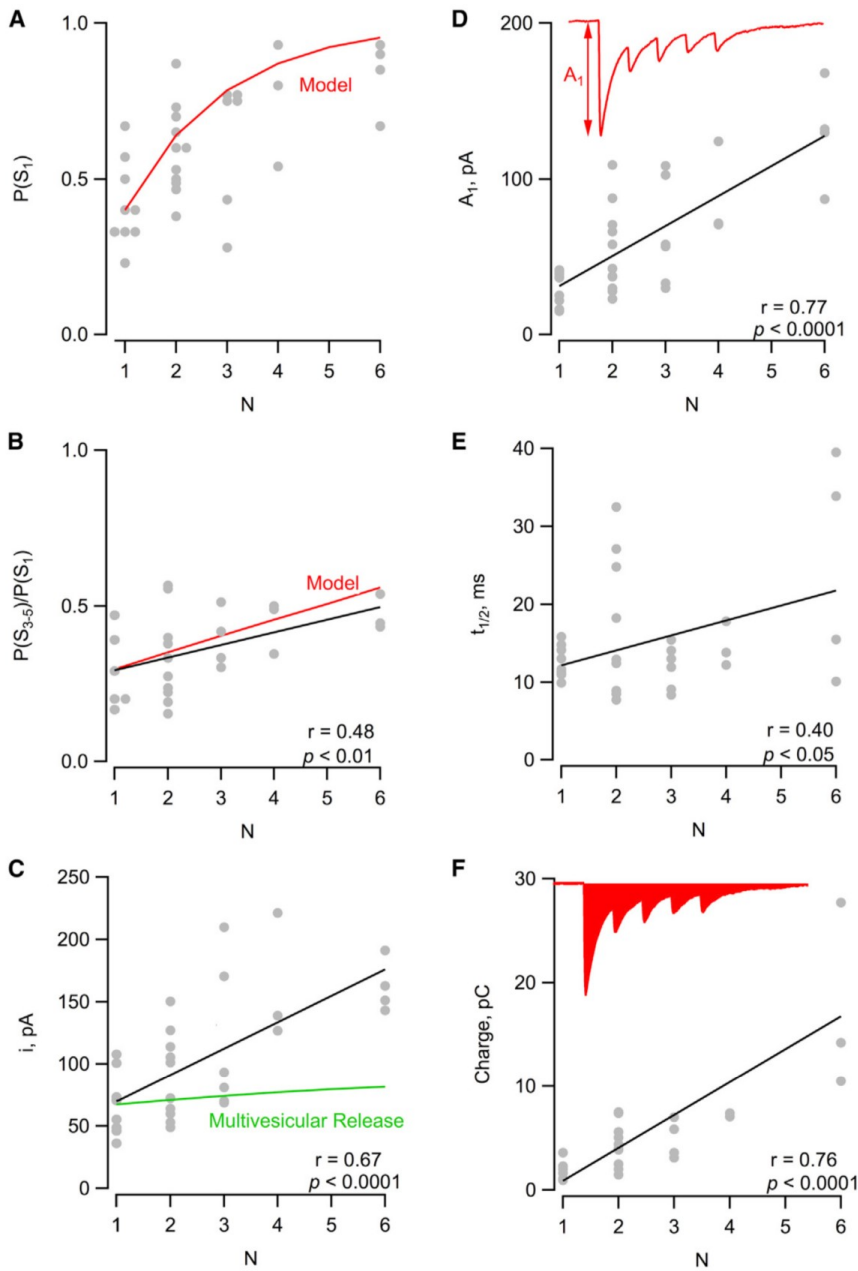


Figure 6. Dependence of Simple Synapse Parameters on Docking Site Number

(A) Dependence of $P(S_1)$ on N (gray circles: experiments; red: model predictions with $p = 0.89$, $\delta = 0.45$, and $R = 3 \text{ s}^{-1}$). (B) Dependence of $P(S_{3-5})/P(S_1)$ on N (circles: experiments; red: model predictions; black: regression line). (C) Plot of i as a function of N . The data show a strong positive correlation, suggesting that synapses with small N values are smaller than synapses with large N values (black: regression line). To assess the participation of multivesicular release in the overall dependence of peak PSC amplitude on N , a normalized plot of the predicted i/q ratio as a function of N is shown (green line, from Figure 4D). This curve displays a shallow dependence on N , implying that quantal size, rather than the number of released vesicles, is the major factor underlying variations of i with N . (D) Mean peak PSC amplitude for the first stimulus (including failures) as a function of N (black: regression line). (E) Half time of PSC decay (calculated for first responses within a train) as a function of N (black: regression line). (F) PSC integral during a five-pulse train as a function of N (black: regression line).

residual amplitude effect seen for elementary synapses in Figure 5B.

In conclusion, the results of Figure 5, together with the control experiments of Figures S5 and S6, indicate that multivesicular release shapes PSC amplitudes and decay kinetics during trains and that these effects depend on N values. These results are in agreement with the model of Figure 4 and demonstrate the predictive power of a description of synaptic function based on several docking sites.

Simple Synapse PSCs as a Function of N

Simulations and experimental results describing simple-synapse parameters

et al., 2009). Local uncaging of DPNI-GABA at single varicosities is able to mimic synaptic currents accurately (Trigo et al., 2009). Two consecutive identical stimulations were applied. At intervals of 10 ms, the second stimulation gave a current response that was $56\% \pm 10\%$ of the first ($n = 6$), consistent with partial saturation of the receptors (Figure S6A). At intervals of 80 or 100 ms, the second response had recovered much of the initial amplitude, but recovery was incomplete, with a ratio between late and early responses of 0.77 ± 0.05 at 80 ms ($n = 10$) and 0.81 ± 0.04 at 100 ms ($n = 11$) (Figure S6B). These results indicate that repeated stimulation at such intervals results in a reduction of the response amplitude by about 20%. This accounts for the

are presented in Figure 6 where results from each experiment ($n = 21-33$) are plotted as a function of the N value that is assigned to it. Both simulated (red curve, from the model of Figure 4) and experimental (circles) values of $P(S_1)$ increase steeply between $N = 1$ and $N = 2$ and saturate for N values of 3 or higher (Figure 6A). $P(S_{3-5})/P(S_1)$ values grow moderately but significantly as a function of N (Figure 6B; black: regression line, $p < 0.01$). The model of Figure 4 (red line in Figure 6B) is close to the regression line, showing that variations in docking site numbers account for the paradoxical changes of synaptic depression with synaptic size illustrated in Figure 2F.

In the same way that i is determined by the size of the postsynaptic density, N is likely determined by the size of the active zone. The correspondence between presynaptic and postsynaptic aspects of the synapse therefore suggests that i and N are correlated. When i was plotted as a function of N , a highly significant correlation was indeed revealed ($p < 0.0001$; Figure 6C). This is a remarkable result since the procedure to determine the value of N entirely rests on an analysis of failure patterns and does not consider PSC amplitudes. Equally noteworthy is the size of the effect: the regression line indicates an increase over a 2.4-fold range from $N = 1$ to $N = 6$. Because receptor saturation limits the augmentation of PSC amplitude that could result from multivesicular release, this large ratio cannot just reflect increased PSC summation with N (simulation: green curve in Figure 6C). The bulk of the effect of N on i therefore reflects changes in the number of postsynaptic receptors, and consequently of the quantum q , as a function of N .

As N increases, a number of parameters are altered, all contributing to producing an increase in synaptic strength. Since both the probability of success (Figure 6A) and the amplitude of successful events (Figure 6C) increase, the mean peak PSC amplitude (including failures) is expected to increase steeply with N due to a combination of these two effects: this is indeed the case (Figure 6D). The regression line ($p < 0.00001$) indicates an increase in the peak amplitude for the first pulse from 30 pA for $N = 1$ to 129 pA for $N = 6$, a ratio of 4.2-fold. Two additional effects contribute to increase synaptic strength during a train. First, the results of Figure 6B indicate that synaptic depression decreases as N increases. Second, the lengthening of PSC decay with multivesicular release (Figure 5) suggests that $t_{1/2}$ may increase as N increases. The examples of Figure 1 (with $N = 6$, showing slowly decaying PSCs) and Figure 2 (with $N = 1$, showing faster decaying PSCs) support this possibility. In line with these expectations, when $t_{1/2}$ for the first pulse in a train was plotted as a function of N , a positive correlation was found, indicating that differences in N exert a significant effect on PSC kinetics (Figure 6E; $p < 0.05$; the regression line indicates a 1.8-fold larger $t_{1/2}$ decay value for $N = 6$ than for $N = 1$). Finally, to examine the overall effect of N on synaptic transmission, we plotted the synaptic charge corresponding to the integral of the mean PSC elicited by a 25 Hz train, finding a very steep relationship to N (Figure 6F). The regression line ($p < 0.0001$) indicates a mean charge increase from 1.2 pC for $N = 1$ to 15.5 pC for $N = 6$, a ratio of 13-fold. Thus, the weight of synaptic signals varies over a very large range for simple synapses, and the value of N stands as the major determinant of this variability.

Changes in Synaptic Properties Induced by Presynaptic Depolarization

The above analysis suggests that the number of docking sites determines intersynaptic variability and that in a given experiment changes in docking sites occupancy account for synaptic depression. We next asked whether it is possible to modulate docking site occupancy by another experimental manipulation.

In MLIs, subthreshold somatic depolarization increases axonal calcium concentration and spontaneous vesicular release (Glitsch and Marty, 1999; Bouhours et al., 2011; Christie

et al., 2011). Consequences on subsequent evoked release involve either an increase or no significant change of the release probability and, in both cases, a drop of the paired-pulse ratio (Bouhours et al., 2011; Christie et al., 2011). Here we examined the patterns of success/failures during trains, interleaving tests at the standard holding potential of -60 mV with tests following 9-s-long prepulses at -80 mV or at -50 mV (Figure 7A). In all experiments, presynaptic traces were examined during depolarizing prepulses, and recordings were discontinued if APs were apparent, indicating voltage-clamp escape. We found in agreement to previous data a decrease with depolarizing prepulses for both the PPR (at -80 mV: 0.64 ± 0.08 ; at -60 mV: 0.31 ± 0.08 ; at -50 mV: 0.17 ± 0.04 ; $n = 9$; effects of hyper- and depolarizing prepulses are significant at $p < 0.01$ and $p < 0.05$ levels respectively) and for the ratio $P(S_{3-5})/P(S_1)$ (values normalized with respect to -60 mV data: 1.311 ± 0.152 at -80 mV, $p < 0.05$; 0.737 ± 0.060 at -50 mV, $p < 0.00001$; Figure 7B, lower panel), while the value of $P(S_1)$ did not vary significantly (Figure 7B, upper panel). Assuming that the N value estimated at -60 mV was not modified by prepulses, we compared estimates of p , δ and R obtained at -60 mV with corresponding values with prepulses at -80 mV and at -50 mV. The results revealed a small decrease of p with hyperpolarizing prepulses (with a mean ratio between -80 mV and -60 mV values of 0.955 ± 0.019 , $p < 0.02$; Figure 7C, upper panel), no significant change of p with depolarizing prepulses, and no significant change in δ with either hyperpolarizing or depolarizing prepulses (Figure 7C, middle panel). Surprisingly, the recovery rate R was markedly affected by prepulses, particularly in the depolarizing direction, with highly significant variations with respect to control (values normalized to -60 mV data: 1.328 ± 0.121 at -80 mV, $p < 0.01$; 0.710 ± 0.078 at -50 mV, $p < 0.0002$; Figure 7C, lower panel). This indicates that a reduction in R is the major reason for the reduced PPR value and for the decreased release probability found at the end of a train after depolarization. It is well established that an elevation of the presynaptic calcium concentration during trains accelerates vesicular replenishment (Neher and Sakaba, 2008). The present results indicate that an elevation of the calcium concentration prior to a train has the opposite effect, perhaps due to enhanced spontaneous release and to an associated decrease in the content of a reserve pool supplying vesicle replenishment. This mechanism (Figure 7D) is in line with the previous finding that the frequency of spontaneous PSCs increases during depolarizing prepulses (Glitsch and Marty, 1999; Christie et al., 2011), which was confirmed in the present experiments (respective values at -60 mV and -50 mV: 0.299 ± 0.098 and 0.365 ± 0.131 Hz; $p < 0.001$, $n = 5$).

Overall, the results suggest that p is modestly sensitive to the prepulse potential, presumably because it is close to saturation, and that R strongly decreases with depolarization, presumably as a consequence of enhanced spontaneous release. It can be shown using Equation 7 below that in the case $p \sim 1$, the late occupancy in a train is proportional to R . Therefore, the change of R alters late release by decreasing docking site occupancy. In summary, the results suggest that docking site occupancy can be specifically modified during synaptic plasticity.

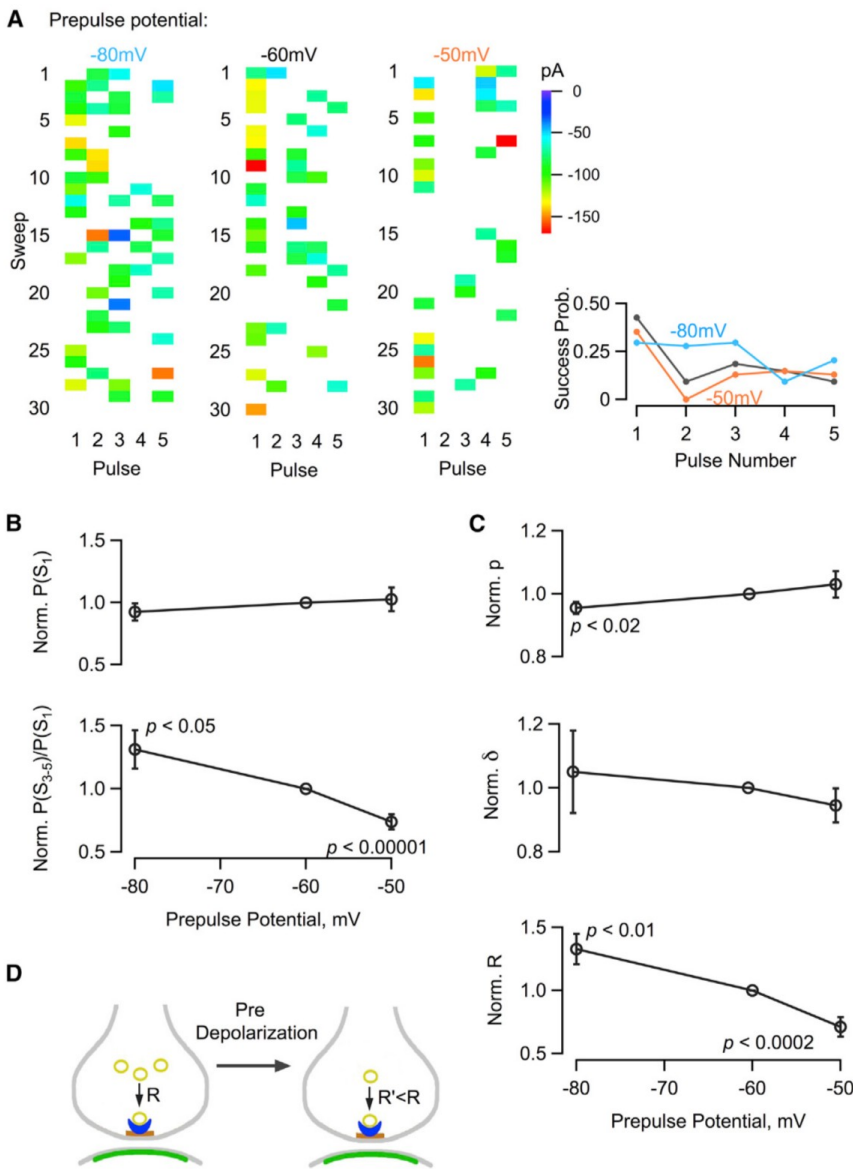


Figure 7. Presynaptic Prepulses Change Vesicular Recruitment Rate

(A) Left: Exemplar experiment showing responses to five-pulse trains delivered from the standard holding potential of -60 mV, preceded by 9-s-long prepulses at -80 mV (left column), at -60 mV (no prepulse; center column), and at -50 mV (right column). The sequence with the three prepulse potentials was repeated as a loop. Right: Plots of $P(S_j)$ for the three potentials, suggesting an increase of synaptic depression with depolarizing prepulses.

(B) Group data ($n = 10$) showing $P(S_1)$ (upper plot) and $P(S_{3-5})/P(S_1)$ (lower plot) as a function of prepulse potential, after normalization to the value at -60 mV.

(C) Normalized calculated values of single site parameters indicate a small decrease of p with hyperpolarizing prepulses (upper panel), no change of δ (middle panel), and a strong decrease of R with depolarizing prepulses (lower panel).

(D) Model of proposed link between the augmentation of spontaneous synaptic activity during depolarizing prepulses, leading to a depletion of reserve vesicles, and the observed decrease in R during subsequent trains.

Error bars represent \pm SEM.

a train. In spite of its simplicity, the model does capture a number of features of the results, including variations of failure rate and multivesicular release during trains, as well as variations among simple synapses.

Variations in Docking Site Numbers Account for Differences between Simple Synapses

The present work suggests that much of the functional variability observed among simple synapses can be accounted for by variations in a single parameter, the number of docking sites N .

Varying N not only accounts for variations of the “presynaptic” parameters, release probability, and paired pulse depression, but also of two major “postsynaptic” parameters: the PSC peak amplitude i and the PSC half decay time $t_{1/2}$. Overall docking site number appears as an integrator of presynaptic and postsynaptic parameters and as a potent organizer of synaptic function.

The relation between i and N uncovered here is very similar to that previously described in the same preparation by Trigo et al. (2012), using a different approach. The close correspondence between the two sets of data would require a highly unlikely coincidence unless the common hypothesis that variable docking site numbers underlie differences among simple synapses is correct. It is well known that the sizes of the active zone and of the postsynaptic density are matched

DISCUSSION

A Stochastic Model for Simple Synapses

The present work describes simple synapse function based on a fixed number of docking sites. At each docking site, exocytosis and vesicle replenishment determine occupancy following single-step transitions. Synaptic release statistics are obtained by combining together those of individual docking sites. Multivesicular release, together with postsynaptic receptor saturation, modulate PSC amplitudes and decay kinetics. As explicated in the Experimental Procedures, the model makes a number of assumptions, some of which remain to be tested. Notably, docking sites are supposed to operate independently of each other; rate constants are assumed to be identical among docking sites within a synapse, as well as across synapses. Furthermore, rate constants are assumed to be constant within

(e.g., Harris and Stevens, 1988; Schikorski and Stevens, 1997). While previous results indicated that the size of the postsynaptic density determines quantal size (Auger and Marty, 1997; Nusser et al., 1997), the present results, together with those of Trigo et al. (2012), suggest that the size of the active zone determines the number of docking sites. Altogether, larger synapses tend to produce larger signals by a series of complementary effects: larger quantum, larger success probability, larger percentage of receptor activation, slower PSC decay kinetics, and less synaptic depression. While the first effect is linked to the number of postsynaptic receptors, all other effects are the consequence of an increased number of docking sites.

It may be noted that in systems (like GABAergic synapses) where receptors are close to saturation, the range of variation of synaptic efficacy would be limited if synaptic size were fixed. In such systems, increasing synaptic size is a particularly efficient way to increase synaptic strength. However, variations in size, receptor numbers, and quantal amplitude also occur at glutamatergic synapses (Harris and Stevens, 1988; Schikorski and Stevens, 1997; Crowley et al., 2007). It remains to be seen whether this is accompanied with changes in the number of docking sites.

In order to minimize the probability of changes of N within an experiment, we kept presynaptic stimulation sparse, and we restricted the duration of data acquisition to 15 min per cell. While our hypothesis of a fixed N value seems justified under these circumstances, the possibility is clearly open that N may change in response to stronger stimuli, or over longer periods of time, and differences in past synaptic activity may contribute to explaining the differences in N values observed among synapses.

A Special Category of Simple Synapses Exhibits a Single Docking Site

An elementary synapse is a simple synapse that has a single docking site ($N = 1$; examples in Figures 2 and 3). It never releases more than one vesicle in response to an AP and therefore obeys the “single-site-single-vesicle” hypothesis (Korn et al., 1982; Silver et al., 2003). This occurred in 27% of our simple synapses (9/33). Elementary synapses are of special interest since their release statistics are particularly simple. This situation is exploited in the present work to investigate the value of docking site occupancy at rest (Figure 3), but many other applications are possible.

Elementary synapses stand out from other simple synapses (with $N > 1$) in several ways. They have a lower success probability ($P(S_1) = 0.417 \pm 0.046$ for $N = 1$ versus 0.662 ± 0.037 for $N > 1$; $n = 9$ and $n = 24$, respectively) and stronger depression ($P(S_{3-5})/P(S_1) = 0.285 \pm 0.050$ for $N = 1$ versus 0.381 ± 0.028 for $N > 1$). Their i value (67.7 ± 8.1 pA versus 116.5 ± 10.4 pA; $p < 0.002$) and $t_{1/2}$ values (12.6 ± 0.6 ms versus 16.2 ± 1.8 ms; $p < 0.02$) are clearly smaller. And finally, they display much weaker changes in amplitudes and decay kinetics of PSCs during trains (Figure 5). The finding of this series of distinctive features of elementary synapses confirms the internal consistency of our analysis and validates the procedure used to estimate N .

Comparison with Previous Models

The classical description of PSC statistics at central synapses involves a fixed quantum q , a release probability p_r , and a number of release units N (Zucker et al., 2009). Here we propose a new variant of this model based on three notions that have been envisaged individually before but have only recently been considered in combination (Trigo et al., 2012): (i) postsynaptic receptor saturation, (ii) presence of several independent docking sites in one active zone, and (iii) partial, time-dependent occupancy of the docking sites.

(i) PSC Amplitude and Decay Kinetics Are Modulated by Postsynaptic Receptor Saturation

At simple MLI synapses, responses appear at first sight to vary in an all-or-none manner, but closer inspection reveals that they vary in size and decay kinetics according to the number of release events. Responses to the first stimulus are larger and slower than later responses. The modulation of the peak amplitude follows the predictions of a model where 76% of the receptors are occupied following one release event. Because receptor activation is not complete following one vesicular release event, multivesicular release increases PSC amplitude according to the number of released vesicles.

Even though the decay kinetics of GABAergic PSCs have long been thought to be largely independent of the amplitude and duration of the GABA pulse in the synaptic cleft, the present data confirms and extends previous evidence (Kondo and Marty, 1998) indicating that multivesicular release modulates PSC decay. GABA_A receptors have two agonist binding sites, and both monoliganded and biliganded receptors contribute to the PSC (Jones and Westbrook, 1995). After removal of the agonist, biliganded receptors must shed one GABA molecule to return to the monoliganded state, from where they relax back to the resting state. It takes therefore longer for biliganded receptors than for monoliganded receptors to return to the basal state. While the extent of the effect depends on kinetic rate constants (Jones and Westbrook, 1995), this suggests that multivesicular release slows PSC decay by favoring the recruitment of biliganded receptors over that of monoliganded receptors.

Receptors at central synapses differ widely in their affinity and decay kinetics. At most GABAergic synapses, vesicular release induces significant receptor occupancy, albeit to different degrees (Auger and Marty, 1997; Nusser et al., 1997; Perrais and Ropert, 1999; Kirischuk et al., 2002; Biró et al., 2006). There is also evidence for a significant degree of receptor occupancy at various types of glutamatergic synapses (climbing fiber synapses onto Purkinje cells: Foster et al., 2002; calyx of Held: Scheuss et al., 2002; parallel fiber input to MLIs: Crowley et al., 2007). Thus, our findings are potentially relevant to both excitatory and inhibitory synapses.

(ii) Within One Simple Synapse, Binomial N Reflects the Number of Docking Sites

The proposal that exocytosis occurs at individual release units can be traced back to Katz (1969), but the nature and very existence of these release units has remained controversial ever since. The strongest functional evidence in favor of release units in central synapses is the fact that fluctuations in synaptic current peak amplitudes decrease at high calcium concentration,

which suggests that the underlying release statistics are binomial rather than Poissonian (e.g., Silver et al., 2003; reviewed in Zucker et al., 2009; Neher, 2010). Previous interpretations of the morphological representation of the number N of release units have varied. According to the single-site-single-vesicle hypothesis, N represents the number of presynaptic varicosities (Korn et al., 1982; Silver et al., 2003). Quantitative studies at the calyx of Held suggest, however, that the number of release competent vesicles is six per active zone and that, therefore, N must be larger than the number of active zones (Neher and Sakaba, 2008). In addition, evidence for multivesicular release has been accumulating at other central glutamatergic (Wadiche and Jahr, 2001; Christie and Jahr, 2006; Crowley et al., 2007) and GABAergic synapses (Biró et al., 2006). These results are difficult to reconcile with the single-site-single-vesicle hypothesis, but they are consistent with the present proposal that N represents the number of docking sites and that several docking sites operate in parallel in one active zone.

(iii) Evidence for Partial Docking Site Occupancy at Rest

Our previous work using calcium uncaging suggested that occupancy of docking sites at rest is less than 1 (Trigo et al., 2012). Two lines of evidence of the present work indicate the same. One is derived from our examination of the conditional probability of release following a failure in elementary synapses (Figure 3). The result that δ is less than 1 can alternatively be derived from modeling the mean frequencies of failures according to the estimated number of docking sites (Figure 4). This finding implies that, at rest, the reaction leading to docking site occupancy is reversible by a mechanism that remains to be elucidated (e.g., reversal of vesicle docking, spontaneous exocytosis, or steric hindrance between docked vesicles). It also implies that the RRP at rest is not fixed. Altogether, synaptic release results from a combination of two stochastic processes, and not of a single process, as commonly assumed: docking site occupancy with probability δ and exocytosis with probability p .

Docking Site Occupancy and Replenishment Rate as Potential Targets of Synaptic Plasticity

The standard description of simple synapses focuses on a single adjustable presynaptic parameter, the release probability p_r (Zucker et al., 2009). In contrast, the present description contains three presynaptic parameters (p , δ , and R), raising the possibility that each of these parameters could be adjusted as a function of specific forms of neuronal activity. The initial release probability is given by a combination of p and δ , whereas late release depends on a combination of p and R . Our results show that applying presynaptic prepulses results in variations of R , leading to changes in docking site occupancy and release probability during the late phase of a train (Figure 7). This demonstrates that docking site replenishment can be modified by previous neuronal activity. It will be interesting in future work to investigate whether manipulations leading to changes in p_r target p , δ , or both. In general, the present description of single site function offers an opportunity to characterize synaptic plasticity in a more specific manner than in previous treatments, thus opening a new path toward underlying cellular mechanisms.

EXPERIMENTAL PROCEDURES

Electrophysiological Recordings

Cerebellar slices were prepared from rats aged PN 12–14. All experiments were performed at room temperature. Recording procedures are detailed in Supplemental Information.

Binomial Model of Simple Synapses

We consider a simple synapse containing N equivalent docking sites. Each docking site has an initial probability δ of being occupied by a release-ready vesicle. An occupied docking site has a probability p to undergo exocytosis, which is assumed to remain constant throughout the train. After exocytosis, the emptied docking site has a probability r to become release competent during one interpulse interval Δt . Assuming a recovery reaction with a single rate constant R , the link between r and R is $r = 1 - e^{-R\Delta t}$. We suppose for simplicity that docking sites are independent of each other and that δ , p , and r are identical across docking sites.

Under the above assumptions, the probability of one docking site to release in response to the j^{th} stimulation is

$$P_D(S_j) = \delta_j p, \quad (3)$$

where δ_j is the docking site occupancy before pulse number j . For $j = 1$, we note $\delta_1 = \delta$.

Because all sites are independent, the probability of having simultaneously a failure at all N sites is

$$P(F_j) = (1 - P_D(S_j))^N = (1 - \delta_j p)^N. \quad (4)$$

Hence, the probability to have at least one vesicular release event in response to pulse number j is

$$P(S_j) = 1 - (1 - \delta_j p)^N. \quad (5)$$

This model can be considered as a probabilistic variant of the previous macroscopic model by Tsodyks and Markram (1997). It assumes that two nested stochastic processes contribute to release statistics, whereas the traditional synaptic model (Equation 9, below) considers a single stochastic process. Here the evolution of $P(S_j)$ during a train is governed by δ_j . For each docking site, the probability of occupancy before pulse $(j + 1)$, δ_{j+1} , is the sum of the probability that an occupied site at pulse j fails to release at pulse j , plus the probability that an occupied site at pulse j releases at pulse j and recovers between pulse j and pulse $(j + 1)$, plus the probability that an unoccupied site at pulse j recovers between pulse j and pulse $(j + 1)$:

$$\delta_{j+1} = \delta_j(1 - p) + \delta_j p r + (1 - \delta_j)r. \quad (6)$$

We note that this equation predicts depression if $\delta > r/r + p(1 - r)$, but that it predicts facilitation if $\delta < r/r + p(1 - r)$. The first inequality applies for any set of (r, p) values if $\delta = 1$, because the ratio $r/r + p(1 - r)$ is less than 1. In general, high values of δ and/or p favor depression, and high values of r favor facilitation. At steady state, $P(S_j)$ reaches a value L , which is independent of j . By entering $P(S_j) = L$ and $\delta_{j+1} = \delta_j$ in Equations 5 and 6, one obtains

$$r = \frac{p\lambda}{p\lambda + p - \lambda}, \quad (7)$$

where $\lambda = 1 - (1 - L)^{1/N}$.

If N is known, Equations 5, 6, and 7 can be used to calculate the unknowns (p , r , and δ) from the measurable parameters $P(S_1)$, $P(S_2)$, and L . The solution for p reads

$$p = \frac{\lambda + 1 + ((\lambda + 1)^2 - 4\lambda B)^{1/2}}{2B} \quad (8)$$

with $B = 1 - P(F_1)^{\frac{1}{N}} - \lambda / (1 - P(F_2)^{\frac{1}{N}} - \lambda)$.

Having calculated p from Equation 8, r can be calculated from Equation 7 and finally δ from Equation 5 with $j = 1$.

Estimating N

To obtain a first estimate for N, we make two simplifying assumptions. First, we assume that the RRP size applying before the first pulse is fixed in one given experiment, with a value $n = \delta N$. Second, we neglect the recovery rate by making $r = 0$. In view of the first assumption, the failure probability after the first pulse takes the previously used form (e.g., Dobrunz and Stevens, 1997; Hanse and Gustafsson, 2001):

$$P(F_1) = (1 - p)^n. \quad (9)$$

This equation follows the predictions of a binomial process with δN units having each a release probability p , whereas in the previous version of the model, we had a binomial process with N units having each a release probability δp . After the first pulse the RRP size drops from the initial value n to the new value $n(1 - p)$. Under the assumption that $r = 0$, and assuming again that the RRP size does not fluctuate around its mean value, we have

$$P(F_2) = (1 - p)^{n(1-p)}. \quad (10)$$

These two equations can be combined to yield

$$n = \frac{\log(1 - P(S_1))}{\log(\log(1 - P(S_2))/\log(1 - P(S_1)))}. \quad (11)$$

Values obtained with Equation (11) ranged between 0 and 3. To obtain N, we assumed that the occupancy δ was close to the value 0.7 previously obtained (Trigo et al., 2012). Therefore, N was initially chosen as the integer closest to the ratio $n/0.7$. Once complete, p , δ , and R calculations were made according to Equations 5, 6, 7, and 8, new N values were estimated due to the fact that the calculated δ value was different from the initial value of 0.7 and, if needed, a new set of calculations was performed in an iterative manner until the value of N became stable. In addition, when the procedure returned the result $N = 1$, indicating an elementary synapse, individual responses were examined to identify potential double vesicular release events. When such responses were found, the experiment was reclassified as $N = 2$ (3 such reclassifications out of 14 experiments that were initially classified as $N = 1$).

For some experiments the calculation led to an apparent value of p that was >1 . Such values were not accepted. Instead, a value $p = 1$ was introduced, and values of δ and R were recalculated according to Equations 5 and 7.

Elementary Synapse Statistics

For elementary synapses $N = 1$.

In this case, Equation 5 applied to the first pulse ($j = 1$) simplifies to

$$P(S_1) = \delta p. \quad (12)$$

The conditional probability to observe a success in response to the second pulse given that a failure was obtained in response to the first pulse is

$$P(S_2|F_1) = \frac{(1 - \delta)r p + \delta(1 - p)p}{1 - \delta p}. \quad (13)$$

Equation 13 indicates that a sequence of failure for the first pulse followed by success for the second pulse can reflect an unoccupied docking site being replenished between the two pulses, and then releasing at the second stimulus, or alternatively an occupied site not releasing during the first stimulus, and releasing during the second one. To understand the implications of this equation it is useful to consider the simplified case where recovery is neglected ($R = r = 0$). Equation 13 then simplifies to

$$P(S_2|F_1) = \frac{\delta p(1 - p)}{1 - \delta p}. \quad (14)$$

By combining with Equation 12, this can be rewritten

$$\frac{P(S_2|F_1)}{P(S_1)} = \frac{(1 - p)}{1 - \delta p}. \quad (15)$$

This ratio is smaller than 1 except for the case $\delta = 1$, where it takes the value of 1.

Solving Equations 12 and 15 given the experimental values $P(S_1) = 0.426$ and $P(S_2|F_1) = 0.117$ gives $p = 0.84$ and $\delta = 0.51$.

SUPPLEMENTAL INFORMATION

Supplemental Information includes six figures and Supplemental Experimental Procedures and can be found with this article online at <http://dx.doi.org/10.1016/j.neuron.2014.12.006>.

ACKNOWLEDGMENTS

This work was supported by a Paris Descartes University PhD fellowship to C.P., a combined CNRS/ Paris Descartes Excellence Chair to F.F.T., and an ERC Advanced grant ("SingleSite") to A.M. We thank Philippe Ascher, Guadalupe Astorga, Jin Bao, David Ogden, and Brandon Stell for comments on the manuscript.

Accepted: November 26, 2014

Published: December 24, 2014

REFERENCES

- Auger, C., and Marty, A. (1997). Heterogeneity of functional synaptic parameters among single release sites. *Neuron* 19, 139–150.
- Auger, C., Kondo, S., and Marty, A. (1998). Multivesicular release at single functional synaptic sites in cerebellar stellate and basket cells. *J. Neurosci.* 18, 4532–4547.
- Balakrishnan, V., Kuo, S.P., Roberts, P.D., and Trussell, L.O. (2009). Slow glycinergic transmission mediated by transmitter pooling. *Nat. Neurosci.* 12, 286–294.
- Biró, A.A., Holderith, N.B., and Nusser, Z. (2006). Release probability-dependent scaling of the postsynaptic responses at single hippocampal GABAergic synapses. *J. Neurosci.* 26, 12487–12496.
- Bouhours, B., Trigo, F.F., and Marty, A. (2011). Somatic depolarization enhances GABA release in cerebellar interneurons via a calcium/protein kinase C pathway. *J. Neurosci.* 31, 5804–5815.
- Branco, T., and Staras, K. (2009). The probability of neurotransmitter release: variability and feedback control at single synapses. *Nat. Rev. Neurosci.* 10, 373–383.
- Christie, J.M., and Jahr, C.E. (2006). Multivesicular release at Schaffer collateral-CA1 hippocampal synapses. *J. Neurosci.* 26, 210–216.
- Christie, J.M., Chiu, D.N., and Jahr, C.E. (2011). Ca^{2+} -dependent enhancement of release by subthreshold somatic depolarization. *Nat. Neurosci.* 14, 62–68.
- Crowley, J.J., Carter, A.G., and Regehr, W.G. (2007). Fast vesicle replenishment and rapid recovery from desensitization at a single synaptic release site. *J. Neurosci.* 27, 5448–5460.
- Dobrunz, L.E., and Stevens, C.F. (1997). Heterogeneity of release probability, facilitation, and depletion at central synapses. *Neuron* 18, 995–1008.
- Ermolyuk, Y.S., Alder, F.G., Henneberger, C., Rusakov, D.A., Kullmann, D.M., and Volynski, K.E. (2012). Independent regulation of basal neurotransmitter release efficacy by variable Ca^{2+} influx and bouton size at small central synapses. *PLoS Biol.* 10, e1001396.
- Foster, K.A., Kreitzer, A.C., and Regehr, W.G. (2002). Interaction of postsynaptic receptor saturation with presynaptic mechanisms produces a reliable synapse. *Neuron* 36, 1115–1126.
- Glitsch, M., and Marty, A. (1999). Presynaptic effects of NMDA in cerebellar Purkinje cells and interneurons. *J. Neurosci.* 19, 511–519.
- Hanse, E., and Gustafsson, B. (2001). Paired-pulse plasticity at the single release site level: an experimental and computational study. *J. Neurosci.* 21, 8362–8369.
- Harris, K.M., and Stevens, J.K. (1988). Dendritic spines of rat cerebellar Purkinje cells: serial electron microscopy with reference to their biophysical characteristics. *J. Neurosci.* 8, 4455–4469.

- Holderith, N., Lorincz, A., Katona, G., Rózsa, B., Kulik, A., Watanabe, M., and Nusser, Z. (2012). Release probability of hippocampal glutamatergic terminals scales with the size of the active zone. *Nat. Neurosci.* *15*, 988–997.
- Jones, M.V., and Westbrook, G.L. (1995). Desensitized states prolong GABA_A channel responses to brief agonist pulses. *Neuron* *15*, 181–191.
- Katz, B. (1969). The release of transmitter substances (The Sherrington Lectures X). (Springfield: Charles C. Thomas Publisher).
- Kirschchuk, S., Clements, J.D., and Grantyn, R. (2002). Presynaptic and postsynaptic mechanisms underlie paired pulse depression at single GABAergic boutons in rat collicular cultures. *J. Physiol.* *543*, 99–116.
- Kondo, S., and Marty, A. (1998). Synaptic currents at individual connections among stellate cells in rat cerebellar slices. *J. Physiol.* *509*, 221–232.
- Korn, H., Mallet, A., Triller, A., and Faber, D.S. (1982). Transmission at a central inhibitory synapse. II. Quantal description of release, with a physical correlate for binomial *n*. *J. Neurophysiol.* *48*, 679–707.
- Llano, I., and Gerschenfeld, H.M. (1993). Inhibitory synaptic currents in stellate cells of rat cerebellar slices. *J. Physiol.* *468*, 177–200.
- Nagwaney, S., Harlow, M.L., Jung, J.H., Szule, J.A., Ress, D., Xu, J., Marshall, R.M., and McMahan, U.J. (2009). Macromolecular connections of active zone material to docked synaptic vesicles and presynaptic membrane at neuromuscular junctions of mouse. *J. Comp. Neurol.* *513*, 457–468.
- Neher, E. (2010). What is rate-limiting during sustained synaptic activity: vesicle supply or the availability of release sites. *Front. Synaptic Neurosci.* *2*, 144.
- Neher, E., and Sakaba, T. (2008). Multiple roles of calcium ions in the regulation of neurotransmitter release. *Neuron* *59*, 861–872.
- Nusser, Z., Cull-Candy, S., and Farrant, M. (1997). Differences in synaptic GABA(A) receptor number underlie variation in GABA mini amplitude. *Neuron* *19*, 697–709.
- Perrais, D., and Ropert, N. (1999). Effect of zolpidem on miniature IPSCs and occupancy of postsynaptic GABA_A receptors in central synapses. *J. Neurosci.* *19*, 578–588.
- Pouzat, C., and Marty, A. (1998). Autaptic inhibitory currents recorded from interneurons in rat cerebellar slices. *J. Physiol.* *509*, 777–783.
- Pouzat, C., and Marty, A. (1999). Somatic recording of GABAergic autoreceptor current in cerebellar stellate and basket cells. *J. Neurosci.* *19*, 1675–1690.
- Sakaba, T. (2008). Two Ca²⁺-dependent steps controlling synaptic vesicle fusion and replenishment at the cerebellar basket cell terminal. *Neuron* *57*, 406–419.
- Scheuss, V., Schneggenburger, R., and Neher, E. (2002). Separation of presynaptic and postsynaptic contributions to depression by covariance analysis of successive EPSCs at the calyx of held synapse. *J. Neurosci.* *22*, 728–739.
- Schikorski, T., and Stevens, C.F. (1997). Quantitative ultrastructural analysis of hippocampal excitatory synapses. *J. Neurosci.* *17*, 5858–5867.
- Sheng, J., He, L., Zheng, H., Xue, L., Luo, F., Shin, W., Sun, T., Kuner, T., Yue, D.T., and Wu, L.-G. (2012). Calcium-channel number critically influences synaptic strength and plasticity at the active zone. *Nat. Neurosci.* *15*, 998–1006.
- Silver, R.A., Lubke, J., Sakmann, B., and Feldmeyer, D. (2003). High-probability unquantal transmission at excitatory synapses in barrel cortex. *Science* *302*, 1981–1984.
- Szule, J.A., Harlow, M.L., Jung, J.H., De-Miguel, F.F., Marshall, R.M., and McMahan, U.J. (2012). Regulation of synaptic vesicle docking by different classes of macromolecules in active zone material. *PLoS ONE* *7*, e33333.
- Trigo, F.F., Papageorgiou, G., Corrie, J.E.T., and Ogden, D. (2009). Laser photolysis of DPNI-GABA, a tool for investigating the properties and distribution of GABA receptors and for silencing neurons *in situ*. *J. Neurosci. Methods* *181*, 159–169.
- Trigo, F.F., Sakaba, T., Ogden, D., and Marty, A. (2012). Readily releasable pool of synaptic vesicles measured at single synaptic contacts. *Proc. Natl. Acad. Sci. USA* *109*, 18138–18143.
- Tsodyks, M.V., and Markram, H. (1997). The neural code between neocortical pyramidal neurons depends on neurotransmitter release probability. *Proc. Natl. Acad. Sci. USA* *94*, 719–723.
- Wadiche, J.I., and Jahr, C.E. (2001). Multivesicular release at climbing fiber-Purkinje cell synapses. *Neuron* *32*, 301–313.
- Xu, J., and Wu, L.-G. (2005). The decrease in the presynaptic calcium current is a major cause of short-term depression at a calyx-type synapse. *Neuron* *46*, 633–645.
- Zucker, R.S., Kullmann, D.M., and Schwarz, T.L. (2009). Release of neurotransmitters. In *From Molecules to Networks*, J.H. Byrne and J.L. Roberts, eds. (Waltham: Academic Press), pp. 217–266.

Neuron, Volume 85

Supplemental Information

Vesicular Release Statistics

and Unitary Postsynaptic Current

at Single GABAergic Synapses

Camila Pulido, Federico F. Trigo, Isabel Llano, and Alain Marty

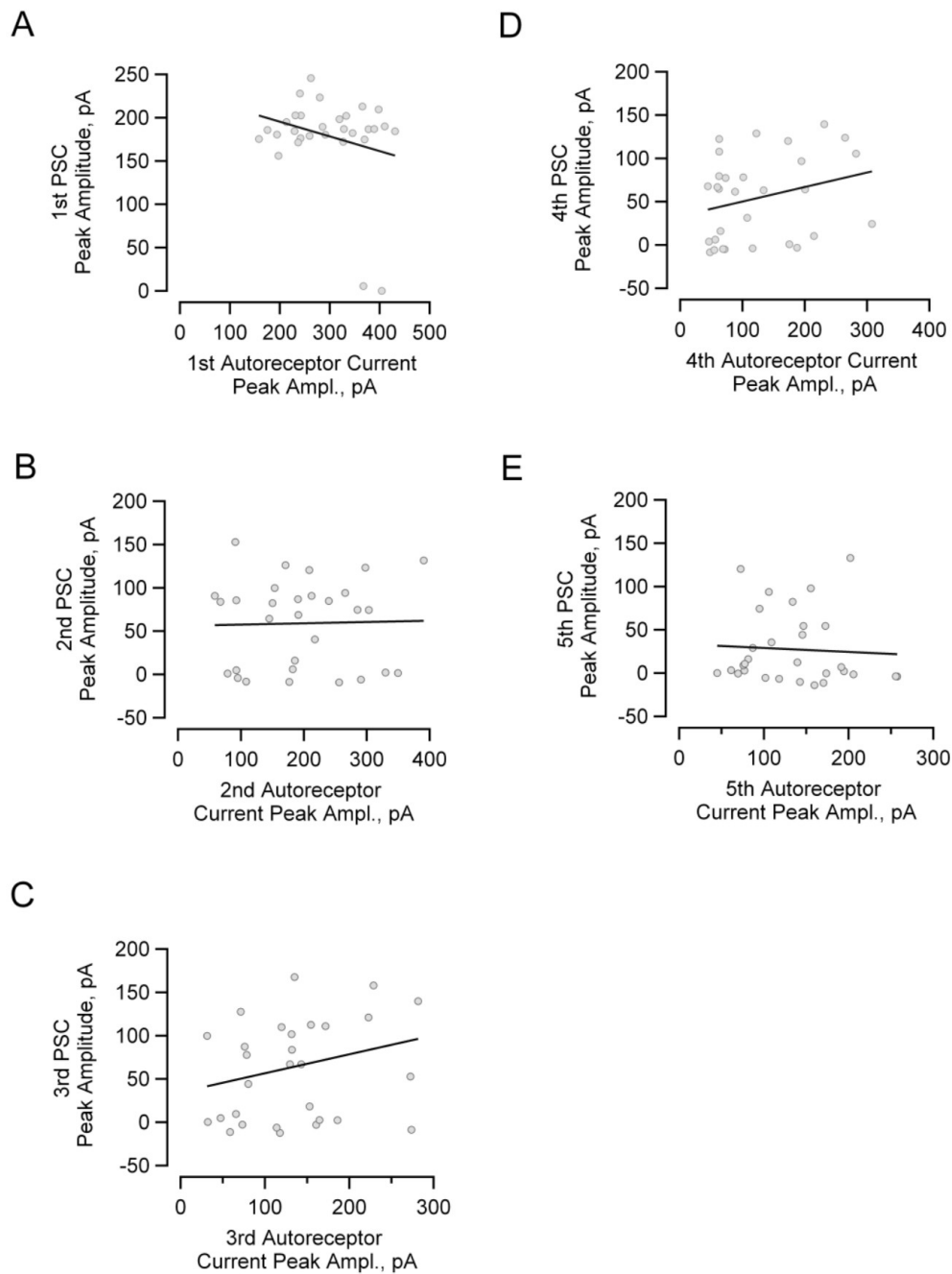


Figure S1, related to Figure 1: Lack of correlation between autoreceptor current and PSC peak amplitudes

To test whether trial-to-trial fluctuations in AP waveform play an important role in determining PSC fluctuations, peak amplitudes were compared for autoreceptor/autaptic current and for PSCs (same data set as in Fig. 1). If fluctuations in presynaptic APs played an important role, a correlation between these two parameters should be apparent, since the two signals are produced by the same action potential waveform. Data were analyzed separately for each pulse number. No significant correlation was observed for any of the 5 stimuli (plots A to E; regression lines in black; $p > 0.05$ for each plot), suggesting that PSC fluctuations are generated downstream of the AP.

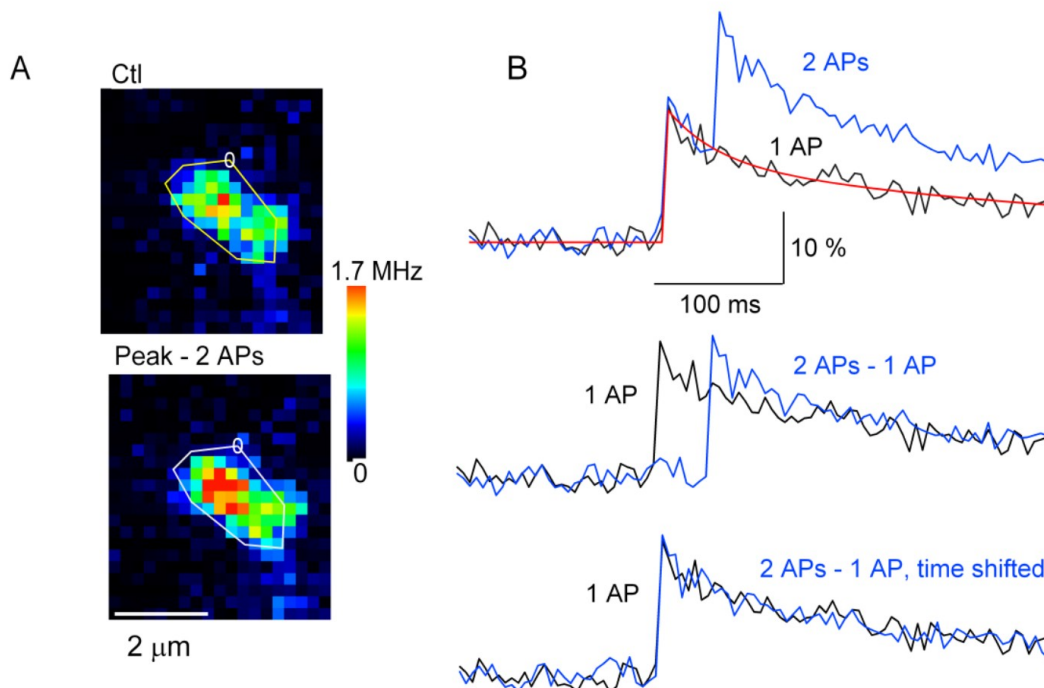


Figure S2, related to Figure 1: Linear summation of local calcium signals in single varicosities

A: Single frame images of an axonal varicosity using two-photon laser scanning microscopy with the calcium indicator Oregon Green 488 BAPTA-6F (200 μ M) applied from the soma. This indicator was employed because it has an optimal affinity for calcium (dissociation constant: \sim 3 μ M), high enough to ensure a large fluorescent signal, yet small enough to avoid indicator saturation with the 1-action-potential (1-AP) or 2-APs stimuli used here. Upper panel: Control. Lower panel: Peak response following a 2-AP stimulus.

B: Upper panel, average fluorescence traces (from 17 trials each; ROI as indicated in A) obtained in response to a single AP (black) and to a pair of APs (blue; 40 ms interval between the 2 stimulations). In agreement with previous results (Collin et al., 2005), the decay of the 1-AP trace can be fitted with a biexponential function (in red; fast component: amplitude 39 %, time constant 38 ms; slow component: amplitude 61 %, time constant 386 ms). Middle panel: comparison of the 1-AP trace with the trace obtained by subtracting the biexponential fit of the 1-AP trace from the 2-APs trace ('2 APs - 1 AP'; in blue). Lower panel: After introducing a 40 ms time shift, the 2 traces of the middle panel are indistinguishable. This indicates that the amounts of calcium entry associated with the first and second AP are the same.

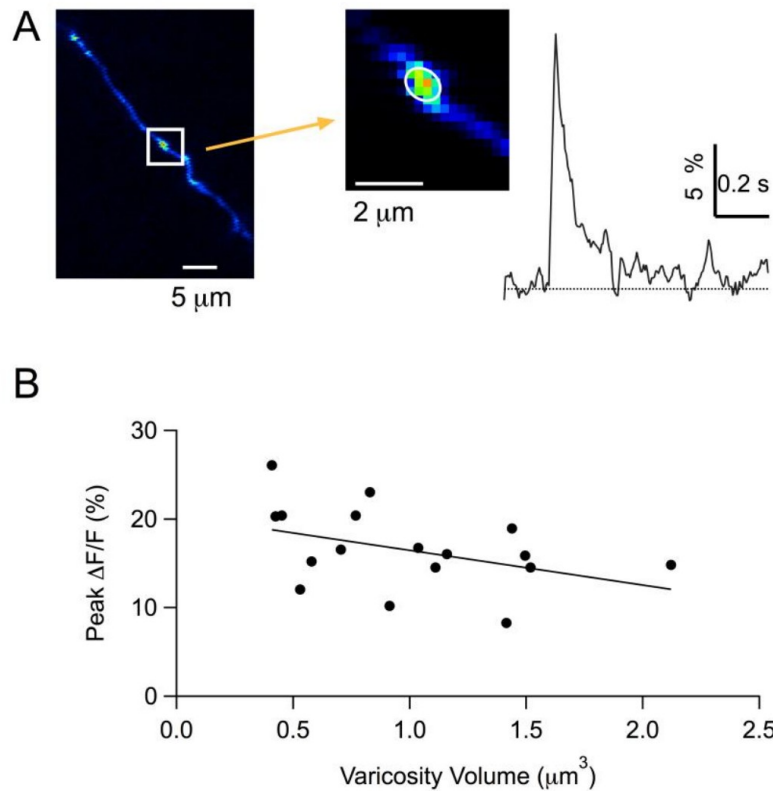


Figure S3, related to Figure 2: Peak AP-evoked calcium as a function of synaptic volume

A: Two-photon images of an axon varicosity (left, large field image; right, expanded view), together with the corresponding calcium response to one AP. Same conditions as in Fig. S2. The varicosity was approximated to an ellipsoid of revolution. Care was taken during the experiment to take images in the plane of symmetry. The short and long axes of the ellipse are noted $2a$ and $2b$ respectively. The symmetry (revolution) axis is the long axis. The ellipsoid volume was calculated as $(4\pi/3)a^2b$, giving $0.42 \mu\text{m}^3$. This analysis is justified since MLI axons are mainly contained in the parasagittal plane, which is the horizontal plane in our two-photon imaging. It avoids the drawback of poor z resolution in 3-dimension reconstructions of two-photon imaging.

B: Group results showing the peak $\Delta F/F$ responses as a function of the volume of the presynaptic varicosity. The regression line has a negative slope with a Pearson regression coefficient of 0.422, which does not reach statistical significance ($p = 0.09$).

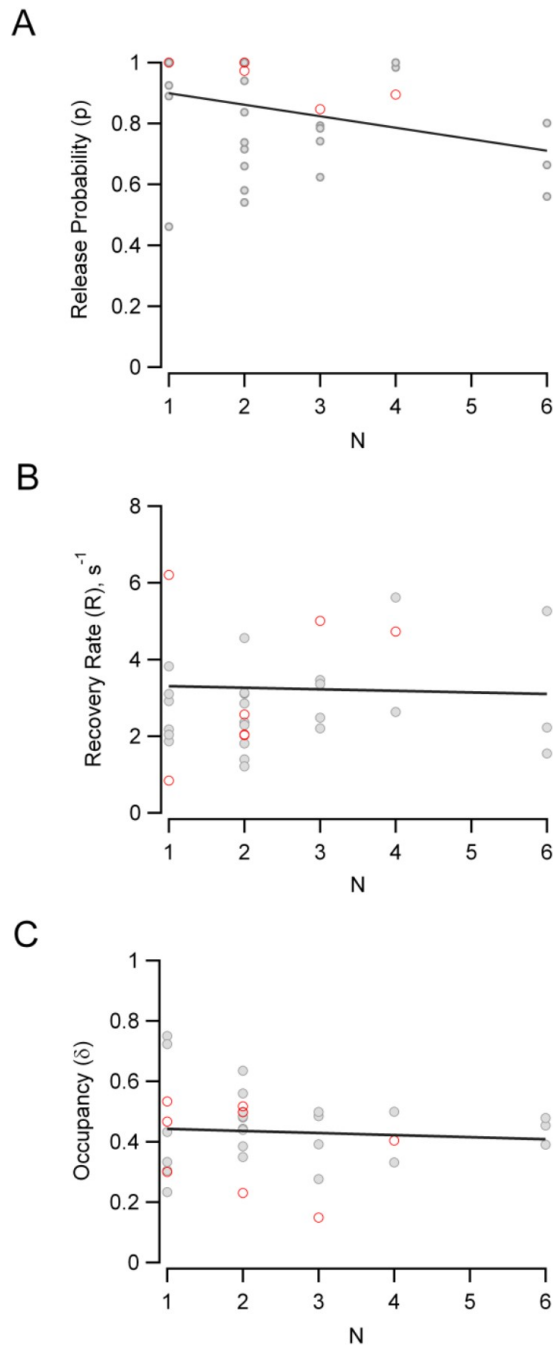


Figure S4, related to Figure 4: Model parameters are independent of docking site number.

Plots of release probability (p : A), recovery rate (R : B) and docking site occupancy (δ : C) as a function of estimated number of docking sites (N). Data were obtained from 33 simple synapse experiments (1-3 values/experiment; note that some of the points are superimposed, particularly for p measurements). Model parameters were obtained as detailed under Experimental Procedures. Closed symbols refer to trains at 25 Hz, and open symbols to trains at 50 Hz. Regression lines (in black) for pooled 25 Hz and 50 Hz data fail to reveal any significant relation of p , R or δ on N ($p > 0.05$). Mean values are $p = 0.89$, $\delta = 0.43$ and $R = 3.4 \text{ s}^{-1}$.

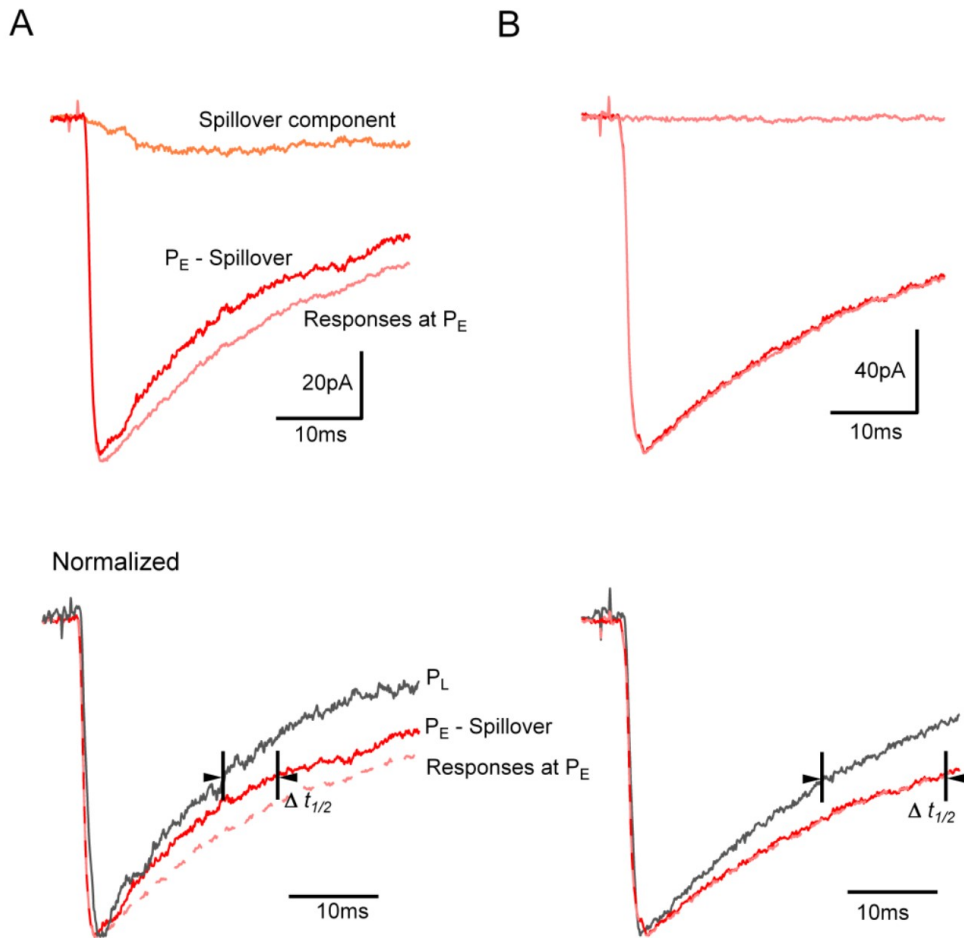


Figure S5, related to Figure 5: Correction for spillover in the analysis of PSC decay

A: Top panel: Mean PSC traces for the first successful response in a train ('Responses at P_E'), and of interleaved failures ('Spillover component') in an experiment displaying spillover (estimated N value for this synapse: N = 2). When present, spillover current had a mean amplitude of a few pA and a risetime on the order of 10 ms. Since spillover and the local PSC originate from different synapses, we assume that they occur independently of each other. The profile of PSCs corrected from spillover ('P_E - Spillover') can therefore be obtained by subtraction of the two preceding traces. Bottom panel: Mean of late traces (black) displays faster decay kinetics than the corrected 'P_E - Spillover' trace.

B: Top panel: In a majority of the cases, no significant spillover component appeared when averaging failures together (example shown: N = 6 synapse). Bottom: In such cases no correction was needed to calculate $\Delta t_{1/2}$ between early and late traces.

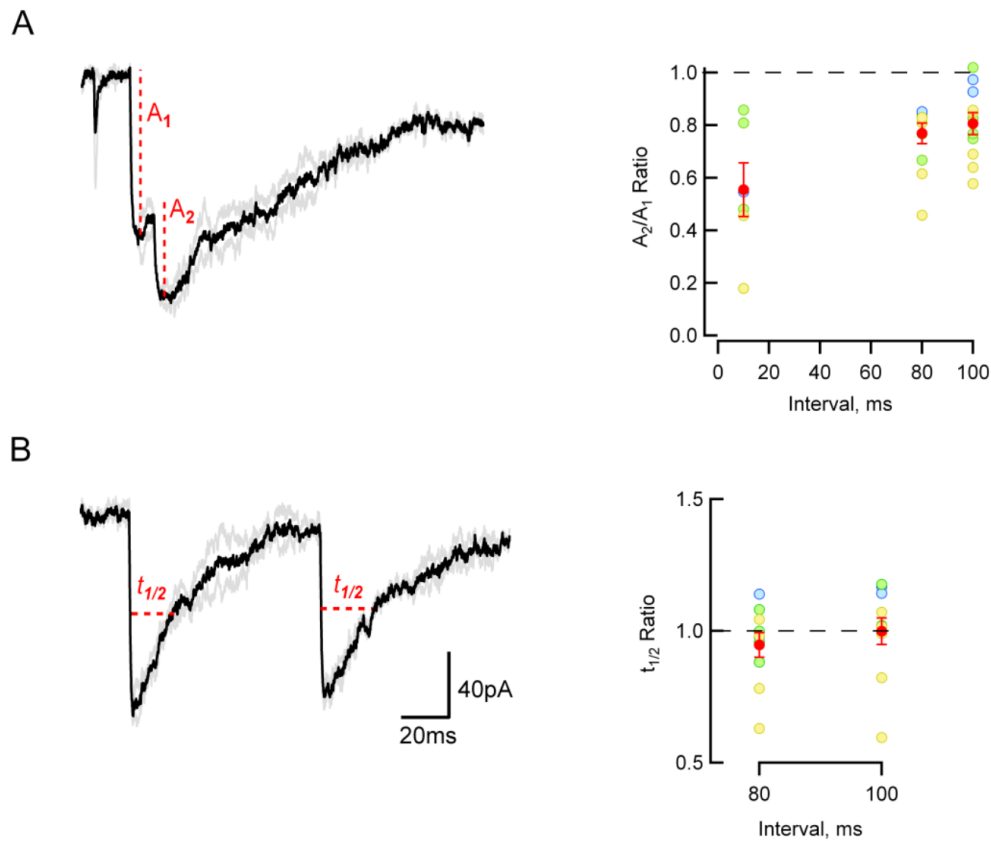


Figure S6, related to Figure 5: Receptor saturation and desensitization following local GABA photolysis

A: Amplitude ratio as a function of stimulus interval. The bath was perfused with 1 mM of the caged GABA, DPNI-GABA, in a HEPES-buffered extracellular solution. To stimulate receptors, a focused laser (2 to 5mW, duration 0.1 ms) was directed to a sensitive spot in the dendritic domain. Two stimulations were applied with intervals of 10, 80 or 100 ms. The corresponding current amplitudes, A_1 and A_2 , were determined as illustrated (grey: individual trials; black: averages). To calculate A_2 , a biexponential fit was performed on the decay of A_1 , in order to obtain a reliable estimate of the starting point of the response. Average values for the A_2/A_1 ratio and associated sem are shown in red in the right panel. For 10 ms intervals, this ratio is 0.56 ± 0.10 , indicating that the first stimulus elicited a significant degree of receptor occupancy. For 80 ms and 100 ms intervals, the ratio takes the respective values of 0.77 ± 0.05 and 0.81 ± 0.04 . Thus even for intervals of 80-100 ms, one exposure to GABA is sufficient to reduce the response amplitude significantly (by 21 %, from the mean of the data at 80 and 100 ms). This presumably reflects a combination of receptor desensitization and residual receptor activation at the time of the second stimulation.

B: The same protocol was used to examine the effect of repeated stimulation on decay kinetics. The ratios of $t_{1/2}$ values obtained at 80 ms and 100 ms intervals were not significantly different from 1. In the right panels, each dot represents averaged results from one varicosity. Dots with identical colors represent varicosities located on the same cell (3 cells, labelled yellow, blue and green).

Supplemental Experimental Procedures

Recording procedures

Sagittal slices (200 μm thick) were prepared from the cerebellar vermis of Sprague Dawley rats (PN 12-14) following the animal care guidelines of our host institution (approval number A-750607). Procedures to record from MLIs were as described (Llano and Gerschenfeld, 1993). The composition of the standard extracellular solution was (in mM): 130 NaCl, 2.5 KCl, 26 NaHCO₃, 1.3 NaH₂PO₄, 10 glucose, 2 CaCl₂, and 1 MgCl₂; osmolarity: 300 mosm/l). This solution was equilibrated with 95 % O₂ and 5 % CO₂ (pH 7.4). The standard internal recording solution contained (in mM): 145 KCl, 4.6 MgCl₂, 0.1 EGTA, 10 HEPES-K, 0.4 NaGTP, 4 Na₂ATP, 10 GABA; pH 7.4; osmolarity: 300 mosm. GABA was included in this solution to prevent emptying of the synaptic vesicles and consequent PSC rundown (Bouhours et al., 2011). In some experiments (Fig. 7) the EGTA concentration was increased to 2 mM in order to provide a better-defined basal calcium concentration. All recordings were at room temperature.

Paired MLI recordings

Dual whole-cell recordings were obtained from MLIs using a double EPC-10 amplifier (Heka, Lambrecht, Germany). The probability to obtain synaptically connected pairs was on the order of 10 %. According to previous work, a connection was considered to involve a simple synapse if the PSC amplitude histogram displayed a single Gaussian peak with a CV value less than 0.35 (Kondo and Marty, 1998). Both pre- and postsynaptic MLIs were maintained in voltage clamp, usually at a holding potential of -60 mV. Peak PSC amplitudes obtained occasionally with another postsynaptic holding potential (-70 mV) were corrected for the difference in driving force. PSCs were elicited by presynaptic voltage steps to 0 mV (1 ms duration). Trains of 5 such pulses (interstimulus interval: either 40 or 20 ms) were applied repetitively, with intervals of 5 or 10 s between trains. Statistical data were derived from sequences of 24-30 trains.

Detection of PSCs during trains

The paired recording traces were analyzed using Igor (Wavemetrics, Lake Oswego, USA). In order to detect PSCs during trains, traces were differentiated, and excursions of the differentiated traces were submitted to a threshold analysis during windows associated with each pulse stimulus. After automated amplitude measurement of each detected event, PSC sequences were displayed as a temperature plot of amplitudes, where 'hot' colors feature large amplitudes, and failures appear in white (examples in Figs. 1D and 2D).

Calcium imaging of presynaptic varicosities

AP evoked calcium signals were studied in MLIs subjected to whole-cell recording with a solution containing (in mM): 140 K gluconate, 5.4 KCl, 4.1 MgCl₂, 9.9 HEPES-K, 0.36 Na-GTP, 3.6 Na-ATP and 100-200 μM of the calcium -sensitive indicator Oregon green 488 BAPTA-6F (Molecular Probes Europe, The Netherlands; K_d for calcium of 5.1 μM estimated from *in vitro* calibrations). Fluorescence was recorded from axonal varicosities using a custom-built 2-photon system based on the design of Tan et al. (1999), with 820 nm excitation provided by a MaiTai Ti-Sapphire laser (Spectra Physics, USA). Raster scans of small fields encompassing the varicosity were performed at dwell times of 5 ms. The MLIs were held at -70 mV and APs were elicited by 1 ms depolarizations to -10 mV. Stimulation protocols alternated between a single AP and 2 APs (interval between APs: 40 ms) and were repeated every 1 to 2 min. Axonal varicosities were identified from the characteristically large amplitude of AP-evoked fluorescence signals (Tan and Llano, 1999; Forti et al., 2000). Fluorescence was analyzed in the pixels encompassing the varicosity in terms of fluorescence changes relative to pre-stimulus values ($\Delta F/F_0$, expressed in %) with software written in the IGOR-Pro programming environment (Wavemetric, Lake Oswego, OR, USA). Averages were performed over 10-17 repetitions.

GABA photolysis

GABA photolysis experiments were done in a HEPES-buffered extracellular solution, whose composition was (in mM): NaCl 128, KCl 4, NaHCO₃ 2.5, HEPES-Na 10, Glucose 25, sodium pyruvate 5, CaCl₂ 2, MgCl₂ 1, pH 7.4 with 1 M NaOH. The intracellular solution used for these experiments was the standard solution with the addition of 40 μM Alexa 488, to aid neurite visualization in order to choose the photolysis location. GABA was photolysed from DPNI-GABA (1-(4-Aminobutanoyl)-4-[1,3-bis(dihydroxyphosphoryloxy)propan-2-yloxy]-7-nitroindoline; Tocris, Bristol, UK) with a 405 nm minimized laser spot, as described previously (Trigo et al. 2009). Briefly, the laser beam (Obis, Coherent, USA) was expanded to fill a 60x water immersion objective. The bath perfusion was turned off and DPNI-GABA was diluted in the bath to a final concentration of 2 mM. A dendritic varicosity was chosen and GABA was photolysed with pulses of 2 to 5 mW, and a duration of 100 μs. The timing of the laser pulses was monitored with a photodiode.

Statistical evaluation of group results

Results of group data analysis are presented as mean \pm s. e. m., or as regression lines. *n* values represent the number of independent experiments. When analyzing means, *p* values are based on Wilcoxon's rank test (either paired or unpaired). When analyzing ratios to control situation, *p*

reflects the area of the normal distribution corresponding to the values of the mean and s. e. m. When analyzing correlations illustrated with regression lines, r represents Pearson's correlation coefficient, and p assesses the probability of correlation given the value of r and the number of degrees of freedom of the data.

Supplemental References

- Collin, T., Chat, M., Lucas, M.-G., Moreno, H., Racay, P., Schwaller, B., Marty, A., and Llano, I. (2005). Developmental changes in parvalbumin regulate presynaptic Ca^{2+} signaling. *J. Neurosci.* 25, 96-107.
- Forti, L., Pouzat, C., and Llano, I. (2000). The spatial distribution of action potential-evoked Ca^{2+} signals in axons of developing rat cerebellar interneurons. *J. Physiol.* 527, 31-47.
- Tan, Y. P., Llano, I., Hopt, A., Würriehausen, F., and Neher, E. (1999). Fast scanning and efficient photodetection in a simple two-photon microscope. *J. Neurosci. Meth.* 92, 123-135.
- Tan, Y. P., and Llano, I. (1999). Modulation by K^+ channels of action potential evoked intracellular Ca^{2+} rises in rat cerebellar basket cell axon. *J. Physiol.* 520, 65-78.

Chapter 2: Changes In IPSC Amplitude And Kinetics With Extracellular Calcium Concentration

The above results suggest that MLI synapses function close to saturation since $P(S1)$, p and δ are all rather close to 1 under control conditions (external calcium concentration: $Ca_o = 2$ mM). By making $p = \delta = 1$ in the simulation of [Figure 4](#) from the paper, the maximum possible response can be calculated. By making the ratio of the simulated maximal response under control conditions (obtained in response to the 1st stimulation) to the overall maximal response, it may be calculated that simple synapses vary in their percentage of saturation from 40 % (for $N = 1$) to 95 % (for $N = 6$).

Assuming the distribution of N values illustrated in [Figure 2E](#) from the paper, the weighted mean percentage is 58 %. This mean that the 1st peak PSC amplitude can at most increase by a factor of 2 when increasing the release probability. To test this prediction, we examined the dependence on Ca_o of mean peak PSC amplitudes, averaged over successes and failures, both in simple synapses and in multisite synapses. The results were pooled together, and were fitted in log-log coordinates with a Hill curve having a slope of 3 ([Figure 11A](#)). With this approach the percentage of saturation was estimated at 57% at hippocampal GABAergic synapses (Bucurenciu et al., 2008). Here the peak PSC amplitude grew by a factor 1.48 ± 0.26 between 2 and 4 mM Ca_o ($n = 9$), and the position of the asymptote of the Hill curve indicated that the percentage of the maximum responsiveness at 2 mM Ca_o is 56 %, close to the predicted 58 % ([Figure 11A](#); note that receptor saturation is not considered in this analysis). The agreement supports the notion that both p and δ vary as a function of Ca_o since if only p were Ca_o dependent, the predicted percentage of responsiveness at 2 mM Ca_o would be 84 %.

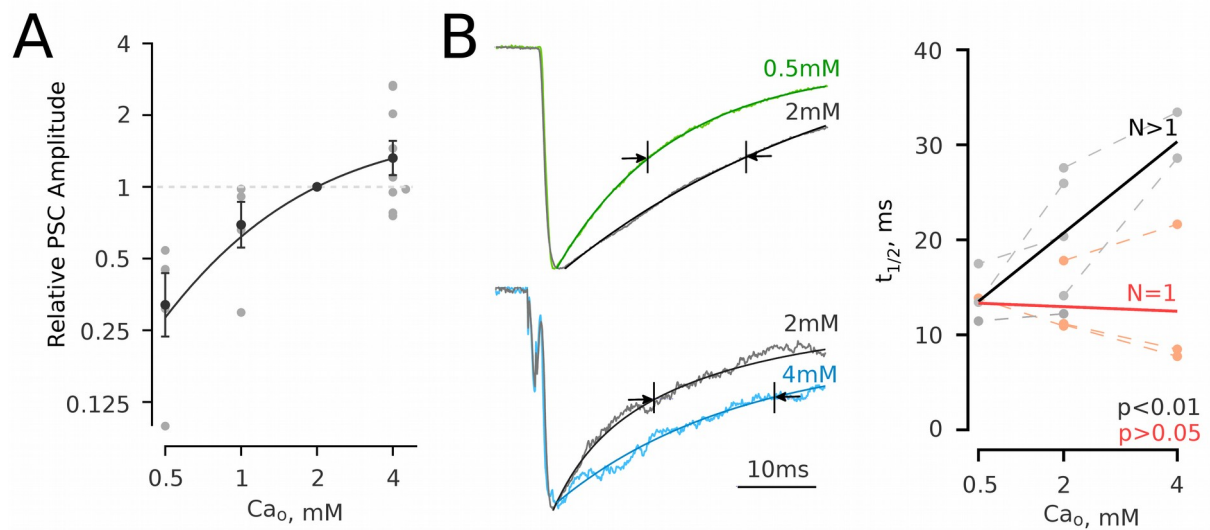


Figure 11. Changes in PSC peak amplitude and kinetics with Ca_o . (A) Variation of the mean peak PSC amplitude as a function of Ca_o . In each experiment (including multisite and simple synapses) the mean PSC amplitude (including failures) was compared at the standard Ca_o value of 2 mM and at one or several test Ca_o values. The data (gray symbols: individual experiments; black symbols: mean \pm sem) are displayed in log-log coordinates and are fitted with a Hill curve having a maximum slope of 3. (B) Comparison of PSC decay kinetics for simple synapses at 0.5, 2 and 4 mM Ca_o . Left, average normalized PSC traces in response to the first stimulus of a train, at 2 mM Ca_o (black) and either 0.5 mM Ca_o (green) or 4 mM Ca_o (blue; this paired recording included an electrical and a chemical connection), for 2 simple synapses with $N > 1$. Note that the decay is in both cases slower at the higher Ca_o value. Right, summary data presenting $t_{1/2}$ values as a function of Ca_o , for a series of 5 paired recordings of simple synapses with $N > 1$, and for 4 further elementary synapses ($N = 1$). Data points from the same experiments are linked together with a dashed line (grey: $N > 1$ experiments; light red: $N = 1$ experiments). The data from $N > 1$ synapses display a significant dependence of $t_{1/2}$ on Ca_o (black regression line), but those for $N = 1$ fail to display a significant dependence (red regression line).

At GABAergic and glycinergic synapses, the PSC decay time has been reported to increase as Ca_o is augmented, an effect that was attributed to neurotransmitter spillover between adjacent synapses, either alone or in combination with multivesicular release (Biró et al., 2006; Balakrishnan et al., 2009). Given the above results indicating a link between number of released vesicles and decay time during a train (Figure 5B from the paper) similar effects are expected when increasing Ca_o . As illustrated in Figure 11B, elevating Ca_o in simple synapse experiments with estimated N values larger than 1 led to increases in PSC half decay time and conversely, reducing Ca_o led to PSC shortening. By contrast in elementary synapses, changes of half decay time were small and inconsistent. Group data analysis revealed a significant slowing of PSC decay with Ca_o in the first class of experiments

($p < 0.01$, $n = 5$), but not in the second ($p > 0.05$, $n = 4$; [Figure 11B](#), right panel). This difference indicates that multivesicular release, rather than GABA spillover, is responsible for the effect, because spillover should occur equally for elementary synapses and for other simple synapses. This was confirmed by examination of failures, as explained above for the data of [Figure 5](#) from paper, which did not reveal a significant spillover component in the experiments where $t_{1/2}$ was increased.

In conclusion, increases in mean number of released vesicles either as a function of pulse number during a train, or as a function of Ca_o , give rise to an increase in the duration of PSC decay.

Chapter 3: Statistics Of Cumulative Released Vesicle Numbers In Elementary GABAergic Synapses

3.1 Introduction

The last step of presynaptic signaling, exocytosis, has been extensively studied in central synapses (Schneppenburger & Neher, 2000; Bollmann et al., 2000), but steps immediately preceding exocytosis remain poorly understood. Current views focus on a special set of vesicles, the readily releasable pool (RRP), that restricts the number of release events elicited by a sudden stimulus. Only vesicles in the RRP can be released, so that RRP exhaustion is a major contributor to synaptic depression following repetitive stimulation. Once exhausted, the RRP is replenished from another pool, the recycling pool. The mechanisms governing RRP replenishment are still unclear, apart from the fact that an elevation of cytosolic calcium speeds up this process (Rizzoli & Betz, 2005).

In the calyx of Held and at mossy fiber-granule cell synapses, two distinct components of the RRP can be distinguished when giving a prolonged presynaptic depolarizing voltage step. In these conditions a fast releasable pool (FRP; about 3 vesicles per active zone at calyx synapses) is first released, followed by the release of a slowly releasable pool (SRP; also about 3 vesicles per active zone) with a time constant about 10 times larger (Sakaba & Neher, 2001; Ritzau-Jost et al., 2014). It has been suggested that only the FRP, not the SRP, contributes to EPSCs during a train of action potentials (Sakaba, 2006). Nevertheless, a recent study suggests that the SRP can be converted to FRP after FRP depletion, and that it does contribute to the steady-state response during prolonged AP trains (Lee, Ho, & Lee, 2012). This raises the possibility that SRP and FRP represent two consecutive stages of maturation along the path of vesicles towards exocytosis.

Whereas previous work on RRP replenishment has focused on measuring RRP size

as a function of previous neuronal activity, Takafumi Miki and Gerardo Malagon, two members of our laboratory, propose a new approach based on the examination of the statistics of released vesicle numbers at single active zones. This question is addressed at single glutamatergic synapses between parallel fiber and molecular layer interneuron, where deconvolution method is used to count released vesicles. Variance analysis of cumulative counted vesicles and Monte Carlo simulations have indicated that vesicles transit through 2 successive states before exocytosis, so that the RRP estimate is up to 2-fold higher than the docking site number (“2-step model”). The transition to the second state has a very rapid rate constant, and is specifically inhibited by latrunculin B and blebbistatin, suggesting the involvement of actin and myosin (Miki et al, manuscript in preparation).

Previously, we showed that some MLI-MLI synapses, called ‘elementary synapses’, display a single docking site. Whereas extensive receptor saturation undermines vesicle counting at single GABAergic synapses containing several docking sites, no such effect occurs at elementary synapses, where one is the maximum number of vesicles able to release by a sudden stimulus. Taking advantage of the single site GABAergic model, We next asked whether 2 successive states before exocytosis are also present in an alternative synaptic type.

3.2 Extension of the 2-step model to single GABAergic synapses

A representative ‘elementary synapse’ experiment is illustrated in [Figure 12A](#). As previously reported, elementary MLI-MLI synapses exhibit severe depression when are repetitively stimulated at 25 Hz. Corresponding vesicle counts s_i are shown in [Figure 12B](#), both as a function of stimulus number (i : columns) and sweep number (lines), each green cell represent the release of one vesicle.

s_i statistics can be modeled by assuming several docking sites operating in parallel. Calling N_1 the number of docking sites and P_i the release probability at one docking site for stimulus number i , the mean and variance of s_i follow the relation:

$$\begin{aligned} \langle s_i \rangle &= N_1 \cdot P_i \\ \text{var}(s_i) &= N_1 \cdot P_i (1 - P_i), \text{ such that} \\ \text{var}(s_i) &= \langle s_i \rangle \left(1 - \frac{\langle s_i \rangle}{N_1}\right) \end{aligned}$$

Thus the variance of s_i follows a binomial model. Note that in the above equation, in contrast to the classical analysis of EPSC amplitudes, the quantal size does not appear. N_1 is the only free parameter, and the initial slope in a plot of $var(s_i)$ as a function of $\langle s_i \rangle$ is always one. The parabolic fits yield to an estimative of N_1 value, the number of docking sites. In the case of the GABAergic 'elementary synapses' experiments, N_1 reaches the value 1 as expected (continuous curve in [Figure 12C](#)).

While the plots of $var(s_i)$ as a function of $\langle s_i \rangle$ provide estimates of N_1 and P_i , they give little information on the replenishment of empty docking sites. To approach this issue, we examined the sum S_i of successively released synaptic vesicles, defined as $S_i = s_1 + s_2 + \dots + s_i$. Without replenishment the sum of released vesicles is constrained by the number of vesicles that were release-ready before stimulation, and values for $var(S_i)$ plotted as a function of $\langle S_i \rangle$ should lie on the $var(s_i)$ parabola.

As illustrated in [Figure 12C](#) (open symbols), the data representing the dependence of $var(s_i)$ on $\langle s_i \rangle$ lie outside the ' N_1 parabola' describing the relation of $var(s_i)$ on $\langle s_i \rangle$. They can however be fitted by another parabola (' N_2 parabola'), also with an initial slope of 1 (discontinuous curve in [Figure 12C](#)), and characterized by a new maximum value N_2 , within $N_2 > N_1$, in this example $N_2 = 2$.

Group results from 'elementary synapses' experiments indicate $N_2 = 1.8 \pm 0.3$ (mean \pm sem; $n = 7$; [Figure 12E](#)), close to $N_2 = 2$. As a further test of the 2-step model, we examined statistics of the sum of vesicle counts across the train, S_5 . Average results ($n = 7$) show that the probability of observing S_5 values in the range from 0 to 2 is significant ($P(S_5 = 0) = 0.33 \pm 0.06$; $P(S_5 = 1) = 0.52 \pm 0.04$; $P(S_5 = 2) = 0.13 \pm 0.03$), but that $P(S_5 > 2)$ is very low (0.012 ± 0.008 ; [Figure 12D](#)). The data differ strikingly from a Poisson distribution with identical mean value (red curve in [Figure 12D](#)), and they suggest a severe restriction to have $P(S_5 \leq 2)$. The 2-step model with $N_2 = 2$ provides precisely this restriction.

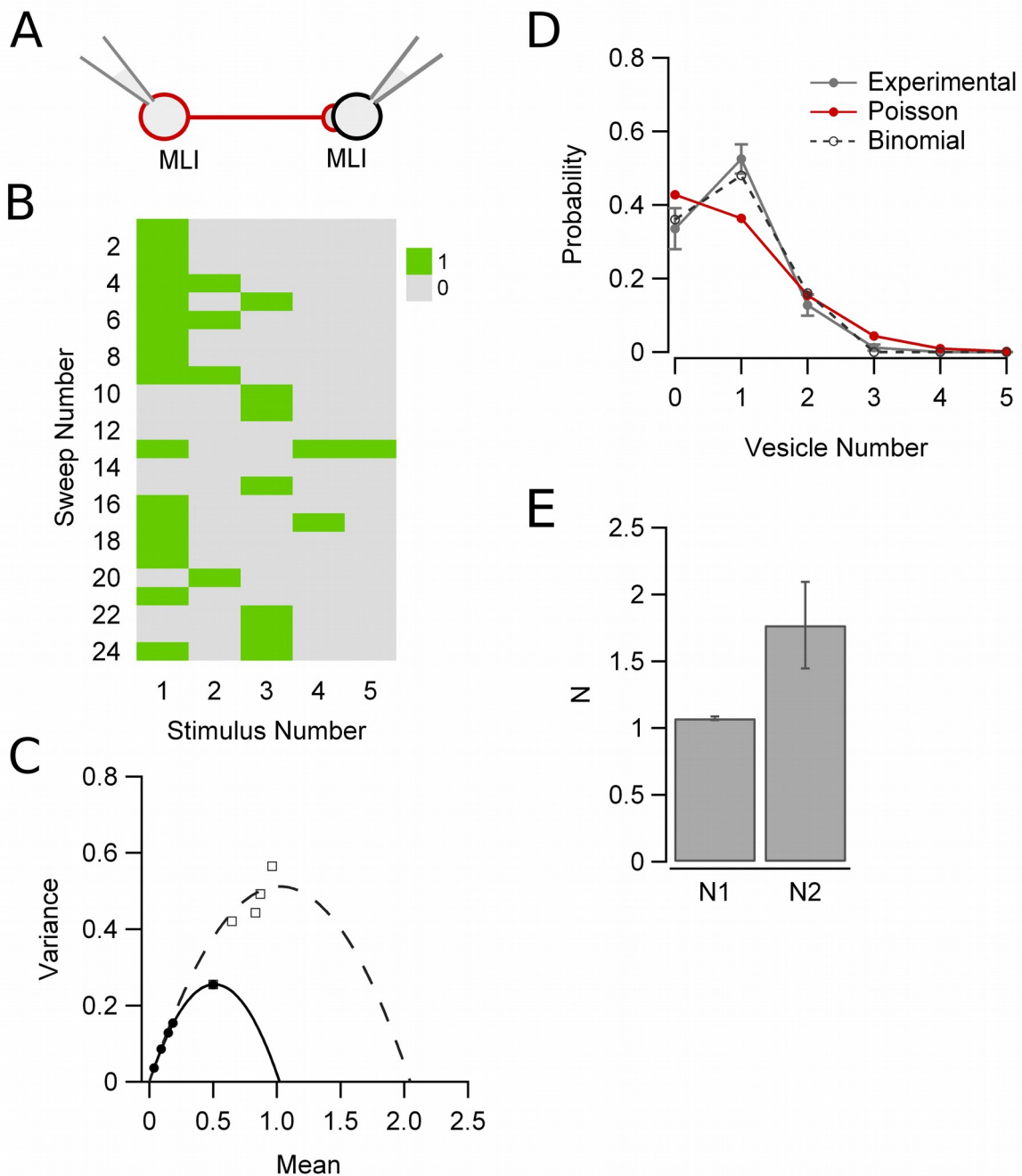


Figure 12. Statistics of cumulative released vesicle numbers in elementary GABAergic synapses. (A) Paired recordings were obtained from synaptically connected MLIs. In some cases these connections involve single synapses having a single docking site; such connections are called ‘elementary synapses’ (Pulido et al., 2015). Trains of 5 APs were applied at a frequency of 25 Hz, with 10 s waiting times between trains. Patterns of success/failures for a representative experiment. Note that 1 vesicle is maximally released following each AP. (B) Plots of $\text{var}(s_i)$ a function of $\langle s_i \rangle$ (giving $N_1 = 1.0$) and of $\text{var}(S_i)$ as a function of $\langle S_i \rangle$ (giving $N_2 = 2.0$) for the experiment shown in A (total number of trains: 54). (C) Distribution of $P(S_5)$ values for 7 elementary synapses, showing an abrupt fall for $i = 3$. A Poisson distribution with same mean as that of $P(S_5)$ is shown for comparison. (D) Group results showing means of N_1 and N_2 values (error bars: \pm sem) across elementary synapses ($n = 7$).

In summary, while $var(s_i)$ vs. $\langle s_i \rangle$ data follow a parabola, as expected from a binomial model, $var(S_i)$ vs. $\langle S_i \rangle$ data cannot be described with the same parabola. Rather, they can partially be approached with another parabola having a maximum vesicle number about twice the value found for the first parabola, or in other words twice the docking site number. These results are consistent with a model supposing two sites in sequence, a replacement site and a docking site. Moreover, these results suggest that the 2-step model applies to elementary MLI-MLI synapses. They therefore suggest that this model is not restricted to PF-MLI synapses, nor to glutamatergic synapses, and that it may be generally applicable.

Chapter 4: Modeling Changes In Synaptic Properties

The results presented in the Figure 7 from the paper suggested that presynaptic depolarization can induce changes in synaptic properties. The results suggested that p is modestly sensitive to depolarization, presumably because it is close to saturation, and that R strongly decreases with depolarization, presumably as a consequence of enhanced spontaneous release (Figure 7 in the paper). Based on this result, we suggested that the augmentation of spontaneous synaptic activity during depolarizing prepulses leads to a depletion of reserve vesicles and to the observed decrease in R during subsequent trains. The change of R alters late release by decreasing docking site occupancy.

In this section, I would like first to show some preliminary data with the aim of evaluating whether a decrease in R is a consequence of enhanced spontaneous release. In such a case, a correlation between the increment in spontaneous synaptic activity and the probability of evoked responses would be expected. Second, I would like to explore how the change in R is affecting the remaining synaptic parameters, by the implementation of Monte Carlo simulations.

4.1 Changes in success probability induced by augmentation of spontaneous synaptic activity.

The vesicle source for spontaneous events is controversial. Some studies suggest that the pool of vesicles and the mechanism of vesicular release are shared between spontaneous release and evoked release (Kaeser & Regehr, 2014; Schneggenburger & Rosenmund, 2015); whereas other studies suggest that there are independent pools (Fredj & Burrone, 2009; Ramirez et al., 2012). Nevertheless, in spite of this controversy, the most parsimonious hypothesis is that most spontaneous release is mediated by a vesicular pool and a molecular mechanism that are shared with evoked release (Kaeser & Regehr, 2014). In such a case, a

previous increase in spontaneous activity due to depolarization, may directly affect the probability of getting an evoked release during a subsequent train of stimulation, which will be represented as a decrease in R.

Following this hypothesis, spontaneous events from interneurons connected by a single synaptic contact were recorded ($n = 8$). The spontaneous postsynaptic currents (sPSCs) were recorded during 9 seconds, while the presynaptic cell was held at three different potentials: -80, -60 and -50mV. If there is an increase in spontaneous release with depolarization, the sPSC events would only increase due to the direct effect of the potential prepulse on the unique release site that is connecting both cells. To test this, all GABAergic sPSCs bigger than 15pA were selected and counted.

The [Figure 13A](#) shows an example of sPSCs (red circles), while the presynaptic cell was held at each potential. During a trial of 9 sec prepulse, 5 events were detected at -80mV, 6 at 60mV and 13 at -50mV. The histogram shows the distribution of amplitudes of the whole experiment at each potential (30 repetitions; [Figure 13B](#), lower panel). The event increments due to depolarization (orange bars) were mostly confined to amplitudes between 10 to 50pA, corresponding to the amplitude distribution of evoked IPSCs (at pulse 1: ~32pA). Immediately after the potential prepulse, the presynaptic cell was held at -60mV and it was stimulated with a train of 5 pulses at 25Hz ([Figure 13A](#) right). In the case of -80mV presynaptic prepulse, where the number of sPSCs decreased, evoked vesicular release occurred all along the train of stimulation, whereas at -60mV just the first pulse elicited an IPSCs and no release was detected with a prepulse at -50mV.

We found in agreement with previous studies (Bouhours et al., 2011) an increase in spontaneous release with depolarizing prepulse (values normalized with respect to -60mV data: 0.96 ± 0.03 at -80mV, ns; 1.09 ± 0.031 at -50mV, $p < 0.02$; $n=8$; [Figure 13C](#)). From the eight experiments that were performed, six presented the depolarizing effect and in these experiments we searched for a correlation between spontaneous and evoked release.

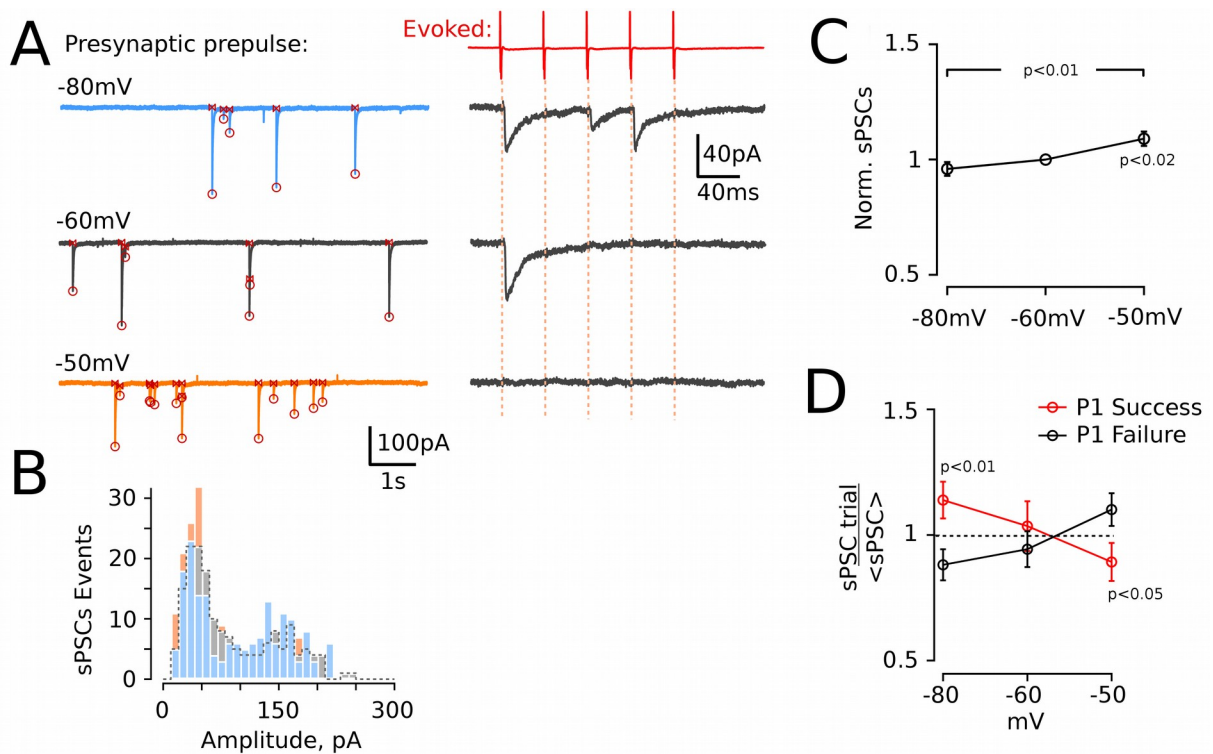


Figure 13. Increase in spontaneous release due to presynaptic depolarization affects evoked release. The recording protocol was as in the Figure 7 from the paper. PSCs were counted during the prepulse. (A) Exemplar experiment showing the postsynaptic spontaneous events during the presynaptic prepulse time at -80mV (blue), -60mV (black) and -50mV (orange, left panel); immediately after taking each of these 3 records, the presynaptic cell was stimulated with the standard train of 5 pulses at -60mV (red trace), and PSCs were recorded (black traces). (B) Histograms of amplitude distribution of the sPSCs during the presynaptic prepulses recorded in A. The amplitude distribution at -60mV is outlined by a dotted line. Note specific increase in PSCs of small amplitude during prepulses at -50mV. (C) Group data ($n = 8$) showing sPSC as a function of prepulse potential, after normalization to the value at -60mV. (D) Proportion of sPSC per 9s trial normalized against the mean as a function of prepulse potential, when there was a success at the first pulse (red trace) or a failure (black trace).

The sPSCs detected at each trial of 9 seconds were normalized with respect to the sPSC mean obtained from 30 repetitions at each presynaptic holding. It was considered as an increase in spontaneous release, when the number of events was larger than the mean. In line with the hypothesis that an increase in the spontaneous release is affecting the evoked release, the results revealed that failures in evoked release at the first pulse of the train were correlated with increments in sPSCs with depolarization ($p < 0.02$ between -80mV and -50mV; Black line in Figure 13D); and reciprocally, successful evoked responses at the first pulse were related with a decrease in preceding sPSC events ($p < 0.02$ between -80mV and -50mV; red line in

Figure 13D). Additionally, when a depolarizing pulse was applied, there was a correlation between getting a success or a failure at first pulse, and when sPSCs decrease or increase, respectively (at -50mV comparing red and black circles: $p < 0.05$; Figure 13D). These results are in concordance with our hypothesis that an increase in spontaneous release is affecting evoked release.

Surprisingly following the -80mV prepulse, when normalized sPSC frequency was larger than 1, there was a higher chance to obtain an evoked release (red circle in Figure 13D); inversely, the chance to get a failure was related with normalized sPSCs smaller than 1 (black circle in Figure 13D; $p < 0.01$). This effect can be explained by a net decrease of sPSC number with hyperpolarization ($p < 0.01$ between -80mV and -50mV; Figure 13C). However, It is still difficult to understand why, when the number of sPSCs decreases compared with the mean of total events at -80mV (which is already low), it is mainly followed by a failure in the evoked event. Moreover, when sPSCs increases, the chance of getting evoked success increases too. Is there a threshold of expected spontaneous release that promotes/enhances success at evoked release? If so, that threshold is balanced at control state (-60mV), because at that holding no significant relation was apparent between the probability of evoked release and the number of spontaneous release events (Figure 13D). Alternatively, this effect with the -80mV prepulse may be related with an additional synaptic release step that is being modulated by the direct effect of calcium influx, and not by the change in spontaneous release itself. Further investigation will be needed to get a coherent conclusion.

Overall, the results suggest that an enhancement of spontaneous release by a depolarization pulse is affecting the success probability of a subsequent train of stimulation. These results suggest a direct link between spontaneous and evoked release. Therefore, they are best explained by the hypothesis that spontaneous and evoked release originate from the same vesicle pool. Furthermore, our results indicate that changes in spontaneous release target the replenishment of docking sites (rate R).

4.2 Simulations of presynaptic parameters.

We used Monte Carlo simulations to explore the implications of the results obtained by changing the prepulse potential. Specifically we examined whether the rate of vesicular recovery in the docking site, R , is the only parameter involved in the strong synaptic depression obtained with a depolarizing prepulse. First, we assumed a model which integrates the four presynaptic parameters quoted in the paper: docking site number (N), occupancy probability (δ), release probability (p) and probability of recovery (r). r was the only non-fixed variable. The other parameters were fixed to values obtained from our previous analysis: 1, 0.45 and 0.89, respectively. In the graphs shown in the [Figure 14](#), the success probability calculated along a train of 5 pulses at 25Hz was compared between different simulated outputs (dotted lines) and representative experimental data recorded at -50mV (orange diamonds).

In our first model, we assumed that the recovery vesicle is coming directly from an infinite pool (1-step model in [Figure 14A](#), upper panel). Since R , which is also represented as a probability² r , dramatically decreases with depolarization, we iterated it between values going from 0 to 0.13, which was the r value at -60mV ([Figure 14A](#), lower panel). In this 1-step model, all simulated responses showed a continuous decline along the train; none reproduced the minimum at stimulus number 2 observed with prepulse at -50mV experimental data. Rather, following a dramatic decrease in the success probability in the second pulse, which is stronger at smaller r values (dotted lines with red tones in [Figure 14A](#), down panel), the probability of response is continuously decreasing later in the train. This result suggests that a simple vesicle pool model cannot explain the time course of synaptic depression during repetitive stimulation, and presumably, that there is another parameter that is being modulated by the depolarizing prepulse.

Recently, it has been suggested that at the calyx of Held the slowly releasing vesicles pool (SRP) are recruited rapidly to become fast-releasing vesicles once the FRP is depleted by a short depolarization (Lee et al., 2012). Moreover, the analysis made in the previous chapter suggests that vesicles transit through 2 successive states before exocytosis (2-step model); previous to the docked vesicle there is an

² $r = 1 - e^{-R\Delta t}$

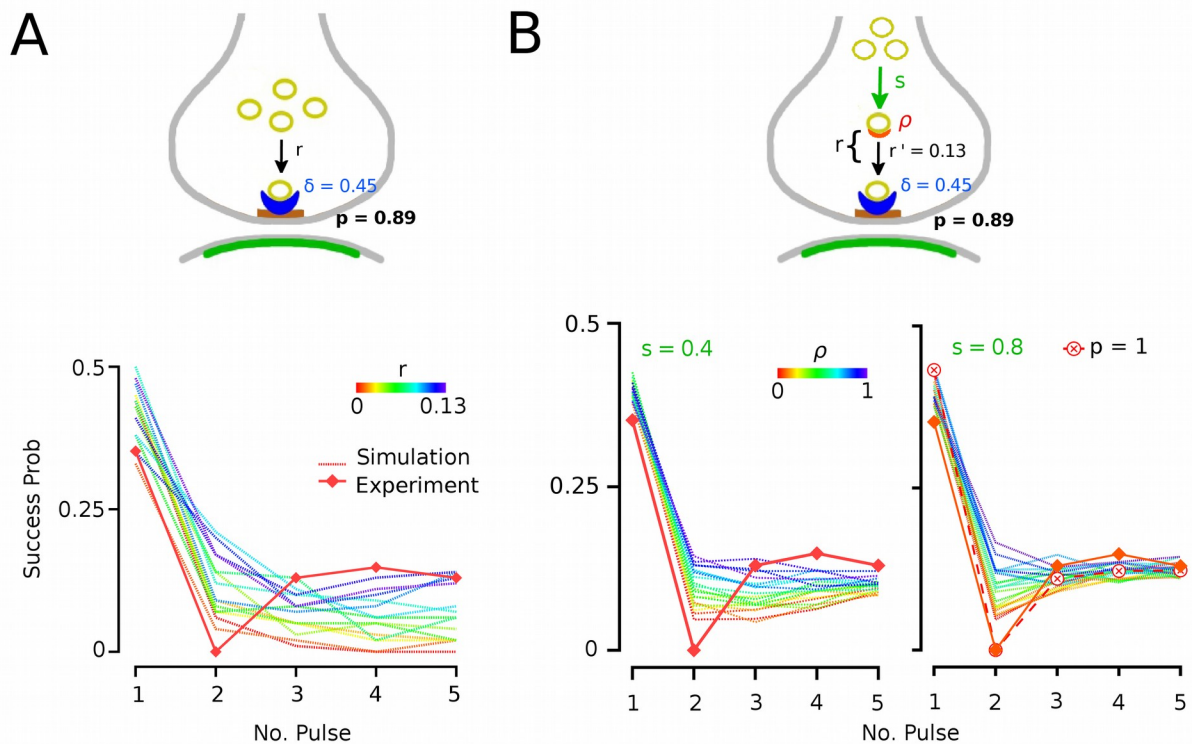


Figure 14. Simulation of synaptic depression during repetitive stimulation in two release models. A series of Monte Carlo simulations of success probabilities against simulation pulse plots (discontinuous color lines) were performed using various variants of a single synapse model assuming 1 docking site. Synapses are submitted to 5-AP trains at 25Hz as in the paper. In A-B, the model assumes an initial occupancy $\delta = 0.8$ and a probability of release of an occupied site $p = 0.89$. (A) 1-step model: emptied docking sites are replenished from an infinite vesicle pool with a fixed transition probability r . Upper panel: scheme describing the 1-step release model on a synapse with a single active zone (Brown) and associated postsynaptic receptors (green). Synaptic vesicles (yellow) are forming the infinite pool and just one is bound to a docking site (blue) before exocytosis. Bottom panel: Plot of probability of success Vs five-pulses trains from the simulated output (lines) when r was iterated from 0 to 0.13 (color code bar); and an exemplar experiment recorded at -60mV, preceded by 9s long pre-pulse at -50mV (orange diamonds). (B) In the 2-step release model a replacement site is associated to the docking site. The replacement site supplies vesicles once the corresponding docking site is empty, with a net probability of recovery r , which is given by probability of occupancy in the replacement site (ρ) and the probability of recovery of the docking site when the replacement site is occupied (r'). Upper Panel: Scheme describing the 2-step model, where a replacement site is added (red). Bottom panel: showing $P(S)$ plot. In order to change r , r' was fixed to 0.13 and ρ was iterated from 0 to 1, and s was fixed at 0.4 (left) and 0.8 (right). One simulation with $p = 1$ was done (orange open circles; right panel).

additional site called the replacement site, which can hold a vesicle with a certain probability of occupancy (ρ). Each replacement site has a probability s of being refilled during one inter-stimulus interval if it is empty. Including this additional step to

our Monte Carlo model, we tested whether the occupancy of the replacement site is affected by the depolarizing prepulse. If so, it would affect the net recovery of the docking site, r , which for this 2-step model is governed by the combination of ρ and the probability of recovery of the docking site with a vesicle coming from the replacement site, r' (Figure 14B, upper panel).

In the 2-step model, we assumed an infinitive reserve pool of vesicles with two fixed s values: 0.4 and 0.8 (Figure 14B, lower panel left and right, respectively); and for simplicity, we assumed that r is changing due to a change in ρ . ρ was assumed to be 1 in the control state (-60mV) and to take a value $0 < \rho < 1$ at depolarized potentials (-50mv). Consequently, r varied between 0.13 (at -60mV) and 0. To evaluate this idea, we iterated ρ from 0 to 1, fixing the docking sites parameters to: $\delta = 0.45$, $p = 0.89$ and $N = 1$ (dotted lines in Figure 14B, lower panel). The simulated results revealed that the amount of synaptic depression is given by ρ ; high depression levels, such as following a depolarization prepulse (orange diamonds), occurs when ρ becomes smaller, making r smaller as expected. This effect was observed both with $s = 0.4$ and with $s = 0.8$, with the difference that recovery of responses from synaptic depression had faster kinetics with $s = 0.8$ for intermediate ρ values (Figure 14B lower panel).

It is known that in MLIs, subthreshold somatic depolarization increases axonal calcium concentration and spontaneous vesicular release (Glitsch & Marty, 1999; Bouhours, Trigo, & Marty, 2011; Christie, Chiu, & Jahr, 2011). Consequences on subsequent evoked release involve an increase of the release probability (Bouhours et al., 2011; Christie et al., 2011). In view of these earlier results, we simulated $p = 1$ and $\rho = 0$, keeping the values of the remaining parameters. Under these conditions, the strong synaptic depression is well emulated, as in depolarizing prepulse of -50mV (Orange open circles in Figure 14B lower panel, right). Overall, the results suggest that r is given by a combination of ρ and r' . Variations in r due to depolarizing prepulse are tentatively related to a decrease in ρ .

From this preliminary interpretation, additional information can be obtained. The simulated cases, where ρ is 1 and r' is 0.13, are supposed to reflect the control conditions where r is 0.13 (dotted lines in Figure 15A). The simulated output was

compared with the experimental data obtained from elementary synapses, where in most of the experiments a dip in response at pulse number 2 was observed. However, the response probability along the simulated train was not comparable with the mean of responses from $N = 1$ data, as shown in the [Figure 15A](#) (-60mV; $n = 6$; black line). Moreover, by making $\rho = 1$ any effect on the response recovery kinetics was observed when s was iterated, the 2-step feature was vanished, tending more to a 1-step model. A better alternative was obtained when the replacement site was not always occupied ($\rho < 1$), for instance ρ at 0.5, in such case different effects on the success probabilities can be observed at the latest pulses when s is changing ([Figure 15B](#)). The results suggest that even in control conditions ρ is smaller than 1. This produces another degree of freedom, the response recovery from synaptic depression, which is governed by the magnitude of s . While this analysis is not sufficient to fully explain how the synaptic parameters are being modulated, it is an useful working hypothesis.

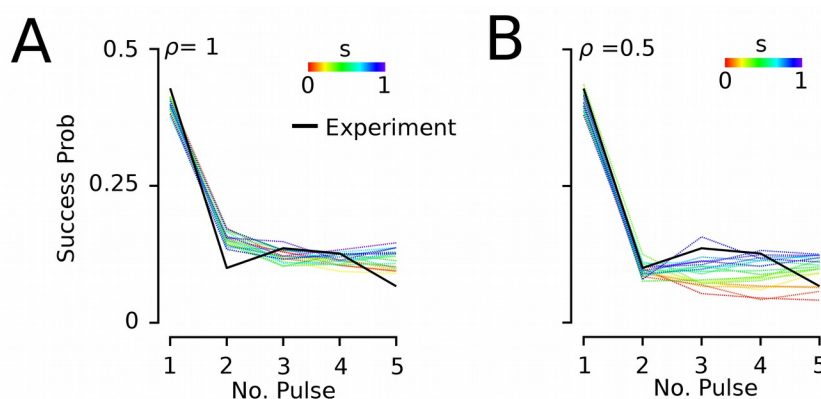


Figure 15. The replacement site may not be fully occupied in control conditions. Using the 2-step model, two more simulations were done iterating s from 0 to 1; with $r' = 0.13$, $p = 0.89$ and $\delta = 0.45$. The computed output (dotted lines) was compared against the mean of responses from experimental elementary synapses ($N = 1$) obtained at -60mV (black line). (A) When ρ was fixed at 1, a continuous declining response was observed when s was iterated. (B) Making ρ smaller than 1, for instance, 0.5 is enough to create a dip at pulse number 2, and response recovery at late pulse numbers for large values of s .

In summary, the results suggest that just adding a replacement site to the model is sufficient to get a recover in the responses at the latest pulses after a synaptic depression. This effect does not only apply to -50mV experiments, it has also been observed at -60mV. Additionally, the results tentatively suggest that the replacement

site is not fully occupied in control conditions. Rather, this replacement site may have an intermediate probability of occupancy, as we have also suggested concerning the docking site ($\delta = 0.45$).

Chapter 5: Developmental Changes In The Synaptic Connectivity Between Cerebellar Interneurons.

The regulation of changes in the neuronal circuits during development has been studied intensively in the last decades. It is of special interest to understand how the system regulates the number of cells in the pre- and postsynaptic population and the number of synaptic contacts between them (Purves & Lichtman, 1980). Traditionally, it has been thought that synapses are strengthening with development (Blue & Parnavelas, 1983; Miller, 1986), however there is extensive evidence that suggests the opposite. In various regions of the central and peripheral nervous system, the postsynaptic cells appear to be innervated by more axons in the early postnatal states than later on (Purves & Lichtman, 1980; Tapia et al., 2012).

In the neuromuscular junction of mature rodents, it has been shown that from the second postnatal week muscle fibers make the transition from double or triple innervations to their adult state of a single innervation (Tapia et al., 2012). Synapse elimination is also characteristic in the central nervous system; for instance, in the cerebellar cortex a decrease has been demonstrated in the number of climbing fibers innervating a Purkinje cell with development. In compensation to axonal loss, it has been also reported that the number of synaptic contacts from the remaining axons could increase with age (Purves & Lichtman, 1980).

These developmental synaptic changes raise a similar question on a more elementary scale: how does the increase in synaptic contacts from a remaining axon affect the synaptic strength? In the interneuron to Purkinje synapse, where presumably the number of varicosities made by a single interneuron increases with age, the impact of these changes on the strength of synaptic interactions was studied as a function of age (Pouzat & Hestrin, 1997). Interestingly, pair-recording experiments show a dramatic reduction with age in the amplitude of the evoked IPSCs and an increase in the number of failures in the Purkinje cell by the activity of

Developmental changes in the synaptic connectivity between cerebellar interneurons.

a single interneuron, which is unexpected when supposedly the number synaptic contacts increases. Moreover, using a classical paired-pulse ratio (PPR) protocol it was shown that with maturation paired-pulse depression is converted into paired-pulse facilitation, suggesting that the probability of release decreases with development. This result explains the apparent discrepancy between the increased synaptic contacts number and the decreased evoked IPSC amplitude.

Changes in the PPR and in the amount of failures could reflect a decrease in the release probability; however, it could also be directly related with a developmental change in the number of docking sites associated at each synaptic contact. We tried to study this hypothesis and we explored whether there is a change in the number of docking sites with development in cerebellar interneuron connected by a single site.

5.1 Docking site number decreases with development.

The simplest way to examine whether there is a synaptic change with age in interneurons is to study miniature postsynaptic currents. We recorded the mPSCs in presence of 100nM TTX from young (12-16 days old; n = 6) and adult rats (30-35 days old; n = 3). The amplitude histogram distribution plotted in the [Figure 16A](#) is left shifted for the events recorded from adult rats (red bars; mean = 72pA) compared with events from young rats (blue bars; mean = 119pA). This finding suggests a change in the synaptic connectivity with development.

In order to know whether the change in the synaptic connectivity is also related with a change in the number of vesicles released per site, simple synapse recordings are fundamental. In adult rats, the probability to find connected pairs dramatically decreases, presumably because the number of inputs in the postsynaptic side coming from different interneurons decreases with age ([Figure 16A](#)). In spite of that, six simple synapses were obtained following the same criteria as in young synaptic pairs. In the [Figure 16B](#) are presented three examples of amplitude distribution: two simple synapses in old rats (red; cell 1: mean = 47pA and CV = 0.3; cell 2: mean = 84pA and CV = 0.145) and one from an elementary synapse (N = 1) in young rat (blue; mean = 61pA and CV = 0.115). The three histograms can be fitted with a single Gaussian with a CV smaller than 0.3.

As in young rats, the presynaptic cells from adult animals were stimulated by 30 trains of five pulses, each were given at 25 Hz with 10s intervals between trains. The mean of the postsynaptic responses from the examples shown ([Figure 16B](#)) displays less depression and more failures compared to the younger animal (N=1; [Figure 16C](#)). Thus, the probability of success for younger rat was 66% for the first pulse, 17% for the second pulse and on average 11% for the third to fifth pulses; while in the case of adult rats the proportions were markedly different. In the cell 2, for instance, the probability of success for the first, second and the average of remaining pulses were 17%, 23.3% and 30%, respectively.

Group results show that success probability in adult rats is low for the first pulse (PS: 0.22 ± 0.053 ; $n = 6$; [Figure 16D](#), left panel) and it is maintained at that state along the train. In some cases facilitation occurs at the second pulse. This behavior is not comparable with any simple synapse from $N = 1$ to $N = 6$ obtained at younger ages, which are shown in light blue- dotted line. The average values of the paired-pulse ratio calculated as the ratio $P(S_{3-5})/P(S_1)$ were 0.35 ± 0.022 at P12-P16 and 1.08 ± 0.15 at P30-P35; this difference was significant ($p < 0.001$; right panel in [Figure 16D](#)). As was already reported for other synapses (Pouzat & Hestrin, 1997), the PPR in MLI synapses also turns from depression to facilitation with age. Paired-pulse facilitation is however not envisaged in our binomial model. Rather, the calculation of docking sites number is based on the measurements of $P(F_2)$ and $P(F_1)$ assuming paired-pulse depression. Therefore, the situation found in the adult precludes the use of the model proposed in the paper to calculate the number of docking sites. An alternative could be an extension of the method presented in the [Figure 12](#).

In [Figure 16E](#), the mean peak PSC amplitude of successful responses for the first pulse is plotted as a function of N, in the case of younger rats, and as a group result in the case of adults. As shown in the paper mean amplitude increases with N at P12-P16 animals ($N1 = 68\text{pA} \pm 8.1$; $N2 = 88\text{pA} \pm 10$; $N3 = 116 \pm 24.4$; $N4 = 162 \pm 29.7$; $N6 = 162 \pm 10.5$), while in P30-P35 rats the distribution of the means remains at small values (mean: $80\text{pA} \pm 23.11$), significantly different from young synapses with $N \geq 3$ ($p < 0.05$), and comparable with values obtained at $N \leq 2$. This result raises the possibility that synaptic contacts in adult rat have a reduced number of docking sites;

Developmental changes in the synaptic connectivity between cerebellar interneurons.

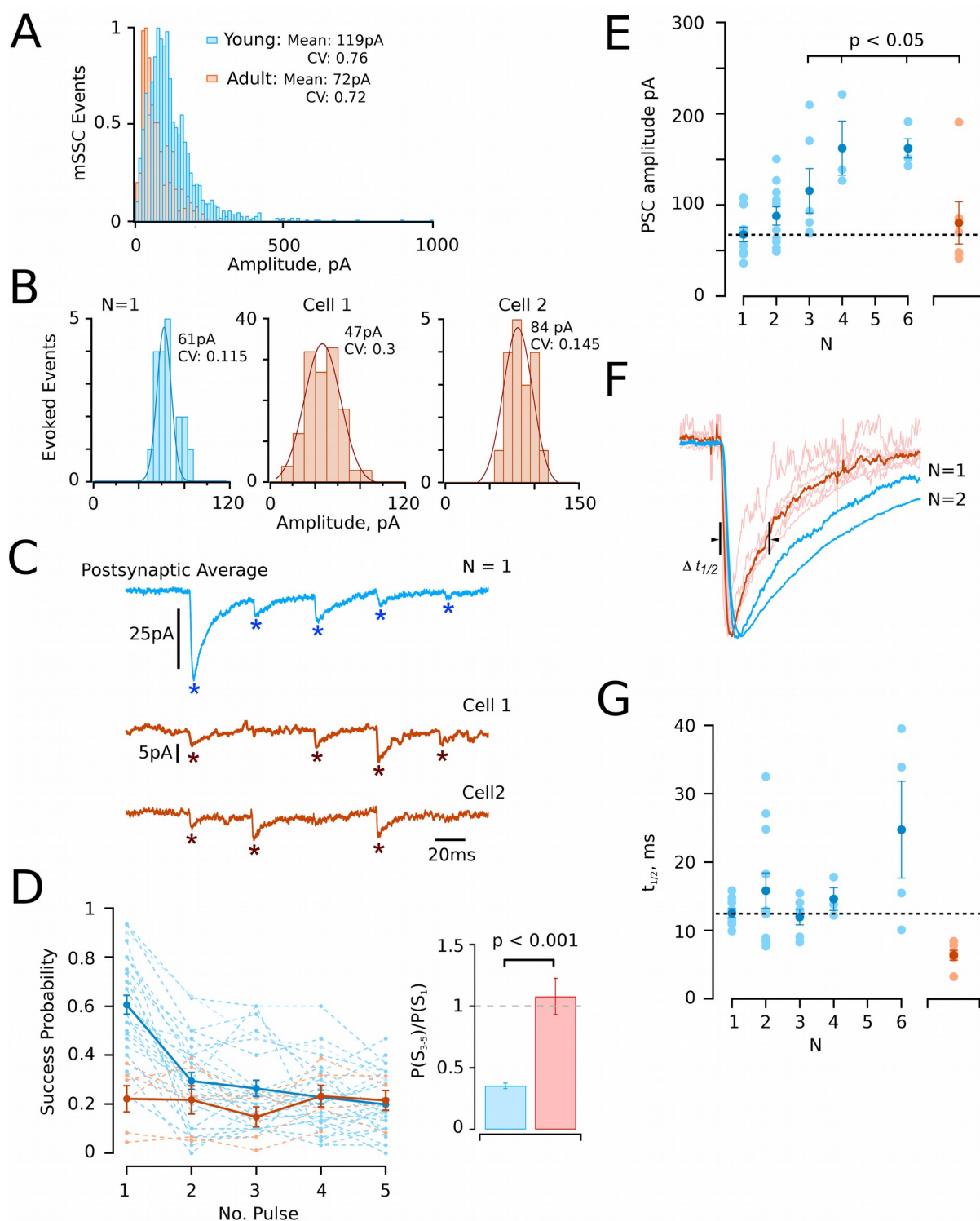


Figure 16. Developmental changes in synaptic parameters. (A) Histogram of amplitude distribution of mPSCs recorded in TTX (100nM) from adult rats (P30-P35; red bars) and younger rats (P12-16; blue bars). (B) Histograms of first peak PSC amplitudes from three examples of connected interneurons: one in younger rat (blue) and two in adult (red). Single Gaussian fits with low CV are diagnostic of a single synaptic site, called “simple synapse”. (C) Average PSCs (30 consecutive trials), showing a clear synaptic depression in the case of younger rats; and a tendency for synaptic →

nevertheless there was one pair with a larger mean amplitude, close to ~ 200 pA.

We tentatively assumed that adult synaptic contacts have a decreased number of docking sites, close to $N = 2$; if so, the mean number of vesicles released per successful event should be also comparable with results obtained with $N \leq 2$ young synapses. In the paper, we showed that differences in multivesicular release exert a significant effect on PSC kinetics; thus the half time of PSC decay, $t_{1/2}$, in adult responses should be comparable to values obtained for small N young synapses. However, this was not the case, the PSC decay kinetics are faster, even when they are compared with responses from elementary synapses (Figure 16F). The group results show that the mean $t_{1/2}$ value from P30-P35 is significantly smaller than the $t_{1/2}$ calculated as a function of N , and it is also significantly different from $N = 1$ ($p < 0.0001$; Figure 16G). These results are in agreement with findings made in other types of GABAergic synapses, where it has been shown that in the GABA receptors there is a decrease in α_3 and an increase in α_1 subunits expression during development, resulting in a faster mIPSC decay (Barberis et al., 2005). Thus, the results not only suggest that likely the number of docking sites decreases, but also that there is a change in postsynaptic receptor with age.

In summary, these results are in concordance with previous findings, where it was shown that during maturation paired-pulse depression is converted to paired-pulse facilitation and the probability of release decreases (Pouzat & Hestrin, 1997).

facilitation in the case of adult rats. The traces shown are from the experiments shown in A. (D) Probability of success of the experimental data from younger (blue) and adult rats (red) is plotted as a function of stimulus number (inter-stimulus interval: 40ms). In the case of P12-P15 traces, release probability at the first pulse is high and from the second pulse synaptic depression occurs. In the case of P30-P35, release probability was maintained at low values along the stimulation train. Sometimes, an increase in $P(S)$ was observed in the latest pulses. (E) Plot of mean peak PSC amplitude of successful responses at the first pulse as a function of N in the case of younger rat (blue) and as a group in adult results (red). The data show that adult responses are similar to the results coming from small synapses ($N \leq 2$) in younger rat. (F) Variations in the kinetics of decay in normalized mean PSC traces in response to the first stimulus of a train. The mean trace (Red line) of all the simple synapses obtained in old animals (light red lines) has a faster decay in comparison with two examples of young animal of $N = 1$ and $N = 2$ (blue lines) (G) Comparison of $t_{1/2}$ values of PSC decay kinetics for simple synapses. The $t_{1/2}$ mean value obtained for adult animals is significantly smaller, even compared with the values obtained in $N = 1$ synapses (dotted line; $p < 0.0001$).

Developmental changes in the synaptic connectivity between cerebellar interneurons.

Moreover, the present results suggest that a developmental reduction in the number of docking sites presumably contributes to the decrease of the postsynaptic current amplitude and success probabilities. However several other factors, both presynaptic and postsynaptic, may play a role, and the results and analysis here presented are not sufficient to reach a definitive conclusion.

DISCUSSION

Looking for the building block of central synaptic transmission has not been a trivial issue; on the contrary, during decades this issue has been in the center of heated discussion. Along this thesis, I was happy to share with you our findings suggesting that docking sites (alternatively called release sites) are the pivotal structures of vesicular release. Our results show that variations among single synapses mainly arise from differing docking site numbers, and that the number of docking sites grows with the synaptic size. Furthermore, our findings suggest a novel model of vesicular release supposing two sites in sequence: a replacement site and a docking site.

1.1 Importance of single synaptic contact recordings and docking sites calculation.

Different methods have been developed in order to calculate the RRP and the docking sites number (N; Rizzoli & Betz, 2005). However, accurate determinations of N and of the RRP are difficult, particularly at large, multisite synapses. This makes the relation between N and RRP size uncertain. Yet determining this relation is essential to develop a quantitative picture of synaptic function at the level of a single active zone.

In the present thesis, we proposed the cerebellar MLIs single synaptic connection as an experimental model to directly estimate the number of docking sites in a given active zone. This synaptic model, previously described by Auger et al. and Kondo et al., features: first, the possibility to discern single synaptic contacts (amplitude distributions fitted by a single Gaussian); second, a high percentage of postsynaptic receptor saturation following release of a single vesicle; and third, multivesicular release in a single active zone.

MLI single contacts (simple synapses) were used as an experimental approach to propose a synaptic model based on a fixed number of independent docking sites. We proposed a probabilistic model to calculate the RRP and the number of docking sites,

DISCUSSION

which is based on the probability of failures between the first two pulses of a train at 25Hz. In addition, a binomial model of simple synapses was proposed to estimate additional synaptic parameters such as release probability (p), initial docking site occupancy (δ) and probability of recovery (r). Our results support the idea that functional variability among synaptic contacts is directly explained by a variation in the docking site number.

Furthermore, our findings reveal for the first time, that docking site occupancy at rest is less than 1 and that it can be modulated by the amount of spontaneous vesicular release that precedes the evoked action potential ([Figure 13](#)). Of course, alternative explanations have to be considered. In summary, these results imply that initial synaptic release is a process governed by two rate constants, and not by one as was typically assumed: exocytosis with probability, p and docking site occupancy with probability δ .

1.2 An extension of the Variance-mean fluctuation analysis method.

Variance-mean fluctuation analysis of the postsynaptic current amplitudes is a well known method to estimate N and to extract additional synaptic information (Clements & Silver, 2000). However, in cases of high postsynaptic receptor saturation, where it has been used (see: Biró et al., 2006), PSC amplitudes are not necessarily proportional to the number of released vesicles. Yet variance-mean fluctuation analysis is an excellent approach to study synaptic plasticity. Here we showed a new variant of this method which has been developed by Malagon et al. and Miki et al. (submitted manuscripts). Instead of measuring fluctuations in the PSC responses at a multi-connected synapse, the fluctuations analysis is directly made on the number of released quanta at a single synapse. The released vesicles are counted following each action potential. This method offers two advantages: first, possible errors linked to receptor saturation are minimized; second, the fluctuations of the counted vesicles compared to the mean signals are maximized, since the variance/mean ratio is inversely proportional to the number of synaptic units.

In this work, we tried to extend this new method to GABAergic synapses and to study the processes underlying docking site replenishment during trains. In GABAergic

single synaptic contacts, we are able to estimate the number of docking sites. If this number is larger than 1, we cannot count quantal released units per action potential due to postsynaptic receptor saturation. However if there is a single docking site (in which case the synapse is called an elementary synapse) receptor saturation does not matter since each evoked response represents one vesicle. Elementary synapses are of special interest since their release statistics are particularly simple. This situation is exploited along this thesis work in many ways ([Figure 3](#) from the paper, [Figure 14](#) and [Figure 15](#)) and now, it is used to implement the new fluctuations analysis method ([Figure 12](#)).

The basic variance-mean analysis of counted vesicles per action potential gives information on docking site number and release probability. In the elementary synapses the estimated $N1$ value was 1, as expected, confirming that the binomial model and fluctuation analysis methods used to calculate the number of docking sites are both in agreement. Additionally, fluctuations of the cumulative release evoked by a series of APs provides information on the organization of the RRP and on its mechanisms of replenishment. In this case, the fitted parabola predicted twice the docking site number ($N2 = 1.8 \pm 0.3$; $n = 7$; [Figure 12E](#)). These results are consistent with a model supposing two sites in sequence, a replacement site and a docking site; which is the current synaptic release model proposed by Miki et al. at the glutamatergic PF-MLI synapses. Altogether, our release model is also in agreement with the fast and slow releasable vesicle pools proposed at different synaptic families (Sakaba & Neher, 2001; Sakaba, 2006; Lee et al., 2012). However, this 2-step model seems at odds with the results reported in Trigo et al. (2012), where kinetics of RRP release appear monophasic instead of biphasic. This disagreement can be presumably attributed to a heterogeneous intracellular calcium contractions in different experiments, but additionally, by the analysis itself which takes in account docked vesicles instead the real number of docking sites. Further experiments involving calcium uncaging at different concentration of EGTA may be needed in order to obtain a biphasic cumulative release, as shown in the calyx of Held.

1.3 2-step Model and its implications in short-term synaptic depression and recovery.

Synaptic depression occurs when the RRP is highly depleted at the first pulse of a train and the replenishment rate is not fast enough to recover the RRP before the arrival of a second action potential (Regehr, 2012). Recovery from synaptic depression is enhanced by high-frequency stimulation of the presynaptic terminal (Dittman & Regehr, 1998; Sakaba & Neher, 2001). In our results, a strong response depression is observed at the second pulse of stimulation, followed by a response recovery from depression mainly since the third stimulation pulse. We observed that short-term synaptic depression and recovery is highly dependent on N . However, even in the most extreme cases of depression, recovery is still occurring. At elementary synapses, for instance, where the amount of depression is highest, there is still, on average, response recovery starting at the third pulse ($P(S1) = 0.43 \pm 0.06$, $P(S2) = 0.1 \pm 0.03$, $P(S3) = 0.14 \pm 0.03$, $P(S4) = 0.13 \pm 0.04$ and $P(S5) = 0.07 \pm 0.02$; $n = 6$; black line in [Figure 15](#)).

In order to have a better understanding of synaptic response recovery, we explored different models of release based on Monte Carlo simulations of elementary synapses. We examined first, a 1-step model of release: After releasing a vesicle following the arrival of an action potential, the refilling vesicle comes directly from a large pool of vesicles, so that the docking site recovery only depends on the recovery probability, r . The 1-step model is illustrated in [Figure 14A](#), and it does not reveal any evidence of recovery from depression along the pulses. Apparently, a simple vesicle pool depletion model cannot explain synaptic depression and recovery.

Work in the calyx of Held suggested the existence of fast and slow sets of releasable vesicles, where calmodulin-dependent refilling supports recovery from synaptic depression by a rapid recovery of the slowly releasing vesicles (Sakaba & Neher, 2001). We have examined whether the introduction of slow and fast vesicles could explain recovery from synaptic depression. Therefore, we explored a 2-step model of exocytosis based on the results presented on [Figure 12](#). The 2-step model posits that empty docking sites are not directly replenished from a large pool, as is commonly assumed, but from a small, most probably very local pool of replacement vesicles

(Figure 14B). This alternative model correlates with models of vesicle tethering cytomatrix proteins, where it is suggested that filamentous structures may play a role in vesicle reloading (Nagwaney et al., 2009; Hallermann et al., 2010; Szule et al., 2012; Hallermann & Silver, 2013).

During a train of stimulation, we suggest that success at the first pulse involves the fast-releasing vesicles, with a probability governed just by two rate constants: p and δ . Whereas the conditional probability to observe a success in response to the second pulse given that a success was obtained in response to the first pulse ($P(S_2|S_1)$) is governed by three additional constant rates: docking site recovery (r'), recruitment site occupancy (ρ) and recovery (s), which slow down the process of release. We associate these late responses with the slow-releasing pool.

Altogether, we showed that the amount of synaptic depression is given by ρ , and the recovery from depression is given by s (Figure 14B bottom plots). Additionally, our model supposes that ρ is less than 1 at rest, otherwise recovery would not occur (Figure 15A). It is important to highlight that our synaptic release model assumes independence between docking sites, implying that synaptic depression is also decreased as the total number of docking sites per active zone increases. The mean paired pulse ratio at elementary synapses ($N=1$) was 0.313 ± 0.056 while at $N = 6$, where the RRP and the probability of success at the second pulse is supposed to be higher, was 0.674 ± 0.02 .

1.4 Spontaneous release offers a way of modulating ρ , the occupancy of the recruitment site.

Our results reveal that application of a depolarizing presynaptic prepulse results in reduced docking site occupancy during subsequent trains. This decrease in occupancy is a consequence of a slow down in the recovery rate along the train. As an explanation, we showed a correlation between the increase in spontaneous postsynaptic currents (sPSCs) with depolarization (Figure 13C) and the faults in evoked release. This finding suggests that spontaneous and evoked release share a common synaptic path, in agreement with previous reports (Kaeser & Regehr, 2014; Schneggenburger & Rosenmund, 2015). However, this effect was only significant when the number of sPSCs in a trial was higher than the mean of sPSCs observed in

DISCUSSION

that experiment ([Figure 13D](#)). Presumably there is a threshold in the number of spontaneous events that affects evoked release.

From these findings, we could expect that the probability of success at the first pulse (PS1) would be affected by the potential prepulse, however this was not the case. PS1 did not significantly vary with holding potential ([Figure 7B](#) upper plot, from the paper). To propose an explanation, we have to consider two previously mentioned findings: first, PS1 is governed by two rate constants, ρ and δ ; and second, the existence of a recruitment site preceding the docking site (2-step synaptic release model). Thus, the augmentation of spontaneous release prevents an increase in PS1, because the RRP is being continuously depleted previous to the action potential arrival. In consequence, the recruitment site is continuously providing vesicles to the empty docking site, preventing a dramatic decrease in PS1. In summary, the balance between the spontaneous release frequency and recovery rate of the docking site with vesicles coming from the recruitment site, maintains in a dynamic equilibrium the initial PS.

Our findings suggest that in a high release probability condition as in the depolarizing prepulse, the recruitment site is actively providing vesicles to the docking site, which necessarily induces a decrease in the initial occupancy of the recruitment site, ρ . The Monte Carlo simulations shown in the [Figure 14B](#) suggest that decreases in ρ value is associated with strong paired-pulse depression effects. From our experimental results we found a decrease in the PPR with depolarization (at -80 mV: 0.64 ± 0.08 ; at -60 mV: 0.31 ± 0.08 ; at -50 mV: 0.17 ± 0.04 ; $n = 9$; effects of hyper- and depolarizing prepulses are significant at $p < 0.01$ and $p < 0.05$). This tentatively suggests that the high degree of depression obtained at -50mV prepulse is a consequence of an initial low occupancy in the recruitment site.

The results shown in this section are promising but are still preliminary, the suggested conclusions are tentative. It will be interesting in future work to investigate whether evoked release is affected by an increase in the rate of spontaneous release (“burst-like”) that exceeds the rate of recovery, rather than a net increase in the number of events. Maybe just the last seconds previous to the evoked action potential are crucial to have an effect on the evoked release.

CONCLUDING REMARKS

Synaptic vesicular release is a highly demanding energy process. Around 24,000 ATP molecules are used presynaptically when a vesicle is released (Harris, Jolivet, & Attwell, 2012). Clearing away calcium and neurotransmitter, and carrying several coordinated interactions between proteins and lipids involved in exocytosis are ATP-dependent processes. Waisting energy is not an option in biological processes, therefore, vesicular release should be highly regulated and limited; with the arrival of an action potential, vesicles cannot be released indiscriminately. As a solution, nature has designed specialized sites in the active zone where vesicular release occurs, the docking sites (originally called release sites). The number of docking sites in a given active zone is limited and in most of the synapses this number is small. In the present thesis, we proposed a model to estimate the number of docking sites in cerebellar MLIs, based on the assumption that at each active zone there is a fixed number of docking sites, which are independent of each other. We found that docking sites at MLIs are in low number, varying between 1 to 6 among active zones.

The existence of docking sites is not just a matter of saving energy, they are the building blocks of synaptic transmission; and their functional role is crucial for the faithful transmission of information, especially in the case of high frequency activity. Thus, docking site modulation is a key step in synaptic plasticity. As we showed here, variations among active zones mainly arise from differing docking site numbers, which account for differences in release probability, as well as in the amplitude and decay kinetics of unitary postsynaptic currents. Presumably, these differences in docking sites number determine intersynaptic variability and moreover, their probability of occupancy is a key parameter controlling single synapse signaling.

Given the low docking site number and the high rate of synaptic activity from some synapses, each docking site has to be rapidly supplied. To face this demand, a secondary vesicle is tethered to the docking site, ready to be used as soon as the primed one is gone. Our results are consistent with this model supposing two sites in

CONCLUDING REMARKS

sequence: a replacement site and a docking site; this mechanism allows a fast response recovery after a high frequency stimulation. Just to keep going!

In a broader perspective, the vesicular release machinery, with its highly coordinated series of proteic, lipidic and molecular interactions, is a complex structure that is difficult to study. 60 years after the discovery of quantal transmission, and we are still along the way... but building knowledge requires solid bases started by others, from which we will continue building. We should not hurry to understand a complex process quickly, errors come promptly if the desire to publish is too high. The results that I presented to you along this thesis are not solving the whole synaptic transmission panorama, but they contribute to its understanding. It just makes me happy to think that our findings, here presented, could be the start of the study of someone else.

PERSPECTIVES

It has been hypothesized that reluctant vesicles are recruited in an actin-dependent manner to become fast-releasing vesicles once these are depleted by a short depolarization (Sakaba & Neher, 2001; Lee et al., 2012). The conversion of slow-releasing vesicles into fast-releasing vesicles may involve the movement of vesicles closer to calcium channels (Neher & Sakaba, 2008). This movement could be made by the filaments tethering the vesicles. It has been shown that deletion in proteins involved in vesicle tethering affects the fast component of recovery from synaptic depression, suggesting that tether filaments support vesicle reloading (Hallermann et al., 2010; Hallermann & Silver, 2013).

Recovery from depression is a calmodulin-dependent process (Sakaba & Neher, 2001), which involves activation of myosin light-chain kinase (MLCK) and an increase of the proportion of fast-releasing vesicles to slow-releasing vesicles. In other words, the MLCK-dependent activation of myosin II regulates the dynamic equilibrium between fast and slow-releasing pools (Lee et al., 2012). Therefore, it will be interesting in future work to investigate whether manipulation of the myosin signaling pathway changes the recovery rate and/or remaining synaptic parameters that promotes vesicular release.

Lysophosphatidic acid (LPAs) is a major member of the lysophospholipids family, which is present in different tissues, including the nervous system (Yung et al., 2015). It has been shown that LPA increases myosin light-chain phosphorylation via LPA1/ Gai/o-protein/ phospholipase C/ MLCK cascade at the presynaptic site, which is known to trigger actomyosin contraction and to induce depression at excitatory synapses (García-Morales et al., 2015). The effect caused by LPA would be comparable to the calmodulin-dependent activation of MLCK, and it may increase the proportion of fast-releasing vesicles to slow-releasing vesicles.

Previously, it was shown that in hypoglossal motoneurons, LPA signaling modulates

PERSPECTIVES

excitatory synaptic transmission through a presynaptic mechanism (García-Morales et al., 2015). Following these findings, we plan to use LPA as a modulator of the response recovery during a train of stimulation. We have therefore performed preliminary experiments exploring LPA effects on the spontaneous release in MLIs. The number of spontaneous events were counted in the presence of TTX [$1\mu\text{M}$] and with and without LPA [$2.5\mu\text{M}$]. GABAergic and glutamatergic events were distinguished by their kinetics. Group results reveal that after normalization with respect to the number of events in control, LPA has a potentiating effect on mEPSC frequency but not on mGPSC (respective mean values: 1.27 ± 0.55 events, and 0.005 ± 0.11 events, $n = 13$; $p < 0.05$). In the case of the spontaneous release amplitude distribution no significant difference was found. This increase in glutamatergic spontaneous events in presence of LPA, opens a new potential way of modulating synaptic release; and it would be interesting to explore whether LPA has a direct effect on the recruitment site, which is represented by the slow-releasing pool.

In the case of GABAergic synapses, we already used depolarization prepulse as a synaptic modulator. Likewise, the increase in spontaneous activity previous to stimulation is a promising alternative that we are interested in exploring further.

BIBLIOGRAPHY

- Abenavoli, A., Forti, L., Bossi, M., Bergamaschi, A., Villa, A., & Malgaroli, A. (2002). Multimodal quantal release at individual hippocampal synapses: evidence for no lateral inhibition. *J. Neurosci.*, *22*(15), 6336–6346.
- Acheson, G. H. (1948). Physiology of neuro-muscular junctions; chemical aspects. *Fed. Proc.*, *7*(3), 447–57.
- Acuna, C., Liu, X., Su, T. C., Acuna, C., Liu, X., Gonzalez, A., & Su, T. C. (2015). RIM-BPs Mediate Tight Coupling of Action Potentials to Ca²⁺-Triggered Neurotransmitter Release. *Neuron*, *87*, 1234–1247.
- Auger, C., Kondo, S., & Marty, A. (1998). Multivesicular release at single functional synaptic sites in cerebellar stellate and basket cells. *J. Neurosci.*, *18*(12), 4532–47.
- Auger, C., & Marty, A. (1997). Heterogeneity of functional synaptic parameters among single release sites. *Neuron*, *19*(1), 139–50.
- Balakrishnan, V., Kuo, S. P., Roberts, P. D., & Trussell, L. O. (2009). Slow glycinergic transmission mediated by transmitter pooling. *Nature Neuroscience*, *12*(3), 286–94.
- Barberis, A., Lu, C., Vicini, S., & Mozrzymas, J. W. (2005). Developmental changes of GABA synaptic transient in cerebellar granule cells. *Molecular Pharmacology*, *67*(4), 1221–1228.
- Barbour, B., & Häusser, M. (1997). Intersynaptic diffusion of neurotransmitter. *Trends in Neurosciences*, *20*(9), 377–384.
- Biró, A. a, Holderith, N. B., & Nusser, Z. (2006). Release probability-dependent scaling of the postsynaptic responses at single hippocampal GABAergic synapses. *J. Neurosci.*, *26*(48), 12487–96.
- Blot, A., & Barbour, B. (2014). Ultra-rapid axon-axon ephaptic inhibition of cerebellar Purkinje cells by the pinceau. *Nature Neuroscience*, *17*(2), 289–295.
- Blue, M. E., & Parnavelas, J. G. (1983). The formation and maturation of synapses in the visual cortex of the rat. II. Quantitative analysis. *Journal of Neurocytology*, *12*(4), 697–712.

BIBLIOGRAPHY

- Bollmann, J. H., Sakmann, B., & Borst, J. G. (2000). Calcium sensitivity of glutamate release in a calyx-type terminal. *Science*, *289*(5481), 953–957.
- Bouhours, B., Trigo, F. F., & Marty, A. (2011). Somatic depolarization enhances GABA release in cerebellar interneurons via a calcium/protein kinase C pathway. *J. Neurosci.*, *31*(15), 5804–15.
- Branco, T., & Staras, K. (2009). The probability of neurotransmitter release: variability and feedback control at single synapses. *Nature Reviews. Neuroscience*, *10*(5), 373–83.
- Bucurenciu, I., Kulik, A., Schwaller, B., Frotscher, M., & Jonas, P. (2008). Nanodomain coupling between Ca²⁺ channels and Ca²⁺ sensors promotes fast and efficient transmitter release at a cortical GABAergic synapse. *Neuron*, *57*(4), 536–45.
- Christie, J. M., Chiu, D. N., & Jahr, C. E. (2011). Ca²⁺-dependent enhancement of release by subthreshold somatic depolarization. *Nature Neuroscience*, *14*(1), 62–68.
- Clements, J. D., & Silver, R. A. (2000). Unveiling synaptic plasticity: A new graphical and analytical approach. *Trends in Neurosciences*, *23*(3), 105–113.
- Couteaux, R., & Pécot-Dechavassine, M. (1970). Synaptic vesicles and pouches at the level of “active zones” of the neuromuscular junction. *C. R. Hebd. Séances Acad. Sci.*, *271*(25), 2346–9.
- De Robertis, E. D. P., & Bennett, H. S. (1955). Some features of the submicroscopic morphology of synapses in frog and earthworm. *J. Biophys. Biochem. Cytol.*, *1*(1), 47–58.
- Del Castillo, J., & Engbaek, L. (1954). The nature of the neuromuscular block produced by magnesium. *J. Physiol.*, *124*(2), 370–84.
- Del Castillo, J., & Katz, B. (1954). Quantal components of the end-plate potential. *J. Physiol.*, *124*, 560–573.
- Del Castillo, J., & Katz, B. (1956). Localization of active spots within the neuromuscular junction of the frog. *J. Physiol.*, *132*, 630–649.
- Dittman, J. S., & Regehr, W. G. (1998). Calcium dependence and recovery kinetics of presynaptic depression at the climbing fiber to Purkinje cell synapse. *J. Neurosci.*, *18*(16), 6147–62.
- Dobrunz, L. E., & Stevens, C. F. (1997). Heterogeneity of release probability, facilitation, and depletion at central synapses. *Neuron*, *18*(6), 995–1008.
- Falk-Vairant, J., Correges, P., Eder-Colli, L., Salem, N., Roulet, E., Bloc, A., ...

- Dunant, Y. (1996). Quantal acetylcholine release induced by mediatophore transfection. *Proc. Natl. Acad. Sci.*, 93(11), 5203–5207.
- Fatt, B. Y. P., & Katz, B. (1952). Spontaneous subthreshold activity at motor nerve endings. *J. Physiol.*, 117, 109–128.
- Fredj, N. Ben, & Burrone, J. (2009). A resting pool of vesicles is responsible for spontaneous vesicle fusion at the synapse. *Nature Neuroscience*, 12(6), 751–8.
- García-Morales, V., Montero, F., González-Forero, D., Rodríguez-Bey, G., Gómez-Pérez, L., Medialdea-Wandossell, M. J., ... Moreno-López, B. (2015). Membrane-Derived Phospholipids Control Synaptic Neurotransmission and Plasticity. *PLOS Biology*, 13(5), e1002153.
- Glitsch, M., & Marty, A. (1999). Presynaptic effects of NMDA in cerebellar Purkinje cells and interneurons. *J. Neurosci.*, 19(2), 511–519.
- Hallermann, S., Fejtova, A., Schmidt, H., Weyhersmüller, A., Silver, R. A., Gundelfinger, E. D., & Eilers, J. (2010). Bassoon speeds vesicle reloading at a central excitatory synapse. *Neuron*, 68(4), 710–723.
- Hallermann, S., & Silver, R. A. (2013). Sustaining rapid vesicular release at active zones: potential roles for vesicle tethering. *Trends in Neurosciences*, 36(3), 185–194.
- Hamill, O. P., Marty, A., Neher, E., Sakmann, B., & Sigworth, F. J. (1981). Improved patch-clamp techniques for high-resolution current recording from cells and cell-free membrane patches. *Pflügers Archiv: European Journal of Physiology*, 391(2), 85–100.
- Harris, J. J., Jolivet, R., & Attwell, D. (2012). Synaptic Energy Use and Supply. *Neuron*, 75(5), 762–777. doi:10.1016/j.neuron.2012.08.019
- Haucke, V., Neher, E., & Sigrist, S. J. (2011). Protein scaffolds in the coupling of synaptic exocytosis and endocytosis. *Nature Reviews Neuroscience*, 12(3), 127–138.
- Heuser, J. E., & Reese, T. (1973). Evidence for recycling synaptic vesicle membrane during neurotransmitter release at the frog neuromuscular junction. *J Cell Biol*, 57, 315–344.
- Holderith, N., Lorincz, A., Katona, G., Rózsa, B., Kulik, A., Watanabe, M., & Nusser, Z. (2012). Release probability of hippocampal glutamatergic terminals scales with the size of the active zone. *Nature Neuroscience*, 15(7), 988–97.
- Holzmann, E., Freeman, A., & Kashner, L. (1971). Stimulation-Dependent Alterations in Peroxidase Uptake at Lobster Neuromuscular Junctions. *Science*, 20(August),

BIBLIOGRAPHY

733–736.

- Horrigan, F. T., & Bookman, R. J. (1994). Releasable pools and the kinetics of exocytosis in adrenal chromaffin cells. *Neuron*, *13*(5), 1119–1129.
- Hurlbut, W. P., Iezzi, N., & Ceccarelli, B. (1990). Correlation between quantal secretion and vesicle loss at the frog neuromuscular junction. *J. Physiol.*, *425*, 501–526.
- Jack, J. J., Redman, S. J., & Wong, K. (1981). The components of synaptic potentials evoked in cat spinal motoneurons by impulses in single group Ia afferents. *J. Physiol.*, *321*, 65–96.
- Kaesler, P. S., & Regehr, W. G. (2014). Molecular mechanisms for synchronous, asynchronous, and spontaneous neurotransmitter release. *Annual Review of Physiology*, *76*, 333–63.
- Katz, B. (1969). *The release of neuronal transmitter substances*. (Liverpool University Press, Ed.). Liverpool.
- Kondo, S., & Marty, A. (1998). Synaptic currents at individual connections among stellate cells in rat cerebellar slices. *J. Physiol.*, *509*(1), 221–232.
- Korn, H., & Faber, D. S. (1991). Quantal analysis and synaptic efficacy in the CNS. *Trends Neurosci.*, *14*(10), 439–445.
- Kriebel, M. E., & Gross, C. E. (1974). Multimodal distribution of frog miniature endplate potentials in adult denervated and tadpole leg muscle. *J. Gen. Physiol.*, *64*(1), 85–103.
- Kuno, M. (1964). Quantal components of excitatory synaptic potentials in spinal motoneurons. *J. Physiol.*, *175*, 81–99.
- Lee, J. S., Ho, W.-K., & Lee, S.-H. (2012). Actin-dependent rapid recruitment of reluctant synaptic vesicles into a fast-releasing vesicle pool. *Proc. Natl. Acad. Sci.*, *109*(13), E765–74.
- Llano, I., & Gerschenfeld, H. M. (1993). Inhibitory synaptic currents in stellate cells of rat cerebellar slices. *J. Physiol.*, *468*, 177–200.
- Llano, I., Marty, A., Armstrong, C. M., & Konnerth, A. (1991). Synaptic- and agonist-induced excitatory currents of Purkinje cells in rat cerebellar slices. *J. Physiol.*, *434*(1), 183–213.
- Llinás, R., Steinberg, I. Z., & Walton, K. (1981). Relationship between presynaptic calcium current and postsynaptic potential in squid giant synapse. *Biophys J*, *33*(3), 323–351.

- Miller, M. W. (1986). Maturation of rat visual cortex. III. Postnatal morphogenesis and synaptogenesis of local circuit neurons. *Brain Research*, 390(2), 271–85.
- Nagwaney, S., Harlow, M. L., Jung, J. H., Szule, J. a, Ress, D., Xu, J., ... McMahan, U. J. (2009). Macromolecular connections of active zone material to docked synaptic vesicles and presynaptic membrane at neuromuscular junctions of mouse. *J. Comp. Neurol.*, 513(5), 457–468.
- Nakamura, Y., Harada, H., Kamasawa, N., Matsui, K., Rothman, J. S., Shigemoto, R., ... Takahashi, T. (2015). Nanoscale distribution of presynaptic Ca(2+) channels and its impact on vesicular release during development. *Neuron*, 85(1), 145–58.
- Neher, E. (2010). What is Rate-Limiting during Sustained Synaptic Activity: Vesicle Supply or the Availability of Release Sites. *Front Synaptic Neurosci*, 2(September), 144.
- Neher, E., & Marty, A. (1982). Discrete changes of cell membrane capacitance observed under conditions of enhanced secretion in bovine adrenal chromaffin cells. *Proc. Natl. Acad. Sci.*, 79(21), 6712–6716.
- Neher, E., & Sakaba, T. (2008). Multiple roles of calcium ions in the regulation of neurotransmitter release. *Neuron*, 59(6), 861–72.
- Pouzat, C., & Hestrin, S. (1997). Developmental regulation of basket/stellate cell-->Purkinje cell synapses in the cerebellum. *J. Neurosci.*, 17(23), 9104–9112.
- Purves, D., & Lichtman, J. W. (1980). Elimination of synapses in the developing nervous system. *Science (New York, N.Y.)*, 210(4466), 153–157.
- Ramirez, D. M. O., Khvotchev, M., Trauterman, B., & Kavalali, E. T. (2012). Vti1a identifies a vesicle pool that preferentially recycles at rest and maintains spontaneous neurotransmission. *Neuron*, 73(1), 121–34.
- Redman, S. (1990). Quantal analysis of synaptic potentials in neurons of the central nervous system. *Physiological Reviews*, 70(1), 165–98.
- Redman, S., & Walmsley, B. (1983). Amplitude fluctuations in synaptic potentials evoked in cat spinal motoneurons at identified group Ia synapses. *J. Physiol.*, 343, 135–145.
- Regehr, W. G. (2012). Short-term presynaptic plasticity. *Cold Spring Harbor Perspectives in Biology*, 4(7), a005702.
- Ritzau-Jost, A., Delvendahl, I., Rings, A., Byczkowicz, N., Harada, H., Shigemoto, R., ... Hallermann, S. (2014). Ultrafast Action Potentials Mediate Kilohertz Signaling at a Central Synapse. *Neuron*, 84(1), 152–163.
- Rizzoli, S. O., & Betz, W. J. (2005). Synaptic vesicle pools. *Nature Reviews*.

BIBLIOGRAPHY

- Neuroscience*, 6(1), 57–69.
- Rudolph, S., Tsai, M.-C., von Gersdorff, H., & Wadiche, J. I. (2015). The ubiquitous nature of multivesicular release. *Trends in Neurosciences*, 1–11.
- Sakaba, T. (2006). Roles of the Fast-Releasing and the Slowly Releasing Vesicles in Synaptic Transmission at the Calyx of Held. *J. Neurosci.*, 26(22), 5863–5871.
- Sakaba, T., & Neher, E. (2001). Calmodulin mediates rapid recruitment of fast-releasing synaptic vesicles at a calyx-type synapse. *Neuron*, 32(6), 1119–1131.
- Scanziani, M., Salin, P. A., Vogt, K. E., Malenka, R. C., & Nicoll, R. A. (1997). Use-dependent increases in glutamate concentration activate presynaptic metabotropic glutamate receptors. *Nature*, 385(6617), 630–4.
- Schikorski, T., & Stevens, C. F. (1997). Quantitative ultrastructural analysis of hippocampal excitatory synapses. *J. Neurosci.*, 17(15), 5858–67.
- Schneggenburger, R., & Neher, E. (2000). Intracellular calcium dependence of transmitter release rates at a fast central synapse. *Nature*, 406(6798), 889–893.
- Schneggenburger, R., & Rosenmund, C. (2015). Molecular mechanisms governing Ca²⁺ regulation of evoked and spontaneous release. *Nature Neuroscience*, 18(7), 935–941.
- Sheng, J., He, L., Zheng, H., Xue, L., Luo, F., Shin, W., ... Wu, L.-G. (2012). Calcium-channel number critically influences synaptic strength and plasticity at the active zone. *Nature*, 15(7), 998–1006.
- Sigworth, F. J. (1980). The variance of sodium current fluctuations at the node of Ranvier. *J. Physiol.*, 307, 97–129.
- Stevens, C. F. (2003). Neurotransmitter Release at Central Synapses. *Neuron*, 40, 381–388.
- Stevens, C. F., & Wang, Y. (1995). Facilitation and depression at single central synapses. *Neuron*, 14, 795–802.
- Südhof, T. C. (2012). The presynaptic active zone. *Neuron*, 75, 11–25.
- Südhof, T. C. (2013). Neurotransmitter release: The last millisecond in the life of a synaptic vesicle. *Neuron*, 80(3), 675–690.
- Szule, J. a., Harlow, M. L., Jung, J. H., De-Miguel, F. F., Marshall, R. M., & McMahan, U. J. (2012). Regulation of synaptic vesicle docking by different classes of macromolecules in active zone material. *PLoS ONE*, 7(3).
- Tapia, J. C., Wylie, J. D., Kasthuri, N., Hayworth, K. J., Schalek, R., Berger, D. R., ... Lichtman, J. W. (2012). Pervasive synaptic branch removal in the mammalian

- neuromuscular system at birth. *Neuron*, 74(5), 816–29.
- Ting, J., Daigle, T., Chen, Q., & Feng, G. (2014). Acute brain slice methods for adult and aging animals: application of targeted patch clamp analysis and optogenetics. *Methods Mol Biol*, 1183, 1–21.
- Tong, G., & Jahr, C. E. (1994). Multivesicular release from excitatory synapses of cultured hippocampal neurons. *Neuron*, 12, 51–59.
- Trigo, F. F., Sakaba, T., Ogden, D., & Marty, A. (2012). Readily releasable pool of synaptic vesicles measured at single synaptic contacts. *Proc. Natl. Acad. Sci.*
- Triller, A., & Korn, H. (1982). Transmission at a central inhibitory synapse. III. Ultrastructure of physiologically identified and stained terminals. *J. Neurophysiol.*, 48(3), 708–736.
- Yung, Y. C., Stoddard, N. C., Mirendil, H., & Chun, J. (2015). Lysophosphatidic Acid Signaling in the Nervous System. *Neuron*, 85(4), 669–682.

BIBLIOGRAPHY

Résumé:

L'élément constitutif des synapses centrales est le site synaptique individuel, comprenant une zone active du côté présynaptique et une densité postsynaptique associée. Du fait de limitations techniques nos connaissances sur le mode de fonctionnement d'un site synaptique restent insuffisantes. Pour faire progresser cette question nous projetons d'effectuer des enregistrements en paires entre interneurons de la couche moléculaire du cervelet. Ces neurones forment des synapses qui ont des signaux élémentaires quantiques de grande taille, et les synapses comprennent parfois un seul site synaptique, ce qui fait qu'ils offrent des avantages décisifs pour ce projet. Les réponses postsynaptiques à des trains de potentiels d'action seront étudiées dans différentes conditions expérimentales. Les résultats seront interprétés par un modèle supposant que les vésicules synaptiques doivent se lier à un petit groupe de sites d'arrimage avant l'exocytose.

Title:

Synaptic Fluctuations in Cerebellar Interneurons Connected by a single synaptic contact

Abstract:

The unitary element of central synaptic transmission is a single synaptic site, with one active zone as presynaptic component and the postsynaptic density as postsynaptic partner. Due to technical limitations there is much uncertainty on the mode of functioning of a single synaptic site. To address this issue it is planned to perform paired recordings between interneurons of the molecular layers of the cerebellum. These neurons form synapses with a large quantal size, and occasionally displaying a single release site, and are thus favorable for this study. Postsynaptic responses will be studied in response to trains of presynaptic action potentials under various conditions. The results will be compared to a model supposing the obligatory binding of vesicles to a small complement of docking sites prior to exocytosis.

Mots clés:

Docking Sites, Single synaptic contacts, GABAergic interneurons.

Keywords :

Docking Sites, Single synaptic contacts, GABAergic interneurons.